

# **Fermion Number Violation and Level Crossing on the Lattice**

Thesis submitted to the University of Glasgow  
for the degree of Doctor of Philosophy

September 1996

**Steven Morrison**

Department of Physics and Astronomy  
University of Glasgow

©Steven Morrison, 1996

ProQuest Number: 11007908

All rights reserved

INFORMATION TO ALL USERS

The quality of this reproduction is dependent upon the quality of the copy submitted.

In the unlikely event that the author did not send a complete manuscript and there are missing pages, these will be noted. Also, if material had to be removed, a note will indicate the deletion.



ProQuest 11007908

Published by ProQuest LLC (2018). Copyright of the Dissertation is held by the Author.

All rights reserved.

This work is protected against unauthorized copying under Title 17, United States Code  
Microform Edition © ProQuest LLC.

ProQuest LLC.  
789 East Eisenhower Parkway  
P.O. Box 1346  
Ann Arbor, MI 48106 – 1346

Ther  
10646  
Copy 1

To my family.

# Acknowledgements

I would like to thank Dr. Colin Froggatt for supervising my research and Dr. Ian Barbour who provided much assistance with the numerical work. Thanks to all of the members of the theory group especially Professor Gordon Moorhouse for his supervision during my first year and Dr. David Sutherland for many useful discussions. I am also grateful to Dr. Simon Hands of the University of Wales, Swansea for useful suggestions and discussions.

I would also like to thank my family and friends for their support and encouragement throughout my studies.

I am grateful to the Particle Physics and Astronomy Research Council for providing a research studentship.

# Declaration

Chapter 1 is a review of fermion number violation and level crossing. The rest of the thesis describes work done by myself with the assistance of Dr. Colin Froggatt and Dr. Ian Barbour. Much of the work described in Chapters 3 and 5 is based on the work of J. Ambjørn, K. Farakos, S. Hands, G. Koutsoumbas and G. Thorleifsson. The method of using the time-dependent Dirac equation to investigate level crossing was suggested by Dr. Simon Hands.

# Summary

The electroweak theory is believed to play an important role in the creation of the baryon asymmetry of the universe. This is due to anomalous fermion number violating processes which are believed to occur rapidly at the high temperatures prevailing in the early universe. However the perturbative methods used to estimate the rate of such processes break down at the very high temperatures occurring above the electroweak phase transition.

Lattice gauge theories provide a useful non-perturbative tool for studying electroweak fermion number violation at high temperature. The most common technique involves measuring the Chern-Simons number  $N_{CS}$  of the gauge field with fermion number violation occurring whenever  $\Delta N_{CS} = \pm 1$ . However the measurement of  $N_{CS}$  on the lattice is known to be problematic. The level crossing picture provides a way of checking that fermion number really is violated in these simulations.

We use two methods to investigate the level crossing phenomenon. In the first level crossing is signalled by the lowest eigenvalue diving to zero and a simultaneous flip in sign of the "generalised chirality" which is a natural label for the eigenstates. This signal is interpreted as showing the lowest eigenvalue crossing zero. To provide further evidence that this is the case we introduce a new method which involves numerically solving the Dirac equation to follow the time development of the fermion states.

Firstly the methods are applied to the  $U(1)$  model in  $1 + 1$  dimensions. Both methods give a clear signal for level crossing, the exact point at which the zero

eigenvalue occurs depending on the Yukawa coupling. Similar results are obtained for the  $SU(2)$  model in  $3 + 1$  dimensions though the signal is affected by fluctuations in the background fields particularly for large Yukawa coupling. A clear signal is only obtained after cooling the backgrounds.

These results provide further evidence that the high temperature configurations with  $\Delta N_{CS} = \pm 1$  observed in lattice simulations are accompanied by fermion number violation.

# Contents

|          |   |           |
|----------|---|-----------|
| <b>1</b> | <b>Introduction</b>                                   | <b>1</b>  |
| 1.1      | Anomalies and Fermion Number Violation . . . . .      | 1         |
| 1.2      | Vacuum Structure and Topology . . . . .               | 3         |
| 1.3      | Fermionic Level Crossing . . . . .                    | 9         |
| 1.4      | Transition Rates . . . . .                            | 12        |
| 1.5      | Baryogenesis and Cosmology . . . . .                  | 14        |
| 1.6      | Numerical Simulations . . . . .                       | 15        |
| <b>2</b> | <b>U(1) Model in 1+1 Dimensions</b>                   | <b>18</b> |
| 2.1      | Introduction . . . . .                                | 18        |
| 2.2      | The Microcanonical Method . . . . .                   | 18        |
| 2.3      | Lattice Gauge-Higgs System . . . . .                  | 21        |
| 2.4      | Numerical Procedure . . . . .                         | 23        |
| 2.5      | Choice of Parameters . . . . .                        | 24        |
| 2.6      | Topological Measurements . . . . .                    | 24        |
| <b>3</b> | <b>Level Crossing in U(1) Model in 1+1 Dimensions</b> | <b>29</b> |
| 3.1      | Introduction . . . . .                                | 29        |
| 3.2      | Lattice Eigenvalue Equations . . . . .                | 30        |
| 3.3      | Eigenvalue and Chirality Measurements . . . . .       | 37        |
| 3.4      | Lattice Dirac Equation . . . . .                      | 42        |
| 3.5      | Transition Probability Measurements . . . . .         | 44        |

|          |  |            |
|----------|--|------------|
| <b>4</b> | <b>SU(2) Model in 3+1 Dimensions</b>                   | <b>68</b>  |
| 4.1      | Introduction . . . . .                                 | 68         |
| 4.2      | Lattice Gauge-Higgs System . . . . .                   | 68         |
| 4.3      | Numerical Procedure . . . . .                          | 71         |
| 4.4      | Choice of Parameters . . . . .                         | 72         |
| 4.5      | Topological Measurements . . . . .                     | 73         |
| <b>5</b> | <b>Level Crossing in SU(2) Model in 3+1 Dimensions</b> | <b>77</b>  |
| 5.1      | Introduction . . . . .                                 | 77         |
| 5.2      | Lattice Eigenvalue Equations . . . . .                 | 77         |
| 5.3      | Eigenvalue and Chirality Measurements . . . . .        | 83         |
| 5.4      | Transition Probability Measurements . . . . .          | 89         |
| <b>6</b> | <b>Conclusions</b>                                     | <b>106</b> |
| <b>A</b> | <b>Lattice Gauge Theory</b>                            | <b>109</b> |
| <b>B</b> | <b>Monte Carlo Methods</b>                             | <b>112</b> |
| <b>C</b> | <b>The Lanczos Algorithm</b>                           | <b>114</b> |
| <b>D</b> | <b>Inverse Iteration</b>                               | <b>116</b> |

# List of Figures

|     |  |    |
|-----|--|----|
| 1.1 | Schematic plot of the potential energy as a function of the gauge and Higgs fields. The minima are vacuum states with different winding numbers $n$ . . . . .  | 8  |
| 1.2 | (a): The initial fermion spectrum. (b): The final fermion spectrum. Open circles denote empty states and filled circles denote occupied states. . . . .  | 11 |
| 2.1 | The Chern-Simons number as a function of time for $\tilde{\lambda} = 0.5$ , $a = 0.2$ , $\frac{T}{gv^3} = 0.095$ . The lattice size is $n = 200$ . . . . .   | 26 |
| 2.2 | The Chern-Simons Number as a function of time for a typical sphaleron transition. . . . .  | 27 |
| 2.3 | The Higgs field during a typical sphaleron transition. (a): $t = 2100$ , $N_H = 0$ . (b): $t = 2137.2$ , $\phi$ crosses zero. (c): $t = 2200$ , $N_H = 1$ . . . . .  | 28 |
| 3.1 | (a): The lowest eigenvalue $E_0$ as a function of time for the configurations (3.3.33) for masses $m = 0, 0.01$ and $0.1$ . (b): The chirality $\Gamma_5$ of the corresponding eigenvector. . . . .                                  | 48 |
| 3.2 | (a): The lowest eigenvalue $E_0$ as a function of time for the configurations (3.3.34) for Yukawa couplings $h = 0.01, 0.05$ and $0.1$ . (b): The generalised chirality $\tilde{\Gamma}_5$ of the corresponding eigenvector. . . . . | 49 |

|      |   |    |
|------|---|----|
| 3.3  | (a): The lowest eigenvalue $E_0$ as a function of time for the configurations (3.3.35) for Yukawa couplings $h = 0.01, 0.05$ and $0.1$ . (b): The generalised chirality $\tilde{\Gamma}_5$ of the corresponding eigenvector. . . .  | 50 |
| 3.4  | (a): The lowest eigenvalue $E_0$ as a function of time for the configurations (3.3.36) for Yukawa couplings $h = 0.01, 0.05$ and $0.1$ . (b): The generalised chirality $\tilde{\Gamma}_5$ of the corresponding eigenvector. . . .  | 51 |
| 3.5  | (a): The lowest eigenvalue $E_0$ as a function of time for the configurations (3.3.37) for Yukawa couplings $h = 0.001, 0.01$ and $0.05$ . (b): The generalised chirality $\tilde{\Gamma}_5$ of the corresponding eigenvector for $h = 0.001$ and $h = 0.01$ . . . . .    | 52 |
| 3.6  | (a): The lowest eigenvalue $E_0$ as a function of time for the configurations (3.3.38) for Yukawa couplings $h = 0.001, 0.01$ and $0.05$ . (b): The generalised chirality $\tilde{\Gamma}_5$ of the corresponding eigenvector for $h = 0.001$ and $h = 0.1$ . . . . .     | 53 |
| 3.7  | (a): The lowest eigenvalue $E_0$ as a function of time for a typical sphaleron transition for the massless Hamiltonian. (b): The chirality $\Gamma_5$ of the corresponding eigenvector. . . . .   | 54 |
| 3.8  | (a): The lowest eigenvalue $E_0$ as a function of time for a typical sphaleron transition for Yukawa couplings $h = 0.1, 0.2$ and $0.3$ . (b): The generalised chirality $\tilde{\Gamma}_5$ of the corresponding eigenvector. . . .                                       | 55 |
| 3.9  | (a): The lowest eigenvalue $E_0$ as a function of time for a typical sphaleron transition for $m = 0$ . (b): The chirality $\Gamma_5$ of the corresponding eigenvector. . . . .   | 56 |
| 3.10 | (a): The lowest eigenvalue $E_0$ as a function of time for a typical sphaleron transition for Yukawa couplings $h = 0.001, 0.01$ and $0.05$ . (b): The generalised chirality $\tilde{\Gamma}_5$ of the corresponding eigenvector for $h = 0.001$ and $h = 0.01$ . . . . . | 57 |

- 3.11 (a):  $\left|\langle E_0^+|\psi\rangle\right|^2$  as a function of time for the configurations (3.3.33) for the massless Hamiltonian. (b):  $\left|\langle E_0^-|\psi\rangle\right|^2$  as a function of time for the configurations (3.3.33) for the massless Hamiltonian. . . . 58
- 3.12 (a):  $\left|\langle E_0^+|\psi\rangle\right|^2$  as a function of time for the configurations (3.3.34) for Yukawa couplings  $h = 0.01, 0.05$  and  $0.1$ . (b):  $\left|\langle E_0^-|\psi\rangle\right|^2$  as a function of time for the configurations (3.3.34) for Yukawa couplings  $h = 0.01, 0.05$  and  $0.1$ . . . . . 59
- 3.13 (a):  $\left|\langle E_0^+|\psi\rangle\right|^2$  as a function of time for the configurations (3.3.35) for Yukawa couplings  $h = 0.01, 0.05$  and  $0.1$ . (b):  $\left|\langle E_0^-|\psi\rangle\right|^2$  as a function of time for the configurations (3.3.35) for Yukawa couplings  $h = 0.01, 0.05$  and  $0.1$ . . . . . 60
- 3.14 (a):  $\left|\langle E_0^+|\psi\rangle\right|^2$  as a function of time for the configurations (3.3.36) for Yukawa couplings  $h = 0.01, 0.05$  and  $0.1$ . (b):  $\left|\langle E_0^-|\psi\rangle\right|^2$  as a function of time for the configurations (3.3.36) for Yukawa couplings  $h = 0.01, 0.05$  and  $0.1$ . . . . . 61
- 3.15 (a):  $\left|\langle E_0^+|\psi\rangle\right|^2$  as a function of time for the configurations (3.3.37) for Yukawa couplings  $h = 0.001$  and  $0.01$ . (b):  $\left|\langle E_0^-|\psi\rangle\right|^2$  as a function of time for the configurations (3.3.37) for Yukawa couplings  $h = 0.001$  and  $0.01$ . . . . . 62
- 3.16 (a):  $\left|\langle E_0^+|\psi\rangle\right|^2$  as a function of time for the configurations (3.3.38) for Yukawa couplings  $h = 0.001$  and  $0.01$ . (b):  $\left|\langle E_0^-|\psi\rangle\right|^2$  as a function of time for the configurations (3.3.38) for Yukawa couplings  $h = 0.001$  and  $0.01$ . . . . . 63
- 3.17 (a):  $\left|\langle E_0^+|\psi\rangle\right|^2$  as a function of time for a typical sphaleron transition for the massless Hamiltonian. (b):  $\left|\langle E_0^-|\psi\rangle\right|^2$  as a function of time for a typical sphaleron transition for the massless Hamiltonian. 64

- 3.18 (a):  $|\langle E_0^+ | \psi \rangle|^2$  as a function of time for a typical sphaleron transition for Yukawa couplings  $h = 0.1, 0.2$  and  $0.3$ . (b):  $|\langle E_0^- | \psi \rangle|^2$  as a function of time for a typical sphaleron transition for Yukawa couplings  $h = 0.1, 0.2$  and  $0.3$ . . . . . 65
- 3.19 (a):  $|\langle E_0^+ | \psi \rangle|^2$  as a function of time for a typical sphaleron transition for the massless Hamiltonian. (b):  $|\langle E_0^- | \psi \rangle|^2$  as a function of time for a typical sphaleron transition for the massless Hamiltonian. 66
- 3.20 (a):  $|\langle E_0^+ | \psi \rangle|^2$  as a function of time for a typical sphaleron transition for Yukawa couplings  $h = 0.001$  and  $0.01$ . (b):  $|\langle E_0^- | \psi \rangle|^2$  as a function of time for a typical sphaleron transition for Yukawa couplings  $h = 0.001$  and  $0.01$ . . . . . 67
- 4.1 The Chern-Simons number as a function of time for  $\beta_G = 12, \beta_H = 0.34, \beta_R = 0.0012$ . The lattice size is  $16^3$ . . . . . 75
- 4.2 The Chern-Simons number as a function of time for a typical sphaleron transition. (a): no cooling. (b): 60 cooling sweeps. . . . . 76
- 5.1 The Chern-Simons Number as a function of time for the configurations (5.3.38). . . . . 84
- 5.2 (a): The lowest eigenvalue  $E_0$  as a function of time for the configurations (5.3.38) for masses  $m = 0, 0.1$  and  $1.0$ . (b): The chirality  $\Gamma_5$  of the corresponding eigenvector. . . . . 92
- 5.3 (a): The lowest eigenvalue  $E_0$  as a function of time for the configurations (5.3.39) for Yukawa couplings  $h = 0.1, 0.5$  and  $1.0$ . (b): The generalised chirality  $\tilde{\Gamma}_5$  of the corresponding eigenvector. . . . 93
- 5.4 (a): The lowest eigenvalue  $E_0$  as a function of time for the configurations (5.3.40) for Yukawa couplings  $h = 0.1, 0.5$  and  $1.0$ . (b): The generalised chirality  $\tilde{\Gamma}_5$  of the corresponding eigenvector. . . . 94

|      |   |     |
|------|---|-----|
| 5.5  | (a): The lowest eigenvalue $E_0$ as a function of time for a typical sphaleron transition (no cooling) for the massless Hamiltonian. (b): The chirality $\Gamma_5$ of the corresponding eigenvector. . . . .  | 95  |
| 5.6  | (a): The lowest eigenvalue $E_0$ as a function of time for a typical sphaleron transition (60 cooling sweeps) for the massless Hamiltonian. (b): The chirality $\Gamma_5$ of the corresponding eigenvector. . . . .   | 96  |
| 5.7  | (a): The lowest eigenvalue $E_0$ as a function of time for a typical sphaleron transition (no cooling) for Yukawa couplings $h = 0.1, 0.3$ and $0.5$ . (b): The generalised chirality $\tilde{\Gamma}_5$ of the corresponding eigenvector. . . . .  | 97  |
| 5.8  | (a): The lowest eigenvalue $E_0$ as a function of time for a typical sphaleron transition (60 cooling sweeps) for Yukawa couplings $h = 0.1, 0.3$ and $0.5$ . (b): The generalised chirality $\tilde{\Gamma}_5$ of the corresponding eigenvector. . . . .   | 98  |
| 5.9  | The generalised chirality $\tilde{\Gamma}_5$ as a function of time for a typical sphaleron transition for 0, 20, 40 and 60 cooling sweeps. (a): $h = 0.1$ . (b): $h = 0.5$ . . . . .  | 99  |
| 5.10 | (a): $ \langle E_0^+   \psi \rangle ^2$ as a function of time for the configurations (5.3.38) for the massless Hamiltonian. (b): $ \langle E_0^-   \psi \rangle ^2$ as a function of time for the configurations (5.3.38) for the massless Hamiltonian. . . . .                                     | 100 |
| 5.11 | (a): $ \langle E_0^+   \psi \rangle ^2$ as a function of time for the configurations (5.3.39) for Yukawa couplings $h = 0.1, 0.5$ and $1.0$ . (b): $ \langle E_0^-   \psi \rangle ^2$ as a function of time for the configurations (5.3.39) for Yukawa couplings $h = 0.1, 0.5$ and $1.0$ . . . . . | 101 |
| 5.12 | (a): $ \langle E_0^+   \psi \rangle ^2$ as a function of time for the configurations (5.3.40) for Yukawa couplings $h = 0.1, 0.5$ and $1.0$ . (b): $ \langle E_0^-   \psi \rangle ^2$ as a function of time for the configurations (5.3.40) for Yukawa couplings $h = 0.1, 0.5$ and $1.0$ . . . . . | 102 |

- 5.13 (a):  $\left|\langle E_0^+|\psi\rangle\right|^2$  as a function of time for a typical sphaleron transition for the massless Hamiltonian. (b):  $\left|\langle E_0^-|\psi\rangle\right|^2$  as a function of time for a typical sphaleron transition for the massless Hamiltonian. 103
- 5.14 (a):  $\left|\langle E_0^+|\psi\rangle\right|^2$  as a function of time for a typical sphaleron transition (no cooling) for Yukawa couplings  $h = 0.1, 0.3$  and  $0.5$ . (b):  $\left|\langle E_0^-|\psi\rangle\right|^2$  as a function of time for a typical sphaleron transition (no cooling) for Yukawa couplings  $h = 0.1, 0.3$  and  $0.5$ . . . . . 104
- 5.15 (a):  $\left|\langle E_0^+|\psi\rangle\right|^2$  as a function of time for a typical sphaleron transition (60 cooling sweeps) for Yukawa couplings  $h = 0.1, 0.3$  and  $0.5$ . (b):  $\left|\langle E_0^-|\psi\rangle\right|^2$  as a function of time for a typical sphaleron transition (60 cooling sweeps) for Yukawa couplings  $h = 0.1, 0.3$  and  $0.5$ . . . . . 105

# Chapter 1

## Introduction

### 1.1 Anomalies and Fermion Number Violation

In classical field theory the existence of a continuous symmetry in the Lagrangian leads, by Noether's Theorem, to a conserved current. However in certain cases the conservation law may be broken in the corresponding quantum theory. This is because the quantisation of the theory involves the introduction of some regularisation scheme in order to obtain finite results. When the process of regularisation does not respect the symmetry additional "anomalous" terms can arise in the divergence of the (classically conserved) current. For example, in classical electrodynamics the vector current  $J_\mu = \bar{\psi}\gamma_\mu\psi$  is conserved

$$\partial^\mu J_\mu = 0 \tag{1.1.1}$$

due to global  $U(1)$  invariance. On the other hand the axial vector current  $J_\mu^5 = \bar{\psi}\gamma_\mu\gamma_5\psi$  obeys

$$\partial^\mu J_\mu^5 = 2im\bar{\psi}\gamma_5\psi \tag{1.1.2}$$

where  $m$  is the mass of the field  $\psi$ . For massless fermions  $J_\mu^5$  is also conserved since for  $m = 0$  the Lagrangian is chirally symmetric. In the corresponding quantum theory  $J_\mu^5$  is not conserved even for  $m = 0$ . If we regularise in such a way as to

maintain vector current conservation  $\partial^\mu J_\mu = 0$  then Eq. (1.1.2) is modified to

$$\partial^\mu J_\mu^5 = 2im\bar{\psi}\gamma_5\psi + \frac{g^2}{8\pi^2}F_{\mu\nu}\tilde{F}^{\mu\nu} \quad (1.1.3)$$

in 3+1 dimensions.  $\tilde{F}^{\mu\nu}$  is the dual of the electromagnetic field tensor  $F_{\mu\nu}$ , defined by  $\tilde{F}^{\mu\nu} = \frac{1}{2}\epsilon^{\mu\nu\rho\sigma}F_{\rho\sigma}$ .

Eq. (1.1.3) can be generalised to nonabelian theories and to different numbers of space dimensions. In particular we have

$$\partial^\mu J_\mu^5 = 2im\bar{\psi}\gamma_5\psi + \frac{g}{2\pi}\epsilon_{\mu\nu}F^{\mu\nu} \quad (1.1.4)$$

for  $U(1)$  theory in 1 + 1 dimensions and

$$\partial^\mu J_\mu^5 = 2im\bar{\psi}\gamma_5\psi + \frac{g^2}{8\pi^2}\text{Tr} [F_{\mu\nu}\tilde{F}^{\mu\nu}] \quad (1.1.5)$$

for  $SU(2)$  theory in 3+1 dimensions. In Eq. (1.1.5)  $F_{\mu\nu}$  is the  $SU(2)$  field tensor,  $F_{\mu\nu} = \frac{\sigma^a}{2}F_{\mu\nu}^a$  where  $\sigma^a$  are the pauli matrices.

Eqs. (1.1.3), (1.1.4) and (1.1.5) are called global anomalies since chiral symmetry is a global symmetry. Such anomalies are harmless in the sense that they do not spoil renormalisability. Furthermore the anomalous term in Eq. (1.1.3) has real physical consequences and is required to explain the observed rate of neutral pion decay  $\pi^0 \rightarrow 2\gamma$ . On the other hand it is crucial for renormalisability that gauge invariance is preserved as reflected in the Ward-Takahashi identities. For purely vector-like theories there are no gauge anomalies.

However if a theory contains axial as well as vector couplings, anomalous contributions to the Ward identities can occur making the theory non-renormalisable. For example consider a chiral theory with a single left handed fermion field coupling to the gauge field. In this case both axial and vector currents are anomalous and in particular the vector current satisfies

$$\partial^\mu J_\mu = -\frac{g}{4\pi}\epsilon_{\mu\nu}F^{\mu\nu} \quad (1.1.6)$$

for  $U(1)$  theory in 1 + 1 dimensions and

$$\partial^\mu J_\mu = -\frac{g^2}{16\pi^2}\text{Tr} [F_{\mu\nu}\tilde{F}^{\mu\nu}] \quad (1.1.7)$$

for  $SU(2)$  theory in  $3 + 1$  dimensions. For the  $U(1)$  theory with a single fermion Eq. (1.1.6) is a gauge anomaly (since in that case the vector current is the gauge current) making the theory non-renormalisable (in the  $SU(2)$  theory there is no such problem). The only hope of maintaining renormalisability is to add further fermion species with charges chosen such that the anomalies cancel between different fermions. In this particular case the charges of left and right handed particles must satisfy  $\sum q_L^2 = \sum q_R^2$  where the sum is over all particle species. Such conditions are useful in constructing extensions of the Standard Model (e.g. Grand Unified Theories) since they place restrictions on the fermion content of such theories.

Eq. (1.1.7) is particularly interesting since it applies to the electroweak theory. Eq. (1.1.7) applies independently for each fermion in the theory and hence the baryon and lepton number currents satisfy

$$\partial^\mu J_\mu^B = \partial^\mu J_\mu^L = -\frac{g^2}{16\pi^2} N_f \text{Tr} [F_{\mu\nu} \tilde{F}^{\mu\nu}] \quad (1.1.8)$$

where  $N_f$  is the number of families. Since the anomaly is the same for the baryon and lepton currents the difference  $J_\mu^{B-L}$  is conserved. At the same time it can be shown that there are no gauge anomalies, the anomalies cancelling between quarks and leptons.

## 1.2 Vacuum Structure and Topology

An important feature of the theories under consideration is their complex vacuum structure [2]. This is easily illustrated in the case of the  $U(1)$  model in  $1 + 1$  dimensions. The Hamiltonian is

$$H = \int dx \left[ \frac{1}{2} E^2 + P^* P + \frac{\lambda}{4} (\phi^* \phi - v^2)^2 + \left( \frac{d}{dx} + igA_1 \right) \phi^* \left( \frac{d}{dx} - igA_1 \right) \phi \right] \quad (1.2.9)$$

in the temporal gauge (the temporal component of the vector field  $A_0 = 0$ ).  $A_1$  is the spatial component of the vector field. Its conjugate momentum is the electric field  $E = \frac{dA_1}{dt}$ .  $\phi$  is the Higgs field with conjugate momentum  $P = \frac{d\phi}{dt}$ . A ground state (vacuum) of this theory is

$$\phi = v, \quad A_1 = 0 \quad (1.2.10)$$

However due to  $U(1)$  gauge invariance so is

$$\phi = e^{i\theta(x)}v, \quad A_1 = -\frac{i}{g} \frac{1}{e^{i\theta(x)}} \frac{d}{dx} e^{i\theta(x)} \quad (1.2.11)$$

Such configurations are known as "pure gauge".

There are thus an infinite number of classical vacua. It is possible to split these vacua into "homotopy classes" as follows. If we identify  $x = -\infty$  and  $x = \infty$  then  $x$  space is topologically equivalent to a unit circle ( $S^1$ ) so  $e^{i\theta}$  defines a mapping

$$e^{i\theta} : S^1 \rightarrow U(1) \quad (1.2.12)$$

Now since  $x = -\infty$  and  $x = \infty$  are identified we can write  $\theta(\infty) = \theta(-\infty) + 2\pi n$  where  $n$  is an integer which measures the number of times  $\theta$  winds clockwise round  $U(1)$  space as  $x$  goes from  $-\infty$  to  $\infty$ . This allows us to split the mappings  $e^{i\theta}$  (and hence classical vacua) into homotopy classes classified by the integer  $n$ .  $n$  is known as the "winding number" and can be written

$$n = \frac{1}{2\pi} \int_{-\infty}^{\infty} dx \left[ -i \frac{1}{e^{i\theta}} \frac{d}{dx} e^{i\theta} \right] \quad (1.2.13)$$

Gauge transformations with  $n = 0$  are called "small" gauge transformations and those with  $n \neq 0$  are "large" gauge transformations. Mappings with a given winding number are homotopic in the sense that they can be continuously deformed into each other by a sequence of mappings.

The winding number defined in Eq. (1.2.13) can be used to define a "Higgs winding number"  $N_H$  for a general Higgs field of the form  $\phi = R e^{i\theta}$ .  $N_H$  is

invariant under small gauge transformations and increases by the integer  $n$  under a large gauge transformation with winding number  $n$ . Note that the phase  $\theta$  and hence  $N_H$  is well defined only if  $R \neq 0$  everywhere.  $N_H$  measures the number of times the Higgs field winds clockwise round the origin as  $x$  goes from  $-\infty$  to  $\infty$ . Now if the Higgs field changes from one vacuum to another with different winding number, the Higgs field must be zero at some point. This is because, as long as  $\phi$  is non-zero everywhere, it has a well defined winding number which cannot change by a continuous transformation.

We can also define a winding number for the  $SU(2)$  theory in 3+1 dimensions. Now we have a Hamiltonian

$$H = \int d^3x \left[ \frac{1}{2} E_i^a E_i^a + \frac{1}{4} F_{ij}^a F_{ij}^a + P^\dagger P + (D_i \phi)^\dagger (D^i \phi) + \frac{\lambda}{4} (\phi^\dagger \phi - v^2)^2 \right] \quad (1.2.14)$$

where  $D_i = \nabla_i - igA_i$  ( $A_i$  is the matrix valued gauge field,  $A_i = \frac{\sigma^a}{2} A_i^a$ ), in the temporal gauge  $A_0^a = 0$ . The conjugate momentum to  $A_i^a$  is the electric field  $E^a = \frac{dA_i^a}{dt}$  while the conjugate momentum to the Higgs doublet  $\phi$  is  $P = \frac{d\phi}{dt}$ . The trivial vacuum of this theory is

$$\phi = \begin{pmatrix} 0 \\ v \end{pmatrix}, \quad A_i = 0 \quad (1.2.15)$$

However due to  $SU(2)$  gauge invariance so is

$$\phi = \Omega \begin{pmatrix} 0 \\ v \end{pmatrix}, \quad A_i = -\frac{i}{g} (\nabla_i \Omega) \Omega^{-1} \quad (1.2.16)$$

where  $\Omega = \Omega(x)$  is any  $SU(2)$  matrix.

If we identify all points at spatial infinity coordinate space is topologically equivalent to a 3-sphere, so we have

$$\Omega : S^3 \rightarrow SU(2) \quad (1.2.17)$$

Again we can define a topological winding number which counts the number of times that  $SU(2)$  space is covered by the mapping  $\Omega$  as we span the coordinate space.

$$n = -\frac{1}{24\pi^2} \int d^3x \epsilon_{ijk} \text{Tr} \left[ \partial_i \Omega \Omega^{-1} \partial_j \Omega \Omega^{-1} \partial_k \Omega \Omega^{-1} \right] \quad (1.2.18)$$

Again  $n$  is necessarily an integer.

We can use Eq. (1.2.18) to define a Higgs winding number  $N_H$  for a general Higgs doublet of the form  $\phi = \Omega R$  where  $R = \begin{pmatrix} 0 \\ |\phi| \end{pmatrix}$  and  $\Omega \in SU(2)$ . If

$\phi = \begin{pmatrix} \phi_+ \\ \phi_0 \end{pmatrix}$  then we have

$$\Omega = \frac{1}{(|\phi_0|^2 + |\phi_+|^2)^{\frac{1}{2}}} \begin{pmatrix} \phi_0^* & \phi_+ \\ -\phi_+^* & \phi_0 \end{pmatrix} \quad (1.2.19)$$

As in the  $U(1)$  theory for topological reasons we can deduce that the Higgs field must have a zero ( $|\phi| = 0$ ) at some point in a transition between two topologically distinct vacua.

The relevance of topologically distinct vacua for fermion number violation can be seen by noting that

$$\begin{aligned} \frac{g}{4\pi} \epsilon_{\mu\nu} F^{\mu\nu} &= \partial^\mu K_\mu \\ K_\mu &= \frac{g}{2\pi} \epsilon_{\mu\nu} A^\nu \end{aligned} \quad (1.2.20)$$

for  $U(1)$  theory in  $1+1$  dimensions and

$$\begin{aligned} \frac{g^2}{16\pi^2} \text{Tr} \left[ F_{\mu\nu} \tilde{F}^{\mu\nu} \right] &= \partial^\mu K_\mu \\ K_\mu &= \frac{g^2}{8\pi^2} \epsilon_{\mu\nu\rho\sigma} \text{Tr} \left[ A^\nu \partial^\rho A^\sigma - \frac{2}{3} i g A^\nu A^\rho A^\sigma \right] \end{aligned} \quad (1.2.21)$$

for  $SU(2)$  theory in  $3 + 1$  dimensions.  $K_\mu$  is the Chern-Simons current. From Eqs. (1.1.6) and (1.1.7) we then have

$$\partial^\mu J_\mu = -\partial^\mu K_\mu \quad (1.2.22)$$

which can be integrated to give

$$\Delta N_F = -\Delta N_{CS} \quad (1.2.23)$$

where  $N_F$  is the fermion number

$$N_F = \int d^d x \psi^\dagger \psi \quad (1.2.24)$$

and  $N_{CS}$  is the Chern-Simons number.

$$N_{CS} = \frac{g}{2\pi} \int dx A^1 \quad (1.2.25)$$

for  $U(1)$  theory in  $1 + 1$  dimensions and

$$N_{CS} = \frac{g^2}{8\pi^2} \int d^3 x \epsilon_{\mu\nu\rho} \text{Tr} \left[ A^\mu \partial^\nu A^\rho - \frac{2}{3} i g A^\mu A^\nu A^\rho \right] \quad (1.2.26)$$

for  $SU(2)$  theory in  $3 + 1$  dimensions. The Chern-Simons number has the same transformation properties as the Higgs winding number, i.e. it is invariant under small gauge transformations and increases by the integer  $n$  under a large gauge transformation with winding number  $n$ . However the difference  $N_{CS} - N_H$  is invariant under large gauge transformations. Now for vacuum states (see Eqs. (1.2.10) and (1.2.15)) the Chern-Simons number is just the topological winding number given by Eq. (1.2.13) for  $U(1)$  in  $1 + 1$  dimensions and Eq. (1.2.18) for  $SU(2)$  in  $3 + 1$  dimensions. Hence fermion number is violated whenever the gauge fields make a transition between two topologically distinct vacuum states.

As discussed above mappings with different winding numbers cannot be continuously deformed into each other by a sequence of mappings. Thus in order for the gauge fields to make a transition between two topologically distinct vacua they must pass through non-vacuum states. The situation is illustrated in figure 1.1.

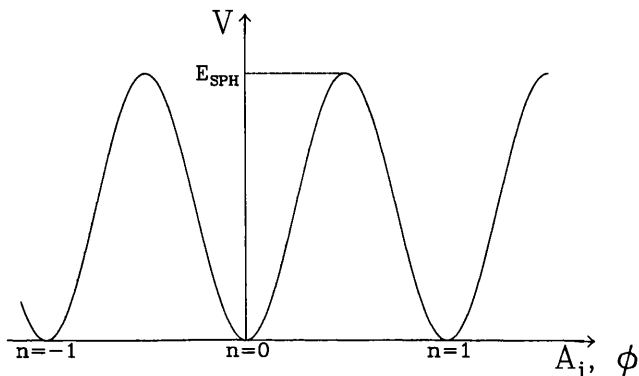


Figure 1.1: Schematic plot of the potential energy as a function of the gauge and Higgs fields. The minima are vacuum states with different winding numbers  $n$ .

Topologically distinct vacua are separated by an energy barrier. The height of the barrier can be found by considering a set of field configurations which continuously interpolate between the two vacua. The configuration corresponding to the top of the barrier is the sphaleron [3], which is a localised unstable time independent solution to the classical equations of motion. It has the form

$$A_1 = \frac{1}{g} \frac{d\beta}{dx}, \quad \phi = i \exp(i\beta) \frac{v}{\sqrt{2}} \tanh\left(\frac{1}{2}v\sqrt{\lambda}x\right) \quad (1.2.27)$$

where  $\beta(x)$  is any real function obeying  $\beta(\infty) - \beta(-\infty) = \pi$  for  $U(1)$  in 1+1 dimensions [4] and

$$A_i = i \frac{\epsilon_{ijk} x_j \sigma_k}{|x|^2} f(\xi), \quad \phi = \frac{v}{\sqrt{2}} i \frac{\sigma^a x^a}{|x|} \begin{pmatrix} 0 \\ 1 \end{pmatrix} h(\xi) \quad (1.2.28)$$

where  $\xi = gv|x|$  for  $SU(2)$  in 3+1 dimensions [3]. The functions  $f(\xi)$  and  $g(\xi)$  obey the boundary conditions  $f(0) = h(0) = 0, f(\infty) = h(\infty) = 1$ . They can

be found numerically by substituting the sphaleron solution into the Hamiltonian and minimising. The sphaleron energy is found to be

$$E_{sph} = \frac{\sqrt{8\lambda}}{3}v^3 \quad (1.2.29)$$

for  $U(1)$  in 1+1 dimensions [4] and

$$E_{sph} = 2\frac{M_W}{\alpha_W}A\left(\frac{\lambda}{\alpha_W}\right) \quad (1.2.30)$$

for  $SU(2)$  in 3+1 dimensions [3].  $\alpha_W = \frac{g^2}{4\pi}$  is the  $SU(2)$  fine structure constant and  $M_W$  the mass of the  $SU(2)$  gauge boson.  $A\left(\frac{\lambda}{\alpha_W}\right)$  varies between 1.5 and 2.7 as the Higgs self coupling  $\lambda$  varies between 0 and  $\infty$ , so that  $E_{SPH}$  is between 8 and 14 TeV depending on the Higgs self-coupling. In each case the Chern-Simons number of the sphaleron is  $\frac{1}{2}$  and its radius is  $\sim \frac{1}{M_W}$ . Another important property of the sphaleron is that its Higgs field is zero at the origin.

### 1.3 Fermionic Level Crossing

The anomalous production of charge has a simple physical interpretation in terms of level shifting of fermionic energy levels. For simplicity consider massless fermions in 1 + 1 dimensions interacting with a homogeneous external  $U(1)$  gauge field  $A_1$  in the temporal gauge  $A_0 = 0$  [8, 9]. If we put the system in a box of length  $L$  and impose anti-periodic boundary conditions the spectrum of the Dirac Hamiltonian is

$$E = k + gA_1 \quad (1.3.31)$$

for states with chirality +1 (right movers) and

$$E = -k - gA_1 \quad (1.3.32)$$

for states with chirality -1 (left movers).  $k$  is quantised due to the anti-periodic boundary conditions,  $k = \frac{(2n+1)\pi}{L}$ .

Now suppose  $A_1$  has the form

$$A_1(t) = \frac{2\pi}{gL}t \quad (1.3.33)$$

where the time  $t$  varies from 0 to 1, i.e. a constant uniform electric field  $\mathcal{E} = \frac{2\pi}{gL}$ . From Eq. (1.2.25)  $t$  is just the Chern-Simons number. The initial gauge field  $A_1(0) = 0$  is the trivial vacuum while the final gauge field  $A_1(1) = \frac{2\pi}{gL}$  is a vacuum with winding number 1. Since  $A_1(0)$  and  $A_1(1)$  are related by a (large) gauge transformation, the initial and final spectra are the same. Now suppose we start with the fermionic vacuum (filled Dirac sea) as shown in figure 1.2a. As the gauge field changes, the energy levels will shift according to Eqs. (1.3.31) and (1.3.32). The energy levels of the right moving states are shifted upwards, while the energy levels of the left moving states are shifted downwards. In particular the uppermost negative energy state with chirality +1 will cross  $E = 0$  to become positive, while the lowermost positive energy state with chirality -1 will cross  $E = 0$  to become negative. The point at which this "level crossing" occurs is when the Chern-Simons number  $t = \frac{1}{2}$ . Thus we end up with a filled positive energy right handed state and an empty negative energy left handed state, i.e. a particle and an antiparticle each with chiral charge +1. This is shown in figure 1.2b. The total change in chiral charge is twice the change in Chern-Simons number, in agreement with the anomaly equation.

For the  $SU(2)$  theory in 3 + 1 dimensions the level crossing phenomenon can also be demonstrated [10, 11]. The level crossing is not dependent on any particular form for the background fields and occurs generally for any set of  $SU(2)$  gauge fields which change continuously from one vacuum to another with different winding number.

If the fermions are massive the situation is quite different. If the fermion in the above example has a mass  $m$  then the energy eigenvalues are bounded below by  $m$  and so cannot cross zero. In the adiabatic limit the initial and final fermion states are the same and chiral charge is conserved. Nevertheless there is still

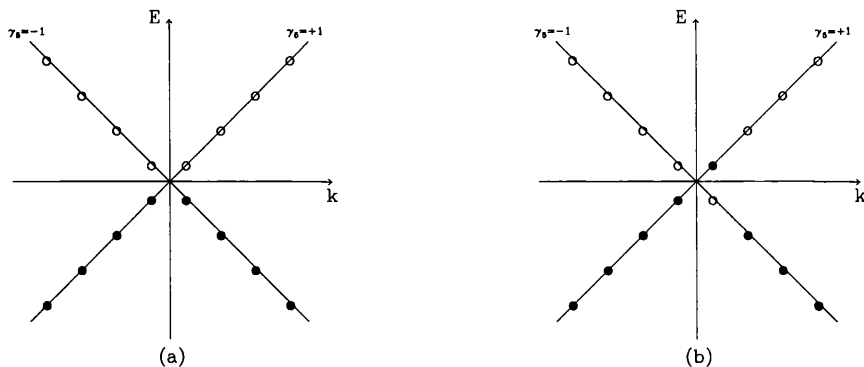


Figure 1.2: (a): The initial fermion spectrum. (b): The final fermion spectrum. Open circles denote empty states and filled circles denote occupied states.

an anomaly given by Eq. (1.1.4). In this case the conservation of chiral charge occurs because the two terms on the r.h.s. of Eq. (1.1.4) cancel for adiabatic fields. For non-adiabatic fields chiral charge will be generated. In this case there is some probability of "hopping" between positive and negative energy states and the initial and final fermion states will differ in chiral charge in agreement with Eq. (1.1.4) [9].

In the above example both left and right handed fermions couple to the gauge field with equal strength. Whenever a right handed particle is created it is accompanied by a left handed hole so fermion number is conserved. However if only the left handed particles couple to the gauge field then only left handed states shift. According to the above discussion we will end up with an antiparticle but now there is no accompanying particle. In this case fermion number is not conserved and the change in fermion number is minus the change in Chern-Simons number in agreement with Eq. (1.2.23).

In the case of chiral fermions the non-conservation of fermion number is independent of the fermion mass (see Eqs. (1.1.6) and (1.1.7)). This appears to

present a problem if the background field is adiabatic, since the existence of the mass gap discussed above prevents level crossing and so fermion number is naively conserved. In fact as emphasised in [12] there is no mass gap since chiral fermions get their mass due to spontaneous symmetry breaking, i.e. from their Yukawa coupling to the Higgs field. Thus, for certain gauge-Higgs configurations, it still may be possible to have a zero eigenvalue. For example it is well known that the  $SU(2)$  sphaleron has a zero eigenvalue [13, 14] though little is known about the existence of zero eigenvalues in more general  $SU(2)$ -Higgs backgrounds. In comparison level crossing in the  $U(1)$ -Higgs theory in  $1+1$  dimensions is relatively well understood. In particular it can be shown [15] that the massless Hamiltonian has a zero eigenvalue if (and only if) the Chern-Simons number is half-integer, while for non-zero Yukawa coupling the zero eigenvalue is displaced from half-integer Chern-Simons number.

## 1.4 Transition Rates

As discussed in Section 1.2 fermion number non-conservation occurs when the gauge fields make a transition between topologically distinct vacua. These vacua are separated by a potential barrier corresponding to the sphaleron configuration (see figure 1.1). Hence at zero temperature the only way that fermion number can be produced is by quantum tunnelling through the barrier [16]. Using standard WKB methods the rate of transitions per unit volume can be calculated and is of the order

$$\Gamma \propto e^{-\frac{4\pi}{\alpha_W}} \quad (1.4.34)$$

The factor in the exponent is the action of the instanton which is a classical solution to the Euclidean equations of motion which interpolates between two neighbouring vacua. Eq. (1.4.34) is so small that it can effectively be ignored.

At finite temperature the rate can be significantly enhanced [18]. At tem-

perature  $T$  the thermal distribution of states is determined by the Boltzmann factor  $e^{-\frac{E}{T}}$ . States with energy  $E > E_{SPH}$  where  $E_{SPH}$  is the barrier height (the sphaleron energy) can overcome the potential barrier classically. The rate of transitions is then just proportional to the number of these states and so we expect

$$\Gamma \propto e^{-\frac{E_{SPH}}{T}} \quad (1.4.35)$$

At temperatures  $T < M_W$  the number of these states is exponentially suppressed and the contribution due to tunneling dominates. On the other hand for  $T \gg M_W$  the main contribution comes from classical motion over the barrier. This allows the rate to be calculated using the semiclassical methods of Langer and Affleck [19]. This method is only valid for  $T \ll E_{SPH}$  (weak coupling). The rate has been calculated in [4] for the  $U(1)$  model in 1+1 dimensions and in [20] for the  $SU(2)$  model in 3+1 dimensions with the results

$$\Gamma = \left( \frac{3E_{SPH}}{\pi T} \right)^{\frac{1}{2}} \frac{\sqrt{M_H^2 M_W}}{4\pi} 2^{\frac{M_W}{M_H} - \frac{3}{4}} e^{-\frac{E_{SPH}}{T}} \quad (1.4.36)$$

for  $U(1)$  in 1+1 dimensions (for  $\lambda \ll g^2$ ) and

$$\Gamma = 0.007 (\alpha_W T)^4 \left( \frac{E_{SPH}(T)}{T} \right) e^{-\frac{E_{SPH}(T)}{T}} \quad (1.4.37)$$

for  $SU(2)$  in 3+1 dimensions (for  $\lambda \sim g^2$ ).

Eqs. (1.4.36) and (1.4.37) for the rates are semiclassical and assume that at high temperatures  $T \gg M_W$  the rate is dominated by classical motion over the top of the barrier. It is assumed that the only quantum effect is in renormalisation of the parameters in the Hamiltonian. It is well known that for the  $SU(2)$  model in 3 + 1 dimensions the renormalised  $W$ -mass is temperature dependent  $M_W = M_W(T)$  [21] and hence the sphaleron energy  $E_{SPH}$  appearing in Eq. (1.4.37) is temperature dependent.

$$E_{sph}(T) = 2 \frac{M_W(T)}{\alpha_W} A \left( \frac{\lambda}{\alpha_W} \right) \quad (1.4.38)$$

Above some critical temperature  $T_C$ ,  $SU(2)$  symmetry is restored, the  $W$  is massless and the sphaleron barrier disappears  $E_{SPH} = 0$ . Hence we expect rapid transitions between topologically distinct vacua. However an exact evaluation of the rate in this region is difficult, since the standard weak coupling methods require  $T \ll E_{SPH}$ . From scaling arguments it is expected to behave as [20]

$$\Gamma = \kappa(\alpha_W T)^4 \quad (1.4.39)$$

where  $\kappa$  is an unknown non-perturbative constant. Estimates of  $\kappa$  using numerical lattice methods give  $\kappa \approx 1$  [5, 6, 7].

## 1.5 Baryogenesis and Cosmology

Experimental evidence suggests that the universe contains far more matter than antimatter. A common measure of this asymmetry is the ratio of the number of baryons to the number of photons.

$$\frac{n_B}{n_\gamma} \approx 10^{-10} - 10^{-9} \quad (1.5.40)$$

Baryogenesis is the creation of this asymmetry from symmetric initial conditions. In 1967 Sakharov showed that any baryogenesis model must satisfy three conditions [17]:

1. Baryon number violation
2. C and CP violation
3. Departure from thermal equilibrium

Initial efforts to explain the asymmetry concentrated on Grand Unified Theories (GUTs) which naturally satisfy all three conditions and can produce results in agreement with Eq. (1.5.40). In such models the baryon asymmetry is created at the GUT symmetry breaking scale (typically  $T \sim 10^{15} GeV$ ).

However the high rate given by Eq. (1.4.39) implies that any B+L asymmetry created above the electroweak phase transition (e.g. at the GUT scale) will be

washed out by rapid electroweak fermion number violating transitions [18]. However since the electroweak theory conserves B-L there still remains the possibility that the current baryon asymmetry is due to a B-L asymmetry created at the GUT scale. This rules out GUTs which conserve B-L (e.g.  $SU(5)$ ).

A more interesting possibility is that the baryon asymmetry was created at the electroweak phase transition (typically  $T \sim 100 GeV$ ). If this is the case then Eq. (1.4.37) provides a constraint on the Higgs mass. If the baryon asymmetry was indeed created at the electroweak phase transition then this asymmetry should survive to the present day. In other words sphaleron processes must come out of equilibrium at the phase transition. Requiring the rate given by Eq. (1.4.37) to be smaller than the expansion rate of the universe at  $T_C$  puts a lower bound on the sphaleron energy which in turn puts an upper bound on the Higgs mass [22]

$$M_H < 45 GeV \quad (1.5.41)$$

to be compared with the LEP bound

$$M_H > 65 GeV \quad (1.5.42)$$

Clearly these bounds are incompatible. This appears to rule out electroweak baryogenesis. However the validity of Eq. (1.5.41) is debatable since it is based on a perturbative treatment of the effective potential. In addition electroweak baryogenesis may still be possible in models with an extended Higgs sector (for a review of electroweak baryogenesis see [23]).

## 1.6 Numerical Simulations

Eqs. (1.4.37) and (1.4.39) for the rate of fermion number violation at finite temperature in the electroweak theory clearly have important consequences for baryogenesis. In particular the high rate of transitions above the electroweak phase transition implies that any baryon asymmetry created above  $T_C$  will be washed

out by electroweak fermion number violation. This will certainly be the case if the coefficient  $\kappa \sim 1$  in Eq. (1.4.39) which is usually assumed. However  $\kappa$  is a non-perturbative constant which has so far only been calculated using numerical lattice simulations [5, 6, 7].

These lattice calculations are based on measuring the change in Chern-Simons number (details will be discussed later in the thesis). From the anomaly fermion number is violated whenever  $\Delta N_{CS} = \pm 1$ . However, on the lattice the measurement of  $\Delta N_{CS}$  is well known to be problematic and it would be useful to have some independent method of checking that fermion number is really violated when  $\Delta N_{CS}$  changes by unity. Fortunately the level crossing picture discussed in Section 1.3 provides just such a method, since  $\Delta N_{CS} = \pm 1$  should be accompanied by fermion eigenvalues crossing zero.

In [24] the lowest eigenvalue was measured for the massless fermion Hamiltonian and shown to dive to zero whenever  $N_{CS}$  changed by one unit. Further evidence that the eigenvalue crosses zero is provided in [25], where the diving of the lowest eigenvalue was shown to be accompanied by a flip in sign of the chirality of the corresponding eigenvector. In addition it was found that level crossing occurs not just for massless fermions but also in the presence of Yukawa interactions. The work described in this thesis is an attempt to provide further evidence for level crossing in lattice simulations.

The method of [25] is based on identifying the chirality of the lattice eigenmodes. However the validity of this method is not obvious. Chirality is not a good label for the eigenmodes since lattice regularisation inevitably breaks chiral symmetry. With this problem in mind we introduce an independent method for investigating the level crossing picture based on solving the time-dependent Dirac equation. In this way we can check directly the time development of the eigenvectors without relying on the measurement of chirality.

As well as the  $SU(2)$  model in  $3 + 1$  dimensions we have also studied the  $U(1)$  model in  $1 + 1$  dimensions. We have studied this model for two main reasons.

Firstly we have a greater analytic understanding of level crossing in this model than in the  $SU(2)$  model. In addition the lower number of dimensions allows us to use larger lattices.

The  $U(1)$  model is discussed in Chapters 2 and 3, while Chapters 4 and 5 deal with the  $SU(2)$  model. For each model fermion number non-conservation is studied firstly by measuring the Chern-Simons number of the gauge field. The level crossing picture is then investigated using the methods of [25] and also by using the Dirac equation as discussed above. Our results are summarised in Chapter 6.

# Chapter 2

## U(1) Model in 1+1 Dimensions

### 2.1 Introduction

In this chapter we discuss the standard numerical method of investigating finite temperature fermion number violation, the real-time microcanonical method, and apply it to the  $U(1)$  theory in 1+1 dimensions. The microcanonical method and its motivation are described in Section 2.2. Section 2.3 describes the discretisation of the  $U(1)$  system and its equations of motion. Details of the numerical procedure, in particular the creation of initial field configurations, are discussed in Section 2.4. Section 2.5 discusses constraints upon our choice of coupling constants. In the final section results are presented for measurements of the Chern-Simons number and the Higgs topology. The methods and notation of [26] are used throughout this chapter.

### 2.2 The Microcanonical Method

The real time microcanonical method was introduced in [27] where it was applied to the process of kink-antikink pair creation in  $\lambda\phi^4$  theory. The method is motivated by the observation that the elementary excitations which combine to

form the sphaleron obey classical statistical mechanics. To see this recall that the sphaleron is an extended object with radius  $r_{SPH} \sim M_W^{-1}$ . The typical momentum of an elementary sphaleron excitation is thus  $k_{ex} \sim r_{SPH}^{-1} \sim M_W$ . The energy of an individual excitation is then

$$E_{ex} = \sqrt{k_{ex}^2 + M_W^2} \approx \sqrt{2}M_W \quad (2.2.1)$$

Now the rate formulae Eqs. (1.4.36) and (1.4.37) are valid for  $T \gg M_W$  so that  $E_{ex} \ll T$  and hence the excitations relevant for the formation of sphalerons obey classical statistics. In the  $SU(2)$  theory the symmetry is restored at  $T > T_C$  and the sphaleron loses its role as the dominant configuration for fermion number violation. Above  $T_C$  it is expected that the configurations responsible for fermion number violation have radius of order the inverse magnetic screening mass  $\sim (\alpha_W T)^{-1}$ . Hence again we have  $E_{ex} \ll T$  (for small  $\alpha_W$ ).

The above discussion suggests that sphaleron formation is well described by classical statistical mechanics provided  $T \gg M_W$ , i.e. in the region where the analytic rate formulae are valid. However classical statistics are ill-defined for systems with an infinite number of degrees of freedom due to the Rayleigh-Jeans divergence. According to the classical theorem of equipartition of energy the total energy of a system with  $N_d$  degrees of freedom is

$$\langle H \rangle = \frac{1}{2}N_d T \quad (2.2.2)$$

which is infinite in the limit  $N_d \rightarrow \infty$ . Of course in any numerical simulation  $N_d$  is necessarily finite. In our simulations we put the system on a spatial lattice with lattice spacing  $a$ . The lattice spacing provides an ultraviolet cut-off  $k_{max} \sim \frac{1}{a}$ . In the case of the full quantum theory modes with momentum  $k > T$  give a negligible contribution to the total energy. Thus the lattice spacing mimics the effect of quantum mechanics on the high energy modes if we set

$$T \approx \frac{1}{a} \quad (2.2.3)$$

The classical approximation suggests the following technique for studying fermion number violation at high temperature. We consider a classical gauge-Higgs system with coordinates  $A, \phi$  and conjugate momenta  $E, P$  (as mentioned above in practice these are defined on a spatial lattice). The probability of any particular state at temperature  $T$  is then dictated by the Boltzmann factor  $e^{-\frac{H}{T}}$ . We pick an initial configuration according to this statistical weight using some Monte Carlo method (see Appendix B). We then allow the system to evolve according to the classical equations of motion. During the time evolution we measure the Chern-Simons number  $N_{CS}$ . From Eq. (1.2.23) fermion number is violated whenever the Chern-Simons number changes by one unit. After letting the system evolve for a sufficiently large time  $t$ , we can then estimate the transition rate  $\Gamma$  by one of two methods.

Firstly we can use the fact that, if the volume  $V$  is not too large, we expect that the fluctuations of  $N_{CS}$  about a given vacuum sector will be small compared to one. Furthermore if the temperature is also not too large we expect transitions with  $\Delta N_{CS} = 1$  to be rare. Hence we expect the measurement of  $N_{CS}$  to consist of plateaus with small fluctuations about a given  $N_{CS}$  and occasional rapid transitions between plateaus. The rate  $\Gamma V$  is then just the inverse of the average plateau time. The estimation of the rate given in [26] using this method agrees with the analytic formula Eq. (1.4.36).

Alternatively we can consider the quantity  $Q(t) = N_{CS}(t) - N_{CS}(0)$  to be the analogue of the coordinate of a Brownian particle jumping between different vacua [28]. We then expect that at large  $t$

$$\langle Q^2(t) \rangle = \Gamma V t \quad (2.2.4)$$

where  $\langle \dots \rangle$  denotes the thermal average over initial field configurations. This formula has been used to calculate the rate in several simulations [29, 30, 31] and again agreement with Eq. (1.4.36) has been found.

## 2.3 Lattice Gauge-Higgs System

The continuum action of the Abelian Higgs model in 1 + 1 dimensions is

$$S = \int dt dx \left[ -\frac{1}{4} F^{\mu\nu} F_{\mu\nu} + (D^\mu \phi)^* (D_\mu \phi) - \frac{1}{4} \lambda (|\phi|^2 - v^2)^2 \right] \quad (2.3.5)$$

where  $D_\mu = \partial_\mu - igA_\mu$  and  $F_{\mu\nu} = \partial_\mu A_\nu - \partial_\nu A_\mu$ . Due to the Higgs mechanism the gauge boson acquires a mass

$$M_W = \sqrt{2}gv \quad (2.3.6)$$

In Eq. (2.3.5)  $A_\mu$ ,  $\phi$  and  $v$  are dimensionless, while the coupling constants  $g$  and  $\lambda$  have dimensions  $[Mass]$  and  $[Mass]^2$  respectively. Following [26] we rewrite Eq. (2.3.5) in terms of dimensionless variables

$$\begin{aligned} \tau &= (gv)t, & y &= (gv)x, \\ \tilde{A}_\mu &= \frac{A_\mu}{v}, & \tilde{\phi} &= \frac{\phi}{v}, & \tilde{\lambda} &= \frac{\lambda}{g^2} \end{aligned} \quad (2.3.7)$$

so that Eq.(2.3.5) becomes

$$S = v^2 \int d\tau dy \left[ -\frac{1}{4} \tilde{F}^{\mu\nu} \tilde{F}_{\mu\nu} + (\tilde{D}^\mu \tilde{\phi})^* (\tilde{D}_\mu \tilde{\phi}) - \frac{1}{4} \tilde{\lambda} (|\tilde{\phi}|^2 - 1)^2 \right] \quad (2.3.8)$$

where  $\tilde{D}_\mu = \partial_\mu - i\tilde{A}_\mu$  and  $\tilde{F}_{\mu\nu} = \partial_\mu \tilde{A}_\nu - \partial_\nu \tilde{A}_\mu$ .

We put this system on a space-time lattice with lattice spacing  $a$  in the spatial direction and  $a_t$  in the temporal direction (for a brief discussion of lattice gauge theories see Appendix A).

$$\begin{aligned} S &= v^2 \sum_j aa_t \left[ \frac{1}{(aa_t)^2} (1 - \text{Re}U_\square) + \frac{2}{a_t^2} (\phi_j^* \phi_j - \text{Re}(\phi_{j+\hat{0}}^* e^{ia_t A_j^0} \phi_j)) \right. \\ &\quad \left. - \frac{2}{a^2} (\phi_j^* \phi_j - \text{Re}(\phi_{j+\hat{i}}^* e^{ia A_j^1} \phi_j)) - \frac{1}{4} \tilde{\lambda} (\phi_j^* \phi_j - 1)^2 \right] \end{aligned} \quad (2.3.9)$$

where  $\hat{1}$  and  $\hat{0}$  are spatial and time-like directions respectively. The Higgs field  $\phi_j$  sits on lattice sites. The temporal component of the vector potential  $A_j^0$  sits on

the link connecting  $j$  and  $j + \hat{0}$  while the spatial component  $A_j^1$  sits on the link connecting  $j$  and  $j + \hat{1}$ .  $U_\square$  is the product of links around an elementary plaquette.

$$\begin{aligned} U_\square &= U_{j,\hat{1}} U_{j+\hat{1},\hat{0}} U_{j+\hat{0},\hat{1}}^* U_{j,\hat{0}}^* \\ U_{j,\hat{0}} &= e^{ia_t A_j^0}, \quad U_{j,\hat{1}} = e^{ia A_j^1} \end{aligned} \quad (2.3.10)$$

Note that Eq. (2.3.9) is written in terms of the dimensionless quantities introduced in Eq. (2.3.7). In particular the lattice spacings  $a$  and  $a_t$  are in units of  $\frac{1}{gv}$ .

In the following we choose the temporal gauge  $A_j^0 = 0$ . The equations of motion follow by the principle of least action. Defining the momenta fields as

$$\begin{aligned} E_j &= a \frac{dA_j^1}{dt} \\ P_j &= a \frac{d\phi_j}{dt} \end{aligned} \quad (2.3.11)$$

in the limit  $a_t \rightarrow 0$  we find the equations of motion

$$\begin{aligned} \frac{dE_j}{dt} &= 2\text{Im} \left( \phi_{j+1} e^{-ia A_j^1} \phi_j^* \right) \\ \frac{dP_j}{dt} &= \frac{1}{a} \left( e^{-ia A_j^1} \phi_{j+1} + e^{ia A_{j-1}^1} \phi_j - 2\phi_j \right) - \frac{1}{2} \tilde{\lambda} a \phi_j \left( |\phi_j|^2 - 1 \right) \end{aligned} \quad (2.3.12)$$

and the Gauss constraint

$$\Delta_j = \frac{1}{a} (E_j - E_{j-1}) + 2\text{Im} (P_j^* \phi_j) = 0 \quad (2.3.13)$$

which is a constant of the motion.

The Hamiltonian is found by taking the  $a_t \rightarrow 0$  limit of Eq. (2.3.9) and writing in the form

$$S = \int dt (E_K - E_P) \quad (2.3.14)$$

where  $E_P$  is the kinetic energy and  $E_K$  is the potential energy. We can then define a Hamiltonian  $H = E_K + E_P$ .

$$\frac{H}{gv^3} = \sum_{j=1}^n a \left[ \frac{1}{2} \left( \frac{E_j}{a} \right)^2 + \left| \frac{P_j}{a} \right|^2 + \left| \frac{\phi_{j+1} - e^{ia A_j^1} \phi_j}{a} \right|^2 + \frac{1}{4} \tilde{\lambda} \left( |\phi_j|^2 - 1 \right)^2 \right] \quad (2.3.15)$$

where  $n$  is the spatial size of the lattice.

## 2.4 Numerical Procedure

The first step in the the numerical procedure is to create a typical equilibrium field configuration at the temperature of interest  $T$ . A simple method is the Metropolis procedure. The problem with this method is that the coordinates  $A_j^1, \phi_j$  and momenta  $E_j, P_j$  are not all independent, since they must satisfy the Gauss constraint, Eq. (2.3.13). If we independently update all the fields and momenta according to the standard Metropolis procedure, then the Gauss constraint will in general not be satisfied. To control this violation of the constraint we use a modified Metropolis procedure in which the Hamiltonian  $H$  is replaced by

$$H' = H + G \sum_{j=1}^n \Delta_j^2 \quad (2.4.16)$$

The larger  $G$  the smaller  $\Delta_j$  and in the limit  $G \rightarrow \infty$  the constraint is exactly satisfied. In practice the use of a finite value of  $G$  means that the constraint will be violated by a small amount after thermalisation. To further reduce the value of  $\Delta_j$  we apply the following "cooling" equations

$$\begin{aligned} \frac{\partial E_j}{\partial t} &= -\frac{\partial}{\partial E_j} \sum_{j=1}^n \Delta_j^2 \\ \frac{\partial \phi_j}{\partial t} &= -\frac{\partial}{\partial \phi_j^*} \sum_{j=1}^n \Delta_j^2 \\ \frac{\partial P_j}{\partial t} &= -\frac{\partial}{\partial P_j^*} \sum_{j=1}^n \Delta_j^2 \end{aligned} \quad (2.4.17)$$

where  $t$  is the cooling "time". These are the Langevin equations [33] without the noise term. In this way we can enforce the Gauss constraint to any desired accuracy. We use a first order discretisation method with discrete time step  $\Delta t = 0.05$  and 1000 cooling sweeps.

Thermalisation is achieved by 5000 Metropolis sweeps through the lattice with 5 hits per site/link in every sweep. The average energy after Metropolis agrees well with that predicted by the classical equipartition theorem

$$\langle H \rangle = \frac{1}{2} N_d T \quad (2.4.18)$$

where  $N_d$  is the number of degrees of freedom (4 per site in this case). The cooling equations, Eq. (2.4.17), have little effect on the energy.

Having obtained an initial configuration in this way we allow the system to evolve in time by numerically solving the Hamiltonian equations of motion, Eqs. (2.3.11) and (2.3.12). We use a first order discretisation method with a discrete time step  $a_t = 0.05$ . The energy is found to be well conserved, as is the Gauss constraint.

## 2.5 Choice of Parameters

In calculating the transition rate for the  $U(1)$  model in 1+1 dimensions, Bochkarev and Shaposnikov [4] worked in the approximation  $\lambda \ll g^2$  or in terms of the dimensionless units used in our simulations (see Eq. (2.3.7))  $\tilde{\lambda} \ll 1$ . In accordance with [26] we thus chose  $\tilde{\lambda} = 0.5$ .

Since the sphaleron radius is  $\sim \frac{1}{M_w}$  ( $\sim 1$  in units of  $gv$ ) we require

$$2a \leq 1 \leq \frac{na}{4} \quad (2.5.19)$$

to ensure that errors due to finite length and finite lattice spacing are negligible. As shown in [26] the choice  $a = 0.2$  and  $n = 200$  is reasonable.

Finally, the rate equation Eq. (1.4.36) is only valid for  $T \ll E_{SPH}$ . Following [26] we chose  $\frac{E_{SPH}}{T} = 10$  (or  $\frac{T}{gv^3} = 0.094$ ). In addition to satisfying the above condition this ensures that the rate is high enough that we can observe sphaleron transitions in our simulations.

## 2.6 Topological Measurements

The main quantity of interest during the time evolution is the Chern-Simons number. In the continuum it is given by

$$N_{CS} = \frac{g}{2\pi} \int dx A^1 \quad (2.6.20)$$

On the lattice Eq. (2.6.20) becomes

$$N_{CS} = \frac{1}{2\pi} \sum_{j=1}^n a A_j^1 \quad (2.6.21)$$

This shares all the properties of the continuum expression. It is an integer for pure gauge (vacuum) configurations. It is invariant under small gauge transformations and changes by an integer under large gauge transformations. Figure 2.1 shows a typical measurement of the Chern-Simons number during the time evolution.  $N_{CS}$  spends most of the time fluctuating around integer values with occasional rapid transitions between integer values. From Eq. (1.2.23) these rapid transitions correspond to fermion number non-conservation. A close up of a particular sphaleron transition is shown in figure 2.2.

We have also investigated the topology of the Higgs field during the sphaleron transition shown in figure 2.2. As discussed in Section 1.2 a winding number can be defined for the Higgs field  $N_H$ . This measures the number of times the Higgs field winds clockwise round the complex plane as  $x$  goes from 0 to  $L$ .  $N_H$  can thus be measured "by eye" by plotting  $\phi_j$  in the complex plane. In practice  $N_H$  is quite large (note  $N_{CS} \sim 8-9$ ) and  $N_H$  difficult to measure. We can reduce  $N_H$  by performing a large gauge transformation  $\phi_j \rightarrow e^{i\theta_j} \phi_j$ . This is compatible with the temporal gauge condition  $A_0 = 0$  provided that  $\theta_j$  is time independent. We chose  $\theta_j$  such that  $\phi_j(t_0) \rightarrow |\phi_j(t_0)|$  at some time  $t_0$  just before the sphaleron transition (we choose  $t_0 = 2000$ ). This ensures that  $N_H$  is zero just before the transition. The behaviour of the (gauge transformed) Higgs field is shown in figure 2.3. As the system evolves  $N_H$  changes from 0 to 1. As discussed in Section 1.2 the Higgs field must cross zero at some point in the process. This is clearly shown with figure 2.3(b) showing the point at which  $\phi$  crosses zero. We find the Higgs field has a zero at  $t_h = 2137.2$ . It is interesting to compare this to the time at which the Chern-Simons number is half-integer  $t_{CS} = 2139.8$ . Thus in this particular case  $t_h < t_{CS}$ . The high temperature Higgs field winds before the gauge field. This is in contrast to the sphaleron which has  $N_{CS} = \frac{1}{2}$  and  $\phi(0) = 0$ .

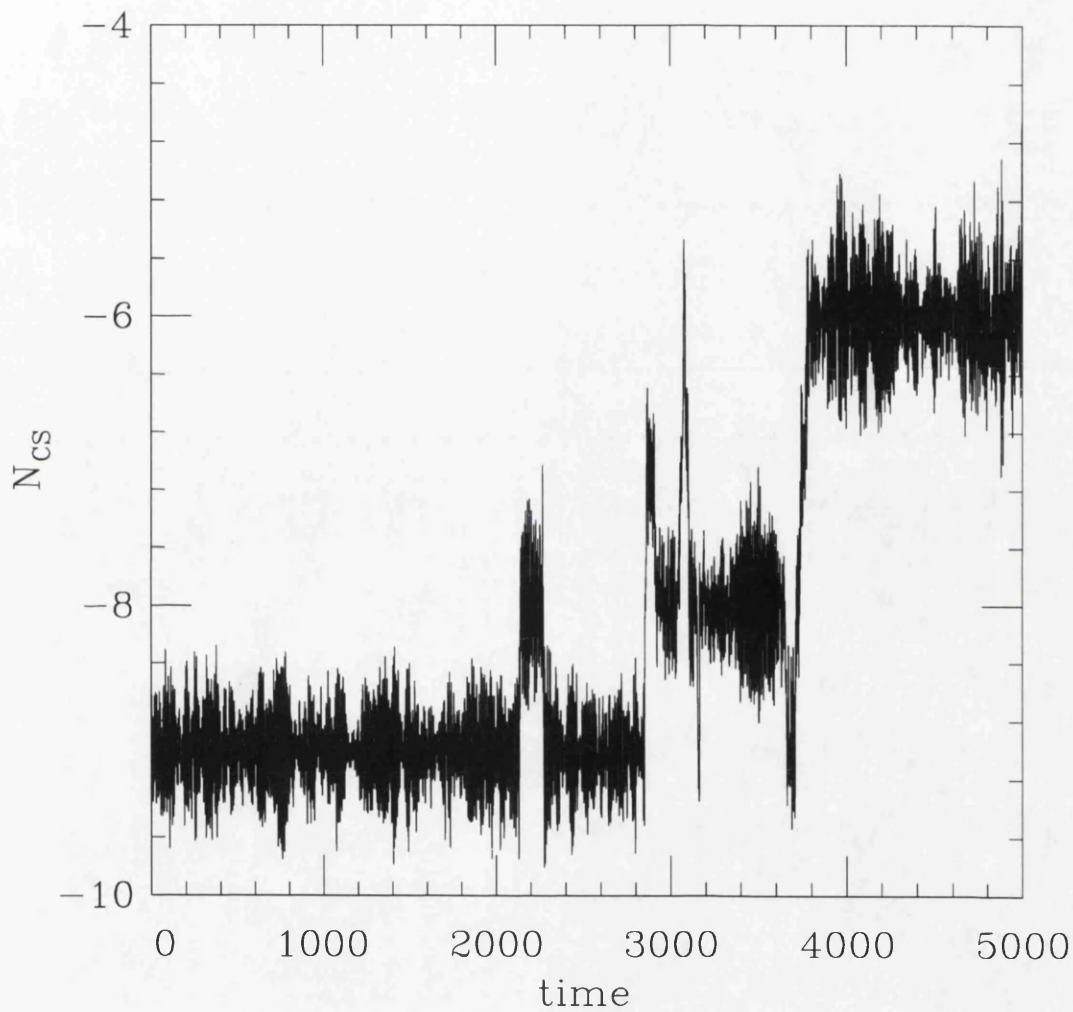


Figure 2.1: The Chern-Simons number as a function of time for  $\tilde{\lambda} = 0.5$ ,  $a = 0.2$ ,  $\frac{T}{gv^3} = 0.095$ . The lattice size is  $n = 200$ .

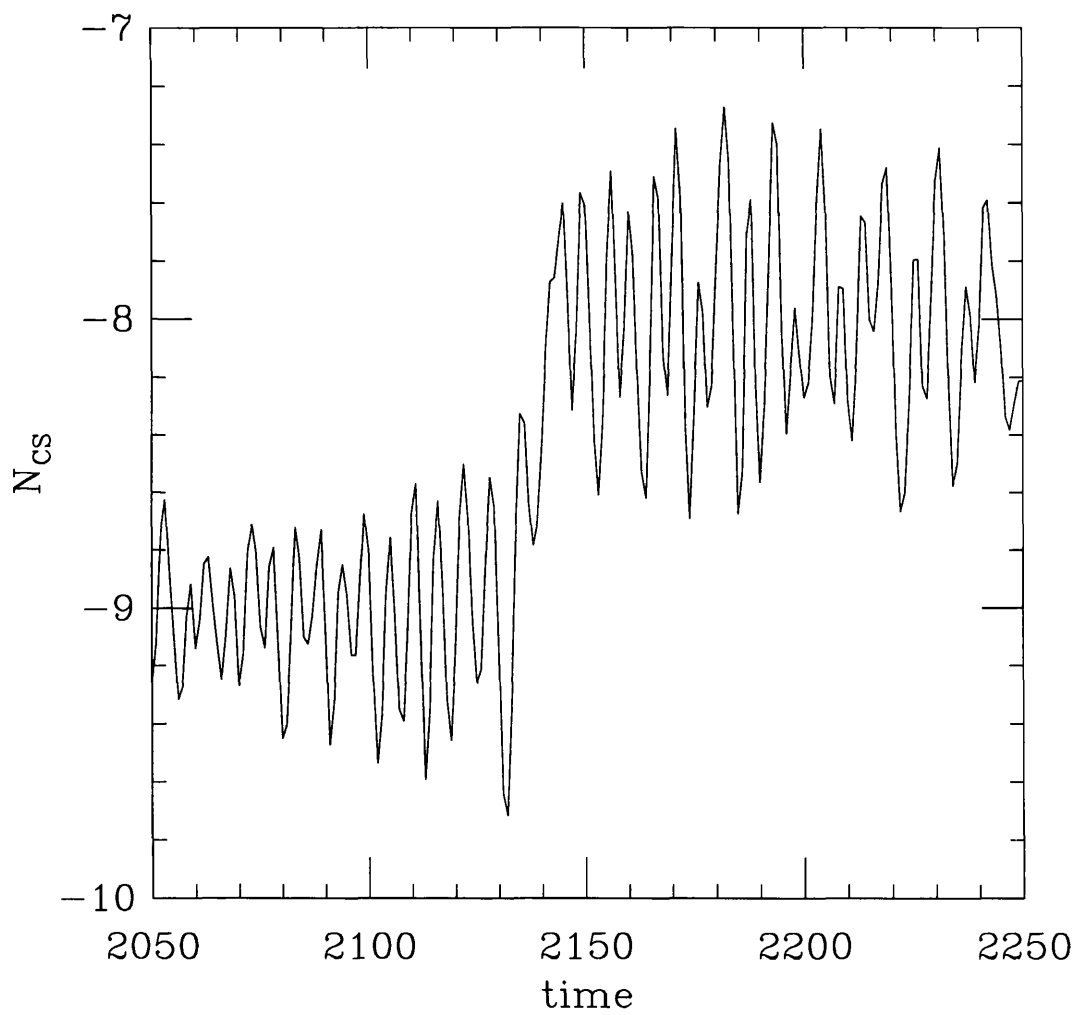


Figure 2.2: The Chern-Simons Number as a function of time for a typical sphaleron transition.

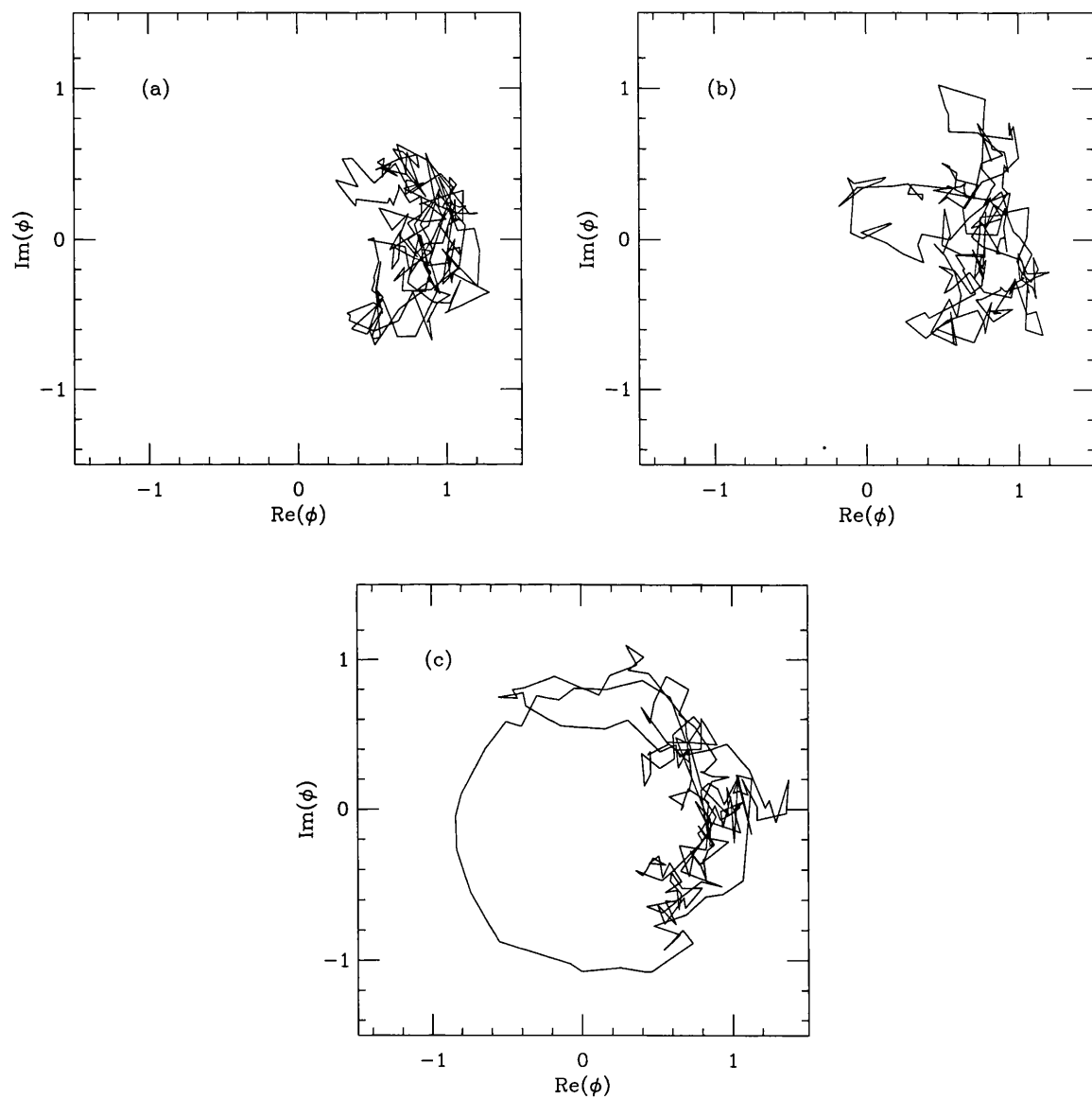


Figure 2.3: The Higgs field during a typical sphaleron transition. (a):  $t = 2100$ ,  $N_H = 0$ . (b):  $t = 2137.2$ ,  $\phi$  crosses zero. (c):  $t = 2200$ ,  $N_H = 1$ .

# Chapter 3

## Level Crossing in $U(1)$ Model in 1+1 Dimensions

### 3.1 Introduction

In the previous chapter fermion number non-conservation was investigated by following the time development of the Chern-Simons number of the  $U(1)$  gauge field. Fermion number should be violated whenever  $N_{CS}$  changes by one unit. As discussed in Section 1.6 an alternative approach is to measure the eigenvalues of the Dirac Hamiltonian. According to the level crossing picture, transitions for which  $N_{CS}$  changes by one unit should be accompanied by the lowest fermion eigenvalue crossing zero. In this Chapter we attempt to verify this picture on the lattice.

In Section 3.2 we describe how to put the Dirac Hamiltonian on the lattice and discuss the fermion doubling problem. By constructing the continuum wavefunctions we show how chirality can be defined on the lattice. In Section 3.3 we present results for the lowest energy eigenvalue and chirality both for "smooth" and high temperature background fields. Section 3.4 describes how level crossing can be checked by solving the time-dependent Dirac equation and Section 3.5

gives results using this method.

## 3.2 Lattice Eigenvalue Equations

The continuum time-independent Dirac equation for a free particle in 1+1 dimensions is

$$\left(-i\alpha\frac{d}{dx} + \beta m\right)\psi = E\psi \quad (3.2.1)$$

where the hermitian Dirac matrices  $\alpha, \beta$  satisfy

$$\{\alpha, \beta\} = 0, \quad \alpha^2 = \beta^2 = 1 \quad (3.2.2)$$

In 1+1 dimensions these relations can be satisfied by 2 by 2 matrices. One specific representation is

$$\alpha = \begin{pmatrix} 1 & 0 \\ 0 & -1 \end{pmatrix}, \quad \beta = \begin{pmatrix} 0 & 1 \\ 1 & 0 \end{pmatrix} \quad (3.2.3)$$

In this representation the upper component of  $\psi$  has chirality +1 and is denoted  $\psi^R$  (right mover) while the lower component has chirality -1 and is denoted  $\psi^L$  (left mover).

$$\begin{aligned} -i\frac{d\psi^R}{dx} + m\psi^L &= E\psi^R \\ i\frac{d\psi^L}{dx} + m\psi^R &= E\psi^L \end{aligned} \quad (3.2.4)$$

We put Eq. (3.2.4) on the lattice in the obvious way by replacing derivatives with centralised differences.

$$\begin{aligned} \frac{-i}{2a}(\chi_{j+1}^1 - \chi_{j-1}^1) + m\chi_j^2 &= E\chi_j^1 \\ \frac{i}{2a}(\chi_{j+1}^2 - \chi_{j-1}^2) + m\chi_j^1 &= E\chi_j^2 \end{aligned} \quad (3.2.5)$$

where  $a$  is the lattice spacing. Naively Eq. (3.2.5) approaches Eq. (3.2.4) in the continuum limit  $a \rightarrow 0$  if we identify  $\chi^1$  with  $\psi^R$  and  $\chi^2$  with  $\psi^L$ . However it

is well known that in the limit as  $a \rightarrow 0$  Eq. (3.2.5) actually gives two copies of Eq. (3.2.4). This is the famous "doubling problem". To see how it arises note that the continuum energy eigenvalues  $E$  are given by

$$E^2 = k^2 + m^2 \quad (3.2.6)$$

while the lattice eigenvalues are given by

$$E^2 = \frac{1}{a^2} \sin^2(ak) + m^2 \quad (3.2.7)$$

The lattice spacing  $a$  provides a momentum cutoff, so that the momenta  $k$  are restricted to the first Brillouin zone

$$-\frac{\pi}{a} < k \leq \frac{\pi}{a} \quad (3.2.8)$$

It is easy to see that as  $a \rightarrow 0$  for fixed  $k$ , Eq. (3.2.7) approaches the continuum expression Eq. (3.2.6). However for finite  $a$  there is an extra degeneracy of fermion states since  $\sin(ka + \pi) = -\sin(ka)$ .

One way of dealing with the doubling problem is to modify the Hamiltonian by the addition of a term which vanishes in the continuum limit but which breaks the degeneracy, by giving the additional states a mass of the order of the cutoff  $\frac{1}{a}$ . This is the Wilson method [34]. An alternative approach is to accept the additional states and interpret Eq. (3.2.5) as describing two fermion "flavours" with common mass  $m$ . This is the staggered fermion method [35] and is the one adopted in this thesis.

For this to be the case we require Eq. (3.2.5) to give two copies of Eqs. (3.2.4) in the continuum limit, one for each of the two flavours. We do this by splitting the  $\chi$  fields according to whether they sit on odd or even sites. From each  $\chi$  field we construct two fields  $\chi^{odd}, \chi^{even}$  as follows

$$\begin{aligned} \chi_j^{odd} &= \chi_{2j-1} \\ \chi_j^{even} &= \chi_{2j} \end{aligned} \quad (3.2.9)$$

Rewriting Eq. (3.2.5) in terms of these two fields gives

$$\begin{aligned}
\frac{-i}{2a} \left( \chi_j^{1,even} - \chi_{j-1}^{1,even} \right) + m \chi_j^{2,odd} &= E \chi_j^{1,odd} \\
\frac{-i}{2a} \left( \chi_{j+1}^{1,odd} - \chi_j^{1,odd} \right) + m \chi_j^{2,even} &= E \chi_j^{1,even} \\
\frac{i}{2a} \left( \chi_j^{2,even} - \chi_{j-1}^{2,even} \right) + m \chi_j^{1,odd} &= E \chi_j^{2,odd} \\
\frac{i}{2a} \left( \chi_{j+1}^{2,odd} - \chi_j^{2,odd} \right) + m \chi_j^{1,even} &= E \chi_j^{2,even}
\end{aligned} \tag{3.2.10}$$

The fields  $\chi^{odd}, \chi^{even}$  sit on a lattice with lattice spacing  $2a$ . First and second central derivatives on this lattice are given by

$$\begin{aligned}
\frac{d\chi_j}{dx} &= \frac{1}{4a} (\chi_{j+1} - \chi_{j-1}) \\
\frac{d^2\chi_j}{dx^2} &= \frac{1}{4a^2} (\chi_{j+1} + \chi_{j-1} - 2\chi_j)
\end{aligned} \tag{3.2.11}$$

In terms of these lattice derivatives we can then rewrite Eq. (3.2.10) as

$$\begin{aligned}
-i \left( \frac{d\chi_j^{1,even}}{dx} - a \frac{d^2\chi_j^{1,even}}{dx^2} \right) + m \chi_j^{2,odd} &= E \chi_j^{1,odd} \\
-i \left( \frac{d\chi_j^{1,odd}}{dx} + a \frac{d^2\chi_j^{1,odd}}{dx^2} \right) + m \chi_j^{2,even} &= E \chi_j^{1,even} \\
i \left( \frac{d\chi_j^{2,even}}{dx} - a \frac{d^2\chi_j^{2,even}}{dx^2} \right) + m \chi_j^{1,odd} &= E \chi_j^{2,odd} \\
i \left( \frac{d\chi_j^{2,odd}}{dx} + a \frac{d^2\chi_j^{2,odd}}{dx^2} \right) + m \chi_j^{1,even} &= E \chi_j^{2,even}
\end{aligned} \tag{3.2.12}$$

Finally we define new fermion fields as linear combinations of the  $\chi$  fields.

$$\begin{aligned}
\psi_j^{1,R} &= \frac{1}{2} (\chi_j^{1,odd} + \chi_j^{1,even}) \\
\psi_j^{1,L} &= \frac{1}{2} (\chi_j^{2,odd} + \chi_j^{2,even}) \\
\psi_j^{2,R} &= \frac{1}{2} (\chi_j^{2,odd} - \chi_j^{2,even}) \\
\psi_j^{2,L} &= \frac{1}{2} (\chi_j^{1,odd} - \chi_j^{1,even})
\end{aligned} \tag{3.2.13}$$

Eq. (3.2.12) can be rewritten in terms of these fields.

$$\begin{aligned}
-i \left( \frac{d\psi_j^{1,R}}{dx} + a \frac{d^2\psi_j^{2,L}}{dx^2} \right) + m\psi_j^{1,L} &= E\psi_j^{1,R} \\
i \left( \frac{d\psi_j^{1,L}}{dx} + a \frac{d^2\psi_j^{2,R}}{dx^2} \right) + m\psi_j^{1,R} &= E\psi_j^{1,L} \\
-i \left( \frac{d\psi_j^{2,R}}{dx} + a \frac{d^2\psi_j^{1,L}}{dx^2} \right) + m\psi_j^{2,L} &= E\psi_j^{2,R} \\
i \left( \frac{d\psi_j^{2,L}}{dx} + a \frac{d^2\psi_j^{1,R}}{dx^2} \right) + m\psi_j^{2,R} &= E\psi_j^{2,L}
\end{aligned} \tag{3.2.14}$$

These are just the "naive" equations for two free fermions  $(\psi^1, \psi^2)$  on a lattice with lattice spacing  $2a$ , but with an extra term of order  $a$  which lifts the degeneracy of the naive Hamiltonian.

For the purposes of our numerical calculations we rewrite Eq. (3.2.5) in terms of dimensionless variables by rescaling the  $\chi$  fields, energy  $E$ , and mass  $m$  according to

$$\chi^{1,2} \rightarrow \frac{1}{a^{1/2}}\chi^{1,2}, \quad E \rightarrow \frac{1}{a}E, \quad m \rightarrow \frac{1}{a}m \tag{3.2.15}$$

so that Eq. (3.2.5) becomes

$$\begin{aligned}
\frac{-i}{2} (\chi_{j+1}^1 - \chi_{j-1}^1) + m\chi_j^2 &= E\chi_j^1 \\
\frac{i}{2} (\chi_{j+1}^2 - \chi_{j-1}^2) + m\chi_j^1 &= E\chi_j^2
\end{aligned} \tag{3.2.16}$$

With this normalisation the total chirality on the lattice is

$$\langle \Gamma_5 \rangle = \sum_{j=1}^{N/2} \left( \psi_j^{\dagger,1,R} \psi_j^{1,R} - \psi_j^{\dagger,1,L} \psi_j^{1,L} + \psi_j^{\dagger,2,R} \psi_j^{2,R} - \psi_j^{\dagger,2,L} \psi_j^{2,L} \right) \tag{3.2.17}$$

Using Eq. (3.2.13) this can be expressed in terms of  $\chi^1, \chi^2$

$$\langle \Gamma_5 \rangle = \sum_{j=1}^N \text{Re} \left( \chi_j^{\dagger 1} \chi_{j+1}^1 - \chi_j^{\dagger 2} \chi_{j+1}^2 \right) \tag{3.2.18}$$

$\chi^1, \chi^2$  can be coupled to the gauge field  $A_j^1$  in the usual gauge invariant way

$$\begin{aligned}
\frac{-i}{2} \left( e^{iaA_j^1} \chi_{j+1}^1 - e^{-iaA_{j-1}^1} \chi_{j-1}^1 \right) + m\chi_j^2 &= E\chi_j^1 \\
\frac{i}{2} \left( e^{iaA_j^1} \chi_{j+1}^2 - e^{-iaA_{j-1}^1} \chi_{j-1}^2 \right) + m\chi_j^1 &= E\chi_j^2
\end{aligned} \tag{3.2.19}$$

As in the free particle case Eq. (3.2.19) actually describes 2 Dirac fermions in the continuum limit. The chirality is modified to

$$\langle \Gamma_5 \rangle = \sum_{j=1}^N \text{Re} \left( \chi_j^{\dagger 1} e^{iaA_j^1} \chi_{j+1}^1 - \chi_j^{\dagger 2} e^{iaA_j^1} \chi_{j+1}^2 \right) \quad (3.2.20)$$

The presence of the link variable  $e^{iaA_j^1}$  between  $\chi_j$  and  $\chi_{j+1}$  ensures that this definition is gauge invariant.

Of particular interest is the massless case. For  $m = 0$  the two components  $\chi^1, \chi^2$  decouple and we can keep only the  $\chi^1$  component.

$$\frac{-i}{2} \left( e^{iaA_j^1} \chi_{j+1}^1 - e^{-iaA_{j-1}^1} \chi_{j-1}^1 \right) = E \chi_j^1 \quad (3.2.21)$$

Since the number of degrees of freedom per site has been reduced from 2 to 1, Eq. (3.2.21) describes a pair of Weyl fermions  $\psi^R, \psi^L$  in the continuum limit. Eq. (3.2.20) for the chirality becomes

$$\langle \Gamma_5 \rangle = \sum_{j=1}^N \text{Re} \left( \chi_j^{\dagger 1} e^{iaA_j^1} \chi_{j+1}^1 \right) \quad (3.2.22)$$

In the continuum  $\Gamma_5$  commutes with the massless Hamiltonian and  $\Gamma_5$  is a good quantum number ( $\psi^R$  has  $\Gamma_5 = +1$  and  $\psi^L$  has  $\Gamma_5 = -1$ ). On the lattice the additional term of order  $a$  (see Eq. (3.2.14)) breaks the chiral symmetry. Thus for finite  $a$ ,  $\Gamma_5 \neq \pm 1$ . Although  $\Gamma_5$  is classically conserved (in the continuum), this conservation law is broken by the chiral anomaly.

$$\Delta \Gamma_5 = -2\Delta N_{CS} \quad (3.2.23)$$

In the next section we will attempt to verify Eq. (3.2.23) by observing the level crossing of energy levels.

Alternatively we can attempt to construct a chiral theory by coupling only  $\chi^1$  to the gauge field. This forbids an explicit mass term, if we want the spectrum to be gauge invariant. As in the continuum we introduce a mass via Yukawa coupling to the Higgs field.

$$\begin{aligned}
\frac{-i}{2} \left( e^{iaA_j^1} \chi_{j+1}^1 - e^{-iaA_{j-1}^1} \chi_{j-1}^1 \right) + h\phi_j^* \chi_j^2 &= E\chi_j^1 \\
\frac{i}{2} \left( \chi_{j+1}^2 - \chi_{j-1}^2 \right) + h\phi_j \chi_j^1 &= E\chi_j^2
\end{aligned} \tag{3.2.24}$$

$h$  is the Yukawa coupling. Since only  $\chi^1$  couples to the gauge field the chirality is modified to

$$\langle \Gamma_5 \rangle = \sum_{j=1}^N \text{Re} \left( \chi_j^{\dagger 1} e^{iaA_j^1} \chi_{j+1}^1 - \chi_j^{\dagger 2} \chi_{j+1}^2 \right) \tag{3.2.25}$$

Again there is a doubling of states so that Eq. (3.2.24) describes 2 flavours of fermions with common Yukawa coupling  $h$ . In the continuum limit Eq. (3.2.24) can be written

$$\begin{pmatrix} -i\alpha(\partial_x + iA) & \beta h\phi^* \\ \beta h\phi & -i\alpha\partial_x \end{pmatrix} \Psi = E\Psi \tag{3.2.26}$$

$\Psi$  is a four component spinor,  $\Psi = \begin{pmatrix} \psi \\ \chi \end{pmatrix}$  where  $\psi = \begin{pmatrix} \psi^{1,R} \\ \psi^{2,L} \end{pmatrix}$ ,  $\chi = \begin{pmatrix} \psi^{2,R} \\ \psi^{1,L} \end{pmatrix}$ .

Note that the two different flavours  $\psi^1, \psi^2$  couple differently to the gauge field. For one of the fermions ( $\psi^1$ ) only the right moving component couples to  $A^1$  as expected from the naive continuum limit of Eq. (3.2.24). On the other hand, for the second fermion ( $\psi^2$ ) only the left moving component couples to  $A^1$ . As discussed in Section 1.1 the  $U(1)$  theory with a single right moving particle has a gauge anomaly which must be cancelled by adding extra fermions with charges satisfying  $\sum q_L^2 = \sum q_R^2$ . Hence the lattice doubler ensures the theory is gauge anomaly free (albeit in the most trivial way). However the lattice doubler also cancels the fermion number anomaly. The total fermion number  $\int dx \Psi^\dagger \Psi = N_F^1 + N_F^2$  is conserved since (see Eq. (1.2.23))

$$\Delta N_F^1 = -\Delta N_F^2 = -\Delta N_{CS} \tag{3.2.27}$$

On the other hand the difference  $N_F^1 - N_F^2$  is anomalous. In the notation of Eq. (3.2.26) we have  $N_F^1 - N_F^2 = \int dx \Psi^\dagger \tilde{\Gamma}_5 \Psi$  where  $\tilde{\Gamma}_5$  is the "generalised" chirality

$$\tilde{\Gamma}_5 = \begin{pmatrix} \gamma_5 & 0 \\ 0 & -\gamma_5 \end{pmatrix} \quad (3.2.28)$$

From Eq. (3.2.27) we have

$$\Delta \tilde{\Gamma}_5 = -2\Delta N_{CS} \quad (3.2.29)$$

The lattice version of  $\tilde{\Gamma}_5$  is

$$\langle \tilde{\Gamma}_5 \rangle = \sum_{j=1}^N \text{Re} \left( \chi_j^\dagger e^{iaA_j^1} \chi_{j+1}^1 + \chi_j^\dagger \chi_{j+1}^2 \right) \quad (3.2.30)$$

which differs from chirality, Eq. (3.2.25), in the sign of the second term. Unlike  $\Gamma_5$ ,  $\tilde{\Gamma}_5$  commutes with the Hamiltonian for finite Yukawa coupling and thus serves as a good label for the energy eigenstates (though the order  $a$  term in the lattice Hamiltonian breaks  $\tilde{\Gamma}_5$  symmetry). Indeed in the continuum  $\tilde{\Gamma}_5$  just labels the particular fermion species. States with  $\tilde{\Gamma}_5 = +1$  correspond to  $\psi^1$  while states with  $\tilde{\Gamma}_5 = -1$  correspond to the doubler  $\psi^2$ . Although classically conserved (in the continuum)  $\tilde{\Gamma}_5$  symmetry is broken by the anomaly which should be reflected by the level crossing of energy eigenstates.

The presence of doubler states with opposite chirality is a general feature of all lattice theories of fermions. Their presence can be derived under very general assumptions. In fact, according to the Nielsen-Ninomiya theorem as long as the Hamiltonian is hermitian, local and translation-invariant there is an equal number of left handed and right handed particles for every set of conserved quantum numbers [36]. As explained above this means that fermion number is conserved for lattice fermions. In terms of the level crossing picture, for every fermion state with generalised chirality  $\tilde{\Gamma}_5 = +1$  (corresponding to species  $\psi^1$ ) crossing zero in one direction there will be a corresponding doubler state (corresponding to species  $\psi^2$ ) with  $\tilde{\Gamma}_5 = -1$  crossing zero in the opposite direction. However in the

continuum limit the doubler decouples and can be ignored. Hence provided the lattice spacing  $a$  is small enough we can still study fermion number violation on the lattice.

### 3.3 Eigenvalue and Chirality Measurements

To investigate the level crossing picture on the lattice we numerically solve Eqs. (3.2.19), (3.2.21) and (3.2.24) for the eigenvalues and eigenvectors of the Dirac Hamiltonian in the presence of background lattice gauge and Higgs fields. Antiperiodic boundary conditions are imposed on the fermion wavefunctions so that there are no zero eigenvalues in the free field case. Appendix C describes the numerical method used to find the eigenvalues. Firstly the Hamiltonian matrix is tridiagonalised using the Lanczos method and then the eigenvalues found using Sturm sequences. Having found the eigenvalues the corresponding eigenvectors are then found using inverse iteration (see Appendix D).

Firstly we investigated the level crossing picture for a set of smooth configurations which interpolate between two topologically distinct vacua. The trivial vacuum with winding number zero is

$$A_j^{(0)} = 0, \quad \phi_j^{(0)} = 1 \quad (3.3.31)$$

while a vacuum with winding number one is given by

$$A_j^{(1)} = \frac{2\pi}{na}, \quad \phi_j^{(1)} = e^{\frac{2\pi i(j-1)}{n}} \quad (3.3.32)$$

where  $a$  is the lattice spacing and  $n$  is the number of lattice sites. We choose our gauge field to smoothly interpolate between  $A^{(0)}$  and  $A^{(1)}$ .

$$A_j(t) = tA_j^{(1)} \quad (3.3.33)$$

where the "time" parameter  $t$  varies from 0 to 1. This is just the lattice version of the gauge field considered in Section 1.3, Eq. (1.3.33), which was shown to result in level crossing, at least for massless fermions.

Firstly we consider the eigenvalues and eigenvectors of the Hamiltonian with an explicit mass term, Eq. (3.2.19) (in the case  $m = 0$ , Eq. (3.2.21)). In this case we can show analytically that level crossing occurs for  $m = 0$ . In addition we know that the zero eigenvalue occurs for  $N_{CS} = \frac{1}{2}$ . Since this can be shown analytically this serves as a test case for our numerical method. Figure 3.1 shows the the lowest positive eigenvalue and the chirality of the corresponding eigenvector for a variety of masses. In each case the lowest eigenvalue falls reaching a minimum at  $t = 0.5$  (corresponding to  $N_{CS} = \frac{1}{2}$ ) before rising again. The chirality is initially positive and switches in sign at  $t = 0.5$  to become negative. From these results we can infer the behaviour of the highest negative energy eigenvalue. To do this we use the fact that due to lattice doubling the eigenvalues come in pairs. From Eq. (3.2.19), if  $(\chi_j^1, \chi_j^2)$  is an eigenvector with eigenvalue  $E$  and chirality  $\Gamma_5$  then  $((-1)^j \chi_j^1, -(-1)^j \chi_j^2)$  is an eigenvector with eigenvalue  $-E$  and chirality  $-\Gamma_5$ . Using this symmetry we can infer that the highest negative energy eigenvalue rises reaching a maximum at  $t = 0.5$  before falling. The chirality of this mode is initially negative and switches sign to become positive.

In the massless case the lowest eigenvalue gets close to zero at  $t = 0.5$  and  $\Gamma_5$  is close to  $\pm 1$ . Now recall that  $\Gamma_5$  is classically conserved in this case (for small lattice spacing). We thus interpret the results as showing a positive chirality mode (right mover) crossing zero from above and a negative chirality mode (left mover) crossing zero from below. The zero eigenvalue occurs for  $N_{CS} = \frac{1}{2}$  as expected for the massless Hamiltonian. The total change in chiral charge is  $\Delta\Gamma_5 = -2$  in agreement with Eq. (3.2.23). On the other hand when the fermion is massive the eigenvalues are bounded from below by the particle mass  $m$  as shown in figure 3.1a and so level crossing cannot occur. As  $m$  is increased  $|\Gamma_5|$  decreases since the mass term breaks chiral symmetry.

These results indicate that our method works well, at least for the analytically understood case of fermions with an explicit mass. We now apply the same method to the less well understood Yukawa case, Eq. (3.2.24). Of particular interest in this

case is the relationship between level crossing and the topology of the Higgs field. With this in mind we have investigated five different Higgs field configurations each with different topological properties. In all five cases the gauge field is as before, Eq. (3.3.33).

**CASE 1.**

$$\phi_j(t) = (1 - t)\phi_j^{(0)} + t\phi_j^{(1)}, \quad A_j(t) = tA_j^{(1)} \quad (3.3.34)$$

In this case the Higgs field smoothly interpolates between  $\phi^{(0)}$  and  $\phi^{(1)}$ .  $\phi$  has winding number  $N_H = 0$  for  $t < \frac{1}{2}$  and  $N_H = 1$  for  $t > \frac{1}{2}$ . The change in winding number occurs at time  $t_h = \frac{1}{2}$  where the Higgs field has zero at the center of the lattice,  $\phi_{\frac{a}{2}+1}(t_h) = 0$ . In this case  $t_h$  coincides with the time at which the Chern-Simons number is half-integer  $t_{CS} = \frac{1}{2}$ . The lowest eigenvalue and generalised chirality are shown in figure 3.2 for a variety of Yukawa couplings  $h$ . For all values of  $h$  we observe the diving of the lowest eigenvalue and corresponding flip in sign of the generalised chirality  $\tilde{\Gamma}_5$  from positive to negative. Since  $\tilde{\Gamma}_5$  is a good quantum number (in the continuum limit) in the Yukawa case, we find  $\tilde{\Gamma}_5 \approx \pm 1$ . As before these results are interpreted using the fact that the eigenvalues come in pairs due to species doubling. From Eq. (3.2.24), if  $(\chi_j^1, \chi_j^2)$  is an eigenvector with eigenvalue  $E$  and generalised chirality  $\tilde{\Gamma}_5$  then  $((-1)^j \chi_j^1, -(-1)^j \chi_j^2)$  is an eigenvector with eigenvalue  $-E$  and generalised chirality  $-\tilde{\Gamma}_5$ . Thus our results also show the rising of the highest negative energy eigenvalue reaching a maximum at  $t = 0.5$ . The generalised chirality of this mode is initially negative and switches sign to become positive. As argued in Section 3.2,  $\tilde{\Gamma}_5$  takes over the role of  $\Gamma_5$  in the current case. In particular it is classically conserved in the continuum limit. Thus we can interpret the results as showing a  $\tilde{\Gamma}_5 = +1$  mode crossing zero from above and a  $\tilde{\Gamma}_5 = -1$  mode crossing zero from below. The zero eigenvalue occurs at  $N_{CS} = \frac{1}{2}$  as in the massless case. As discussed in Section 3.2  $\tilde{\Gamma}_5 = +1$  states correspond to one fermion  $\psi^1$  (with fermion number  $N_F^1$ ) and states with  $\tilde{\Gamma}_5 = -1$  to the doubler  $\psi^2$  (with fermion number  $N_F^2$ ). So we have  $\Delta N_F^1 = -\Delta N_F^2 = -\Delta N_{CS}$

and  $\tilde{\Gamma}_5 = -2\Delta N_{CS}$  in agreement with the anomaly equations, Eqs. (3.2.27) and (3.2.29).

**CASE 2.**

$$\phi_j(t) = (1 - \sqrt{t})\phi_j^{(0)} + \sqrt{t}\phi_j^{(1)}, \quad A_j(t) = tA_j^{(1)} \quad (3.3.35)$$

As above the Higgs field interpolates between the two vacua. However in this case the Higgs zero occurs at  $t_h = \frac{1}{4}$ , i.e.  $t_h < t_{CS}$ . The lowest eigenvalue and generalised chirality are shown in figure 3.3. As before the results show the diving of the lowest eigenvalue and chirality flip suggestive of level crossing. However the exact point at which we have a zero eigenvalue  $t_0$  depends upon the Yukawa coupling  $h$  with  $t_0$  varying continuously from  $t_{CS}$  to  $t_h$  as  $h$  is increased. This shift of  $t_0$  away from  $t_{CS}$  for finite  $h$  has been shown analytically in the continuum[15].

**CASE 3.**

$$\phi_j(t) = (1 - t^2)\phi_j^{(0)} + t^2\phi_j^{(1)}, \quad A_j(t) = tA_j^{(1)} \quad (3.3.36)$$

This is similar to CASE 3 except now we have  $t_h = \frac{1}{\sqrt{2}}$  i.e.  $t_h > t_{CS}$ . The results are shown in figure 3.4. As in CASE 3,  $t_0$  varies continuously with increasing  $h$  from  $t_{CS}$  towards  $t_h$ .

**CASE 4.**

$$\phi_j(t) = \phi_j^{(0)}, \quad A_j(t) = tA_j^{(1)} \quad (3.3.37)$$

In this case only the gauge field varies while the Higgs field is frozen in the trivial vacuum ( $N_H = 0$ ). The results are shown in figure 3.5. For small Yukawa coupling we have level crossing with  $t_0$  increasing as  $h$  is increased. At some threshold Yukawa coupling  $t_0 = 1$ . For  $h$  greater than this threshold there is no level crossing.

**CASE 5.**

$$\phi_j(t) = \phi_j^{(1)}, \quad A_j(t) = tA_j^{(1)} \quad (3.3.38)$$

This is similar to CASE 4 except here the Higgs field is frozen in the vacuum with winding number  $N_H = 1$ . The results are shown in figure 3.6. As in CASE 4

level crossing occurs for small  $h$ . As  $h$  is increased  $t_0$  decreases and level crossing disappears above some threshold value of  $h$ .

Armed with these results we can now apply the same procedure to the case of the "high temperature" fields discussed in Chapter 2. Previously we identified fermion number violation by measuring the Chern-Simons number of the gauge field. Now we shall attempt to observe fermion number violation directly by measuring the lowest eigenvalue and chirality in these high temperature backgrounds.

In Section 2.6 a particular "sphaleron" transition was described. The Chern-Simons number for this transition is shown in figure 2.2. Since  $\Delta N_{CS} = 1$  we expect this transition to be accompanied by the level crossing of energy eigenstates. In the massless case we know that level crossing must occur with the zero eigenvalue occurring at half-integer  $N_{CS}$ . This is clearly shown in figure 3.7 which shows the lowest eigenvalue and chirality of the massless Hamiltonian.

For the Yukawa case the lowest eigenvalue and generalised chirality are shown in figure 3.8. For small Yukawa coupling the results are similar to the massless case with level crossing occurring at time  $t \sim t_{CS}$ , where  $N_{CS}$  is half-integer. As  $h$  is increased we still have level crossing but the time  $t_0$  at which this occurs is displaced from  $t_{CS}$ , decreasing as  $h$  increases. This is expected for a general Higgs configuration as shown in the trial configurations discussed above. From our trial results we expect  $t_0$  to approach  $t_h$ , the time where the Higgs field has a zero, as  $h$  is increased. In Section 2.6 we showed by direct measurement that for this particular transition  $t_h = 2137.2$ , i.e.  $t_h < t_{CS}$ . Thus we expect  $t_0$  to decrease towards  $t = 2137.2$  as  $h$  is increased and this is what we observe.

Results for a second sphaleron transition are shown in figure 3.9 for the massless Hamiltonian and figure 3.10 for the Hamiltonian with the Yukawa term. The Chern-Simons number is half-integer at time  $t_{CS} = 2275.9$  resulting in level crossing in the massless case as shown in figure 3.9. For the Yukawa case we have level crossing for small Yukawa coupling. The time of level crossing  $t_0$  decreases as  $h$

is increased indicating that  $t_h < t_{\frac{1}{2}}$  as above. In fact in this case  $t_h$  occurs before the time scale shown in figure 3.10 so that level crossing disappears off the figure for large  $h$ . Hence in this case the winding number of the Higgs field has already changed before the time scale shown in these figures. The Higgs topology is thus similar to CASE 5 discussed above in which the Higgs winding number doesn't change but is frozen at  $N_H = 1$ .

### 3.4 Lattice Dirac Equation

In the previous section it was shown that transitions with  $\Delta N_{CS}$  are accompanied by the diving of the lowest eigenvalue and a flip in sign of the chirality (or generalised chirality in the Yukawa case). This was interpreted as showing the lowest eigenvalue crossing zero leading to the violation of fermion number. This interpretation relies on the assumption that chirality (generalised chirality) commutes with the Hamiltonian in the massless (Yukawa) case and is thus a constant of the motion.

For example suppose  $\Gamma_5$  is initially  $+1$  and flips in sign to become  $-1$ . Then if we initially choose  $|\psi\rangle$  to be the lowest positive energy eigenstate of  $H$  and evolve  $|\psi\rangle$  according to the time-dependent Dirac equation the chirality of  $|\psi\rangle$  will remain  $+1$ . Furthermore in the adiabatic limit where the background fields change slowly with time  $|\psi\rangle$  will remain an eigenstate of  $H$ . As  $H$  slowly varies  $|\psi\rangle$  evolves into the closest  $\Gamma_5 = +1$  eigenstate. So as long as the chirality of the lowest positive energy eigenstate is  $\Gamma_5 = +1$ ,  $|\psi\rangle$  will remain in the lowest positive energy eigenstate. However when  $\Gamma_5$  changes to  $-1$   $|\psi\rangle$  cannot remain as the lowest positive energy eigenstate since  $\Gamma_5$  is conserved. At this point the closest  $\Gamma_5 = +1$  eigenstate is the highest negative energy eigenstate. Hence we expect  $|\psi\rangle$  to evolve into the highest negative energy eigenstate of  $H$ . This leads to the conclusion that the  $\Gamma = +1$  state crosses zero from above leading to creation of chiral charge.

Of course on the lattice  $\Gamma_5$  is not conserved. As explained in the previous section the lattice Hamiltonian contains an order  $a$  term which explicitly breaks chiral symmetry. This is unlikely to be a problem in our 1 + 1 dimensional model since as shown in the previous section we measure  $\Gamma_5$  to be very close to  $\pm 1$  indicating that chirality is close to being a good quantum number. However it would be useful to have some independent method to check that the state really does cross zero. The above discussion suggests the following method to verify the level crossing picture directly.

Let  $|E_0^+(t)\rangle$  be the lowest positive energy eigenstate and  $|E_0^-(t)\rangle$  be the highest negative energy eigenstate. At some time  $t_i$  before the zero eigenvalue we pick our initial state  $|\psi(t_i)\rangle = |E_0^+(t_i)\rangle$ , i.e.  $|\psi\rangle$  is the lowest positive energy eigenstate of  $H$ . We then evolve the state according to the time-dependent Dirac equation. As  $|\psi\rangle$  evolves we measure the probability of finding  $|\psi\rangle$  in the states  $|E_0^+\rangle$  and  $|E_0^-\rangle$ . According to the above discussion for adiabatic background fields we expect  $|\psi\rangle$  to remain in the lowest positive energy eigenstate  $|\psi\rangle = |E_0^+\rangle$  until the point where we have a zero eigenvalue and chirality flip where it should evolve into the highest negative energy eigenstate  $|\psi\rangle = |E_0^-\rangle$ .

The above discussion assumes the background fields are adiabatic. This assumption will not be satisfied for general gauge-Higgs backgrounds. In particular the high temperature fields vary quite rapidly with time. For these more general backgrounds we do not expect  $|\psi\rangle$  to remain in one particular energy eigenstate but to gradually disperse among all possible states with the same chirality as  $|E_0^+(t_i)\rangle$ . However provided the backgrounds do not vary too rapidly we still expect the above method to give useful results.

We want to evolve the state  $|\psi\rangle$  according to the Dirac equation.

$$i \frac{d}{dt} |\psi(t)\rangle = H(t) |\psi(t)\rangle \quad (3.4.39)$$

where  $H$  is the fermion Hamiltonian. An important property of Eq. (3.4.39) is that the time evolution operator is unitary. This ensures that the norm of the

state  $|\psi\rangle$  is preserved. This property is obviously crucial for the reliability of our method and so we use the following discrete version of Eq. (3.4.39)[42]

$$\left(1 + \frac{1}{2}i\Delta t H(t)\right) |\psi(t + \Delta t)\rangle = \left(1 - \frac{1}{2}i\Delta t H(t)\right) |\psi(t)\rangle \quad (3.4.40)$$

Using these equations the norm of  $|\psi\rangle$  is preserved exactly. We solve Eq. (3.4.40) numerically using Lanczos matrix inversion (see Appendix D).

### 3.5 Transition Probability Measurements

Firstly we followed the time development of  $|\psi\rangle$  for the trial configurations discussed in Section 3.3. In each case  $|\psi\rangle$  was initially chosen to be the lowest positive energy eigenstate of the Hamiltonian and the probabilities of finding  $|\psi\rangle$  in the states  $|E_0^+\rangle$  and  $|E_0^-\rangle$  at subsequent times were measured.

Firstly consider the massless case, i.e. consider the massless Hamiltonian in the uniform gauge field background, Eq. (3.3.33), which has  $t_{CS} = \frac{1}{2}$ . Recall that in the massless case the Hamiltonian has a zero eigenvalue at  $t_0 = t_{CS}$  and so we expect level crossing to occur at this point. Figure 3.11a shows  $|\langle E_0^+(t)|\psi(t)\rangle|^2$ , i.e. the probability of finding  $|\psi\rangle$  in the lowest positive energy eigenstate at time  $t$ .  $|\langle E_0^+(t)|\psi(t)\rangle|^2$  is initially one by our initial choice of  $|\psi\rangle$ . It remains very close to one until  $t_0$ , i.e. it remains in the lowest positive energy eigenstate. At  $t_0$  it dives to zero. As discussed in the previous section this is just as expected for an adiabatic background. Since  $\Gamma_5$  flips in sign at  $t_0$ ,  $|\psi\rangle$  cannot remain in  $|E_0^+\rangle$  since chirality is approximately conserved. We thus expect  $|\psi\rangle$  to evolve into  $|E_0^-\rangle$  at  $t_0$ . To check that this is the case we measure  $|\langle E_0^-(t)|\psi(t)\rangle|^2$ , i.e. the probability of finding  $|\psi\rangle$  in the highest negative energy eigenstate. This is shown in figure 3.11b.  $|\langle E_0^-(t)|\psi(t)\rangle|^2$  remains close to zero until  $t = t_0$  at which point it jumps to one. After  $t_0$ ,  $|\langle E_0^-(t)|\psi(t)\rangle|^2$  remains very close to one. The lowest positive energy eigenstate evolves almost entirely into the highest negative energy eigenstate, confirming the level crossing picture.

These results indicate that the simple uniform gauge field background, Eq. (3.3.33), is consistent with the adiabatic approximation whereby the background field varies so slowly with time that  $|\psi\rangle$  remains a particular energy eigenstate with unit probability. Hence the level crossing picture is particularly clear here. For more general backgrounds the adiabatic approximation will not be valid.

We can see this applying the same procedure to the Hamiltonian with a Yukawa term. Now our background field contains a Higgs field which will in general make the adiabatic approximation invalid. Thus we expect  $|\psi\rangle$  not to evolve completely into  $|E_0^- \rangle$  but to disperse into other nearby states (consistent with chirality conservation). This dispersion will depend upon the particular background. This in turn will depend upon the Yukawa coupling and on the topology of the Higgs field. To investigate this we have solved the Dirac equation in all 5 different gauge-Higgs backgrounds discussed in Section 3.3 for a variety of Yukawa couplings. The results are shown in figures 3.12 - 3.16.

Firstly consider CASE 1 given by Eq. (3.3.34). Recall that in this case the Higgs field has a zero at  $t_h = t_{CS}$  and that for all values of Yukawa coupling  $h$  we have a zero eigenvalue at this point. Figure 3.12a and 3.12b show  $|\langle E_0^+(t)|\psi(t)\rangle|^2$  and  $|\langle E_0^-(t)|\psi(t)\rangle|^2$  respectively. For small values of  $h$  the results are similar to the massless case with  $|\langle E_0^+(t)|\psi(t)\rangle|^2 \approx 1$  for  $t < t_0$  and  $|\langle E_0^-(t)|\psi(t)\rangle|^2 \approx 1$  for  $t > t_0$ . As  $h$  is increased we see a gradual fall in both  $|\langle E_0^+(t)|\psi(t)\rangle|^2$  and  $|\langle E_0^-(t)|\psi(t)\rangle|^2$  away from 1. This indicates that the additional Yukawa term makes the Hamiltonian "less adiabatic", so that  $|\psi\rangle$  doesn't remain as the lowest eigenstate but gradually disperses among other eigenstates consistent with  $\tilde{\Gamma}_5$  conservation. In the current case this non-adiabatic behaviour increases for increasing Yukawa coupling  $h$ . However the essential features suggestive of level crossing still remain. In particular  $|\langle E_0^+(t)|\psi(t)\rangle|^2$  and  $|\langle E_0^-(t)|\psi(t)\rangle|^2$  are discontinuous at  $t_0$  while  $|\langle E_0^+(t_0 - \Delta t)|\psi(t_0 - \Delta t)\rangle|^2 \approx |\langle E_0^-(t_0 + \Delta t)|\psi(t_0 + \Delta t)\rangle|^2$ . This suggests that  $|E_0^- \rangle$  takes over from  $|E_0^+ \rangle$  at  $t_0$  and that the lowest eigenvalue crosses zero.

In the other 4 Yukawa cases the results are similar with the level crossing

picture being verified in each case. As above the presence of the Yukawa term results in non-adiabatic behaviour with  $\left|\langle E_0^+(t)|\psi(t)\rangle\right|^2$  and  $\left|\langle E_0^-(t)|\psi(t)\rangle\right|^2$  falling away from 1 as  $|\psi\rangle$  disperses among the other eigenstates, the amount of dispersion being dependent on the Yukawa coupling. In CASE 1 we found that the behaviour was similar to the massless case for small  $h$ ,  $h \sim 0.1$ , and became "less adiabatic" as  $h$  was increased. However this is not a general rule as can be seen in figure 3.16 for example. Figure 3.16a shows strongly non-adiabatic behaviour for very small  $h$ ,  $h = 0.001$ . In this case the behaviour is "more adiabatic" for the larger  $h$ ,  $h = 0.1$ . On the other hand for very small  $h$  the results are similar to the massless case (as they must be by continuity, since the massless case corresponds to  $h = 0$ ). Clearly the relationship between the "non-adiabatic" fall in the overlaps and the Yukawa coupling is complicated and depends upon the particular background being studied.

We now apply the method to the high temperature fields discussed in Chapter 2. In Section 3.3 the lowest eigenvalues and chiralities for two different high temperature "sphalerons" were presented and showed the diving of the lowest eigenvalue and flip in chirality suggestive of level crossing.

Results for the first sphaleron in the massless case are shown in figure 3.17 (the corresponding lowest eigenvalue and chirality are given in figure 3.7). From figure 3.17a we can see the behaviour is far from adiabatic. By time  $t_0$ ,  $\left|\langle E_0^+(t)|\psi(t)\rangle\right|^2$  has fallen to  $\sim 0.2$ . However we still see the sharp discontinuity in  $\left|\langle E_0^+(t)|\psi(t)\rangle\right|^2$  and  $\left|\langle E_0^-(t)|\psi(t)\rangle\right|^2$  suggestive of level crossing. The picture is improved considerably in the Yukawa case (the corresponding lowest eigenvalue and generalised chirality are given in figure 3.8). This is shown in figure 3.18 for 3 values of the Yukawa coupling,  $h = 0.1, 0.2$  and  $0.3$ . All 3 values of  $h$  give similar results.  $\left|\langle E_0^+(t)|\psi(t)\rangle\right|^2$  remains very close to 1 until  $t_0$  where it drops sharply to zero. The "non-adiabatic fall" in  $\left|\langle E_0^+(t)|\psi(t)\rangle\right|^2$  away from 1 is very small in all 3 cases with the effect slightly increasing as  $h$  increases from 0.1 to 0.3. Of course for smaller values of  $h$  we get similar results to the massless case (which corre-

sponds to  $h = 0$ ) i.e. a large non-adiabatic effect. As discussed above for the trial configurations there is no simple relationship between the overlaps and  $h$  with this depending strongly on the particular background under consideration.

For the second sphaleron in the massless case the results are much better as shown in figure 3.19 (the corresponding lowest eigenvalue and chirality are given in figure 3.9). From these figures we can see that the behaviour is almost adiabatic with only a very slight fall in  $|\langle E_0^+(t)|\psi(t)\rangle|^2$  and  $|\langle E_0^-(t)|\psi(t)\rangle|^2$ . The Yukawa case shown in figure 3.20 (the corresponding lowest eigenvalue and chirality are shown in figure 3.10) shows increased non-adiabatic behaviour for the smaller value of  $h$ ,  $h = 0.001$ . Note the results in this case are very similar to the trial CASE 5 where the Higgs field was frozen in the second vacuum. In the current case this is not surprising since as discussed in Section 3.3 the winding number of the Higgs field has already changed before the time scale on these figures and so the topology here is similar to that in CASE 5.

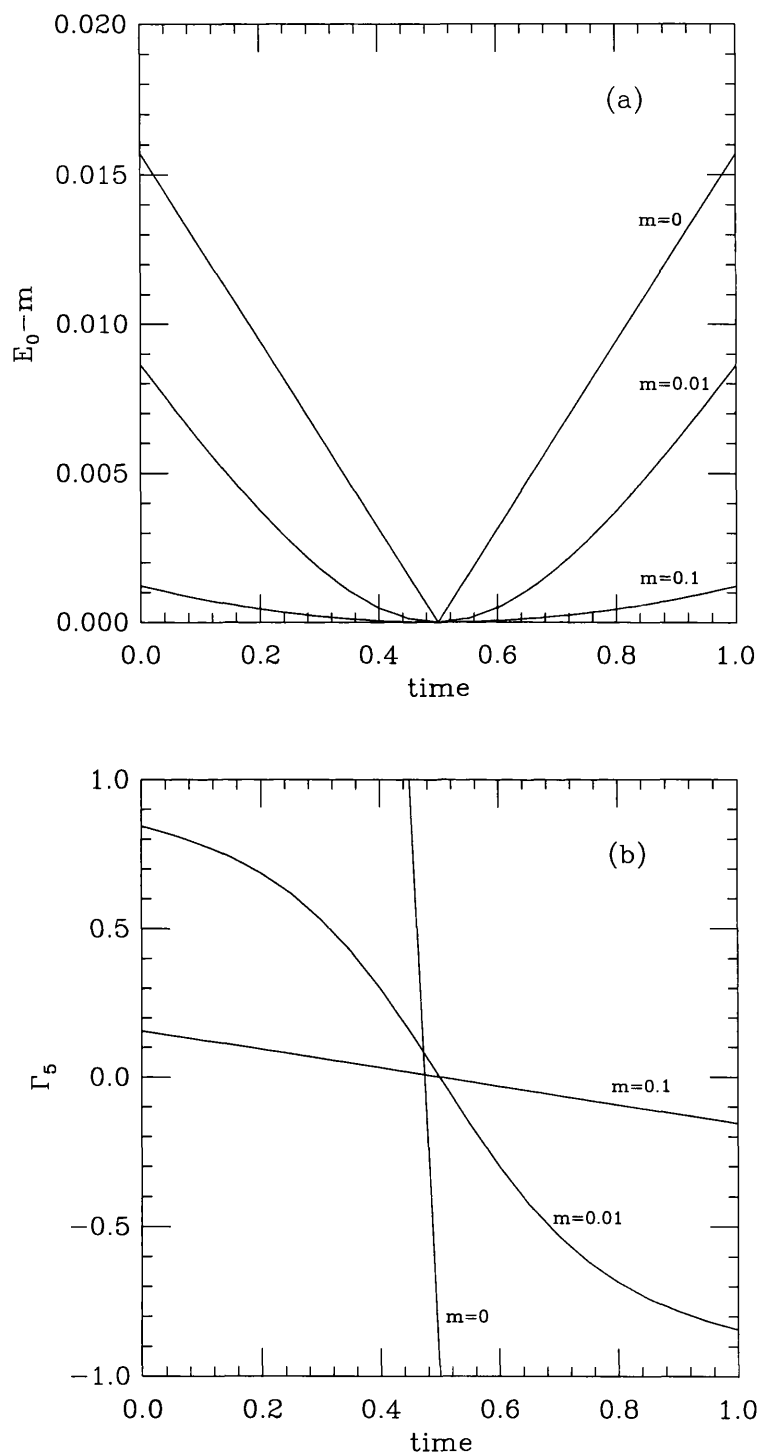


Figure 3.1: (a): The lowest eigenvalue  $E_0$  as a function of time for the configurations (3.3.33) for masses  $m = 0, 0.01$  and  $0.1$ . (b): The chirality  $\Gamma_5$  of the corresponding eigenvector.

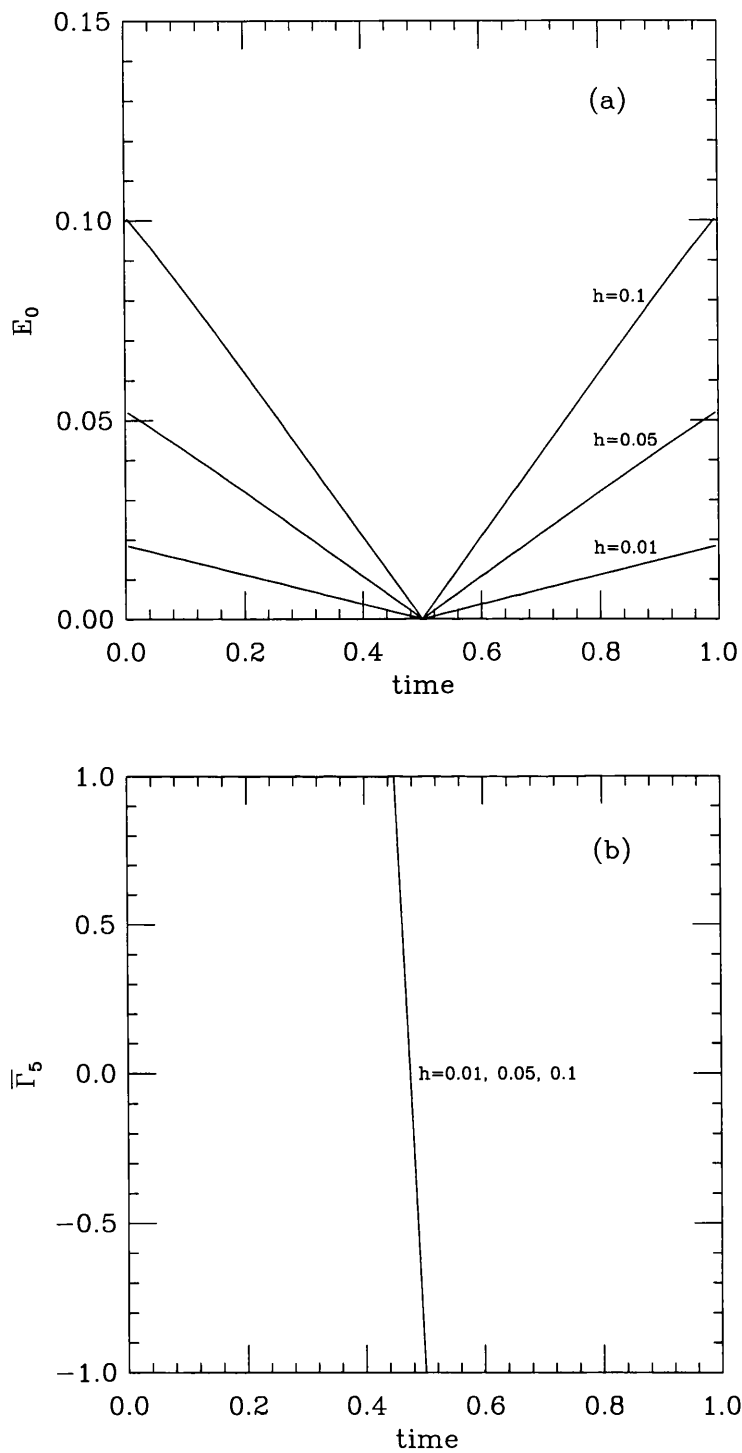


Figure 3.2: (a): The lowest eigenvalue  $E_0$  as a function of time for the configurations (3.3.34) for Yukawa couplings  $h = 0.01, 0.05$  and  $0.1$ . (b): The generalised chirality  $\tilde{\Gamma}_5$  of the corresponding eigenvector.

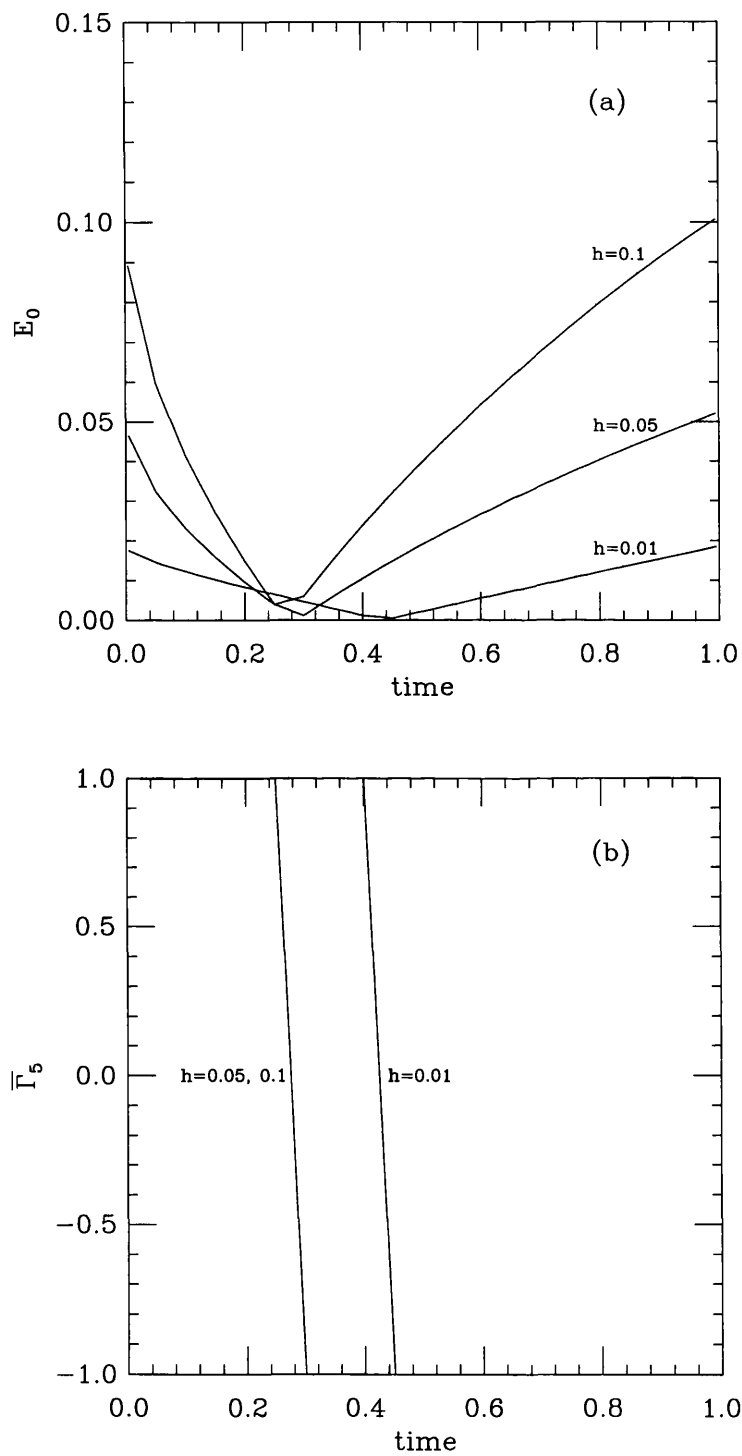


Figure 3.3: (a): The lowest eigenvalue  $E_0$  as a function of time for the configurations (3.3.35) for Yukawa couplings  $h = 0.01, 0.05$  and  $0.1$ . (b): The generalised chirality  $\tilde{\Gamma}_5$  of the corresponding eigenvector.

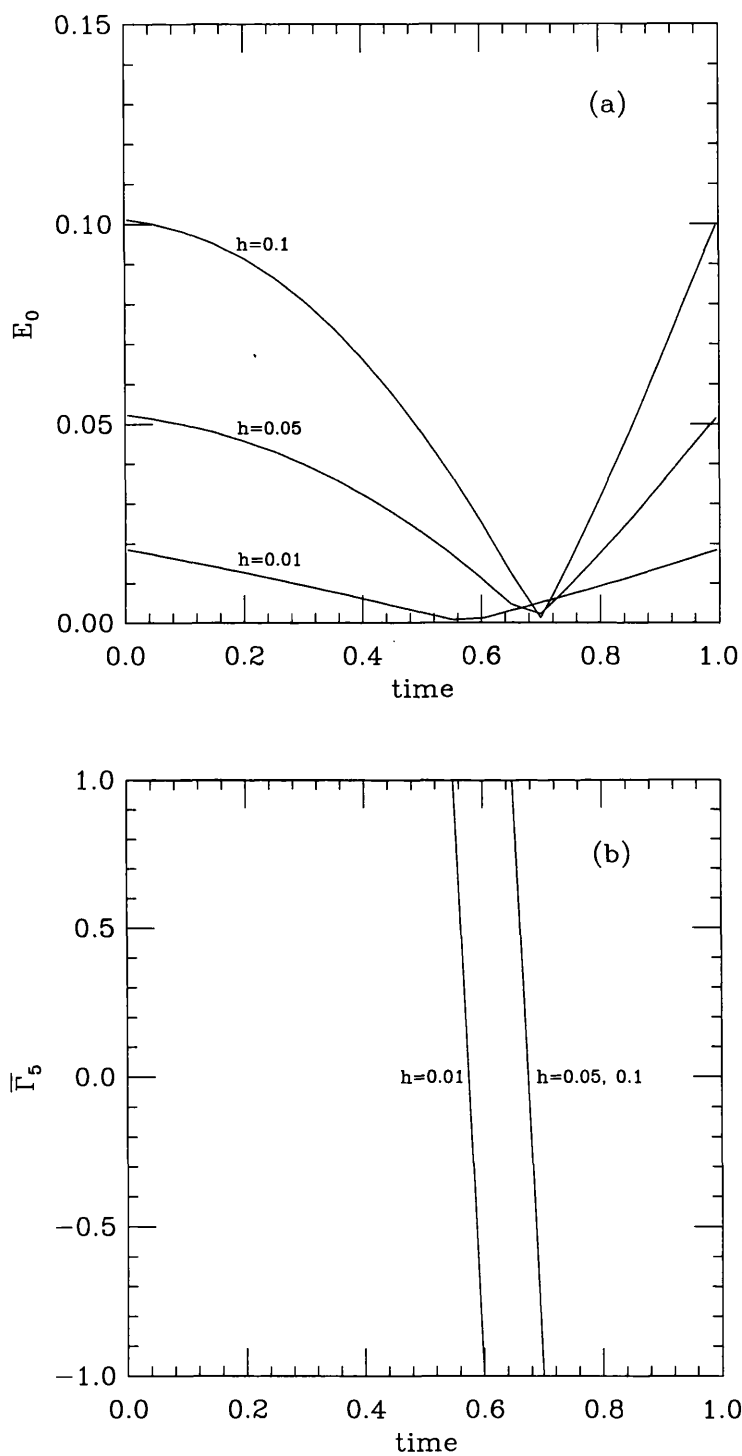


Figure 3.4: (a): The lowest eigenvalue  $E_0$  as a function of time for the configurations (3.3.36) for Yukawa couplings  $h = 0.01, 0.05$  and  $0.1$ . (b): The generalised chirality  $\tilde{\Gamma}_5$  of the corresponding eigenvector.

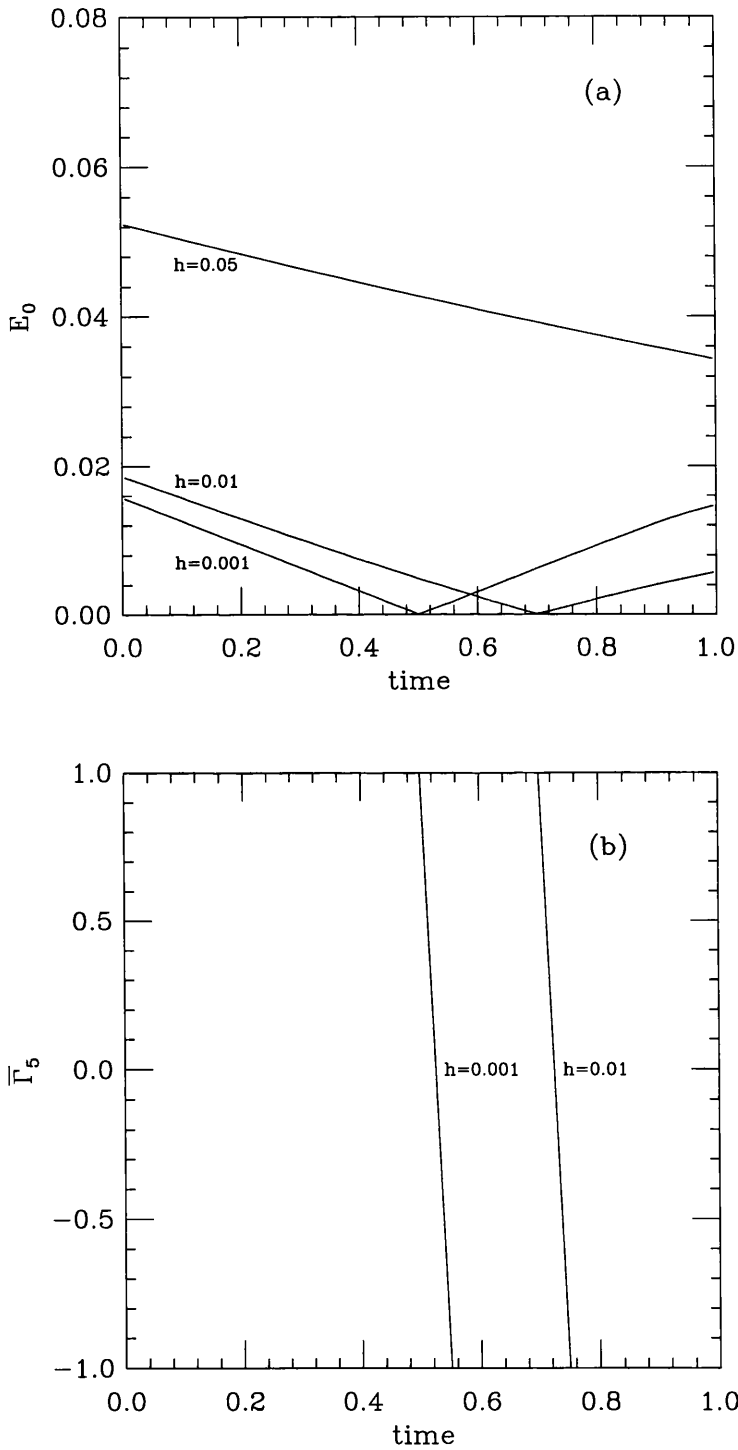


Figure 3.5: (a): The lowest eigenvalue  $E_0$  as a function of time for the configurations (3.3.37) for Yukawa couplings  $h = 0.001, 0.01$  and  $0.05$ . (b): The generalised chirality  $\tilde{\Gamma}_5$  of the corresponding eigenvector for  $h = 0.001$  and  $h = 0.01$ .

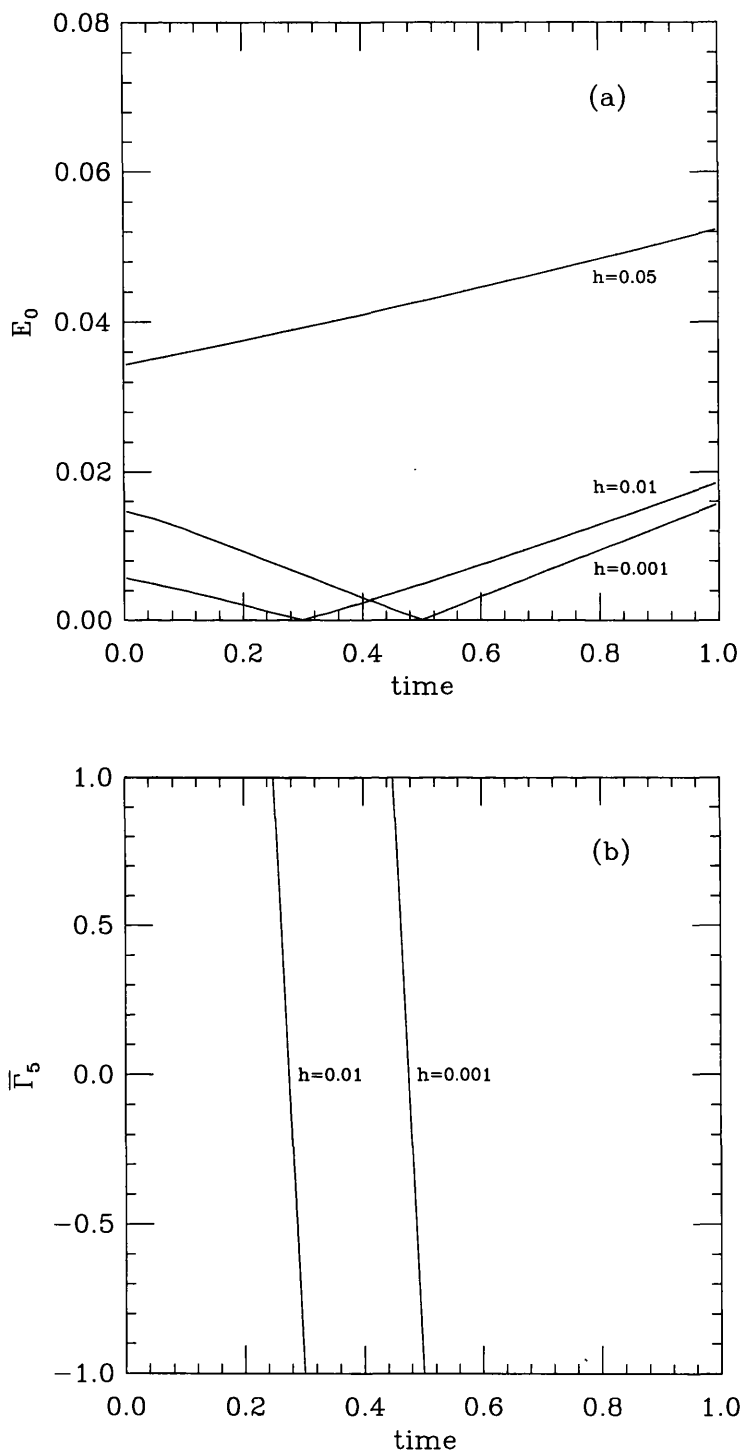


Figure 3.6: (a): The lowest eigenvalue  $E_0$  as a function of time for the configurations (3.3.38) for Yukawa couplings  $h = 0.001, 0.01$  and  $0.05$ . (b): The generalised chirality  $\tilde{\Gamma}_5$  of the corresponding eigenvector for  $h = 0.001$  and  $h = 0.1$ .

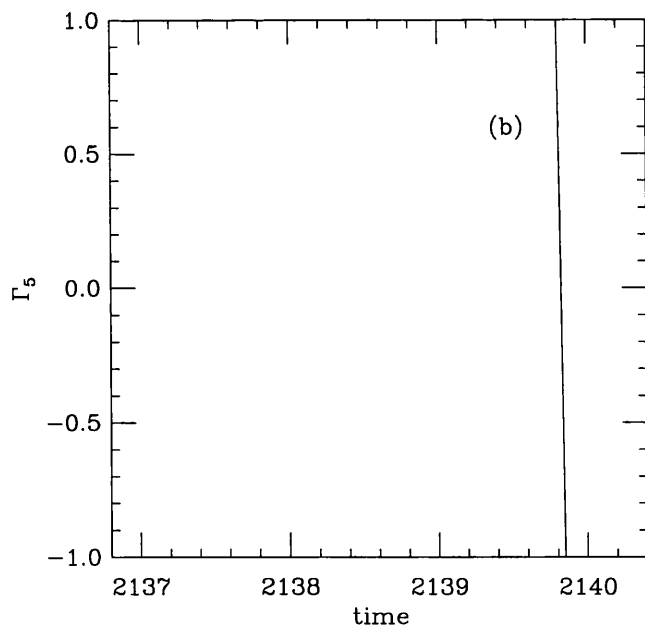
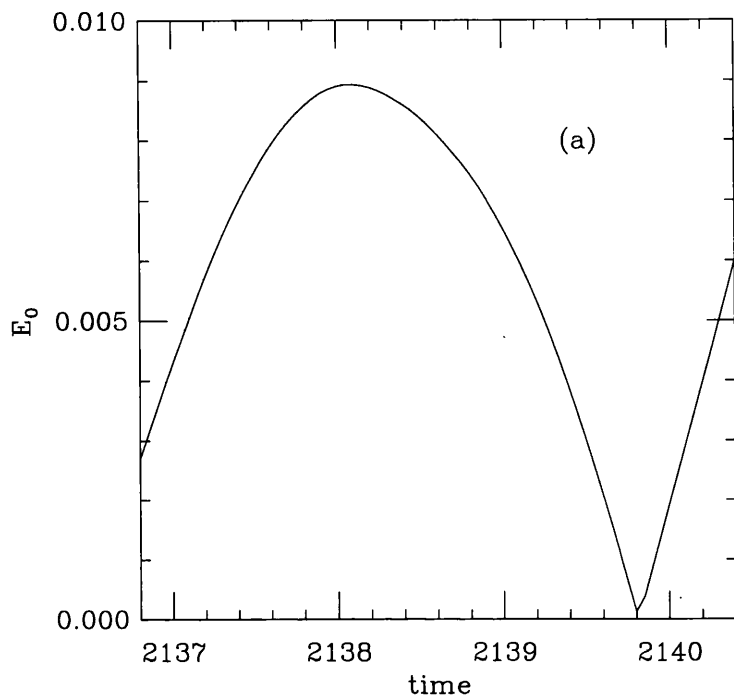


Figure 3.7: (a): The lowest eigenvalue  $E_0$  as a function of time for a typical sphaleron transition for the massless Hamiltonian. (b): The chirality  $\Gamma_5$  of the corresponding eigenvector.

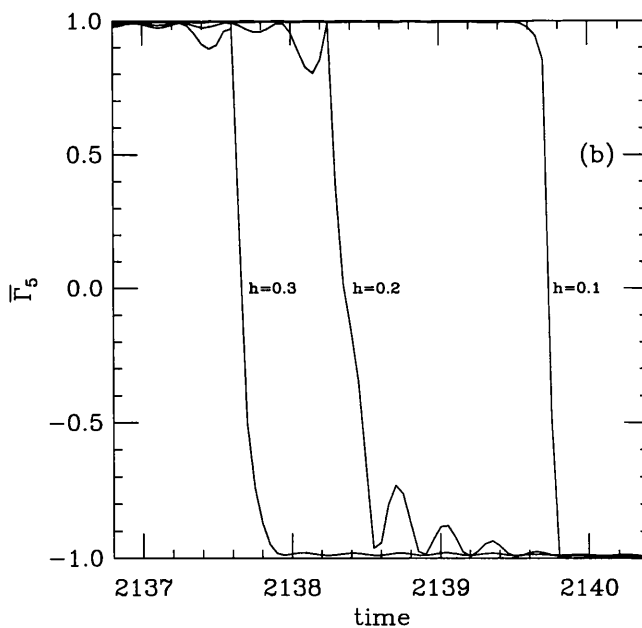
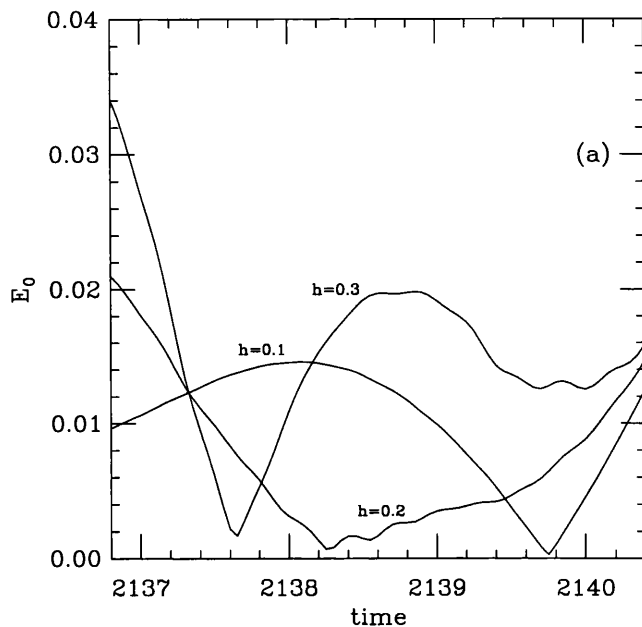


Figure 3.8: (a): The lowest eigenvalue  $E_0$  as a function of time for a typical sphaleron transition for Yukawa couplings  $h = 0.1, 0.2$  and  $0.3$ . (b): The generalised chirality  $\tilde{\Gamma}_5$  of the corresponding eigenvector.

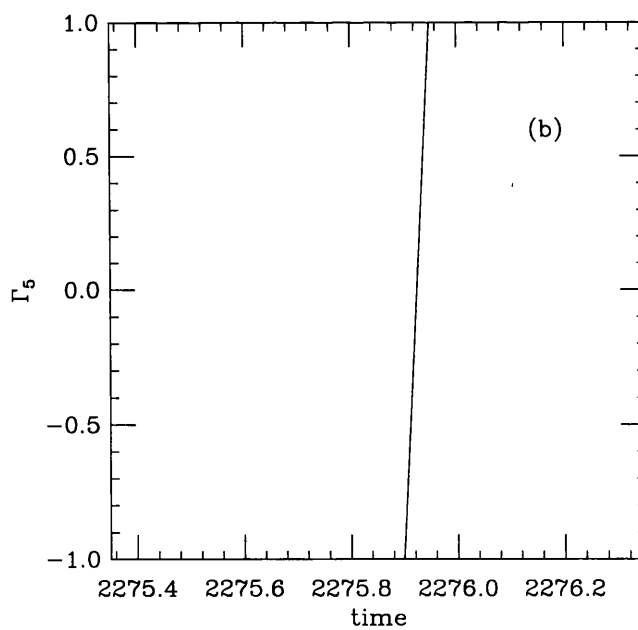
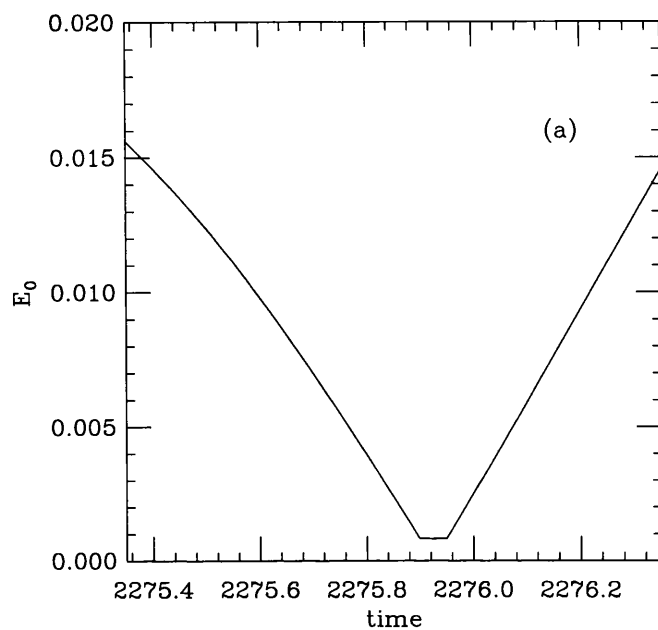


Figure 3.9: (a): The lowest eigenvalue  $E_0$  as a function of time for a typical sphaleron transition for  $m = 0$ . (b): The chirality  $\Gamma_5$  of the corresponding eigenvector.

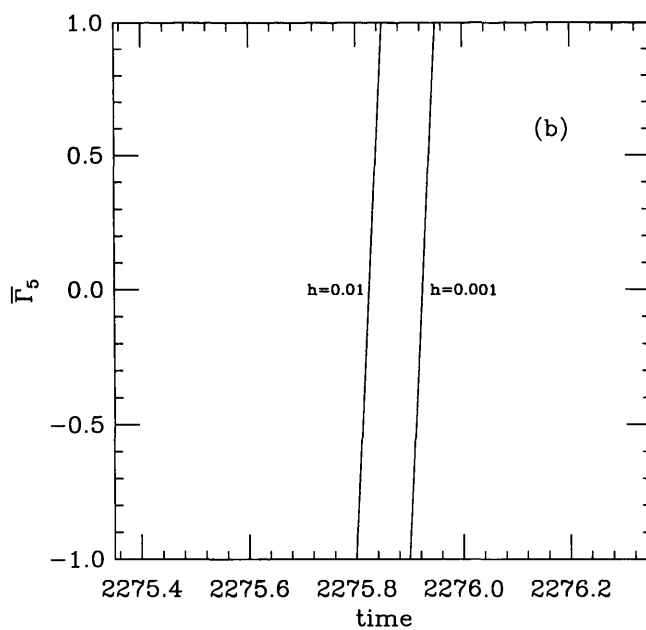
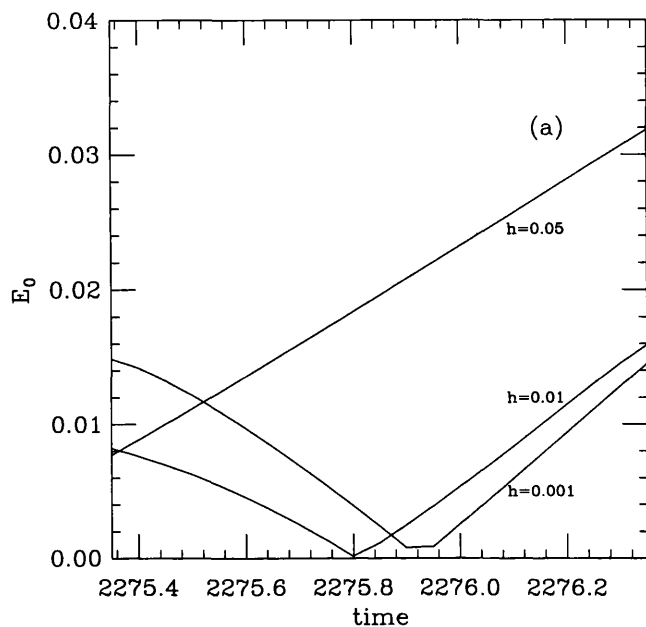


Figure 3.10: (a): The lowest eigenvalue  $E_0$  as a function of time for a typical sphaleron transition for Yukawa couplings  $h = 0.001, 0.01$  and  $0.05$ . (b): The generalised chirality  $\tilde{\Gamma}_5$  of the corresponding eigenvector for  $h = 0.001$  and  $h = 0.01$ .

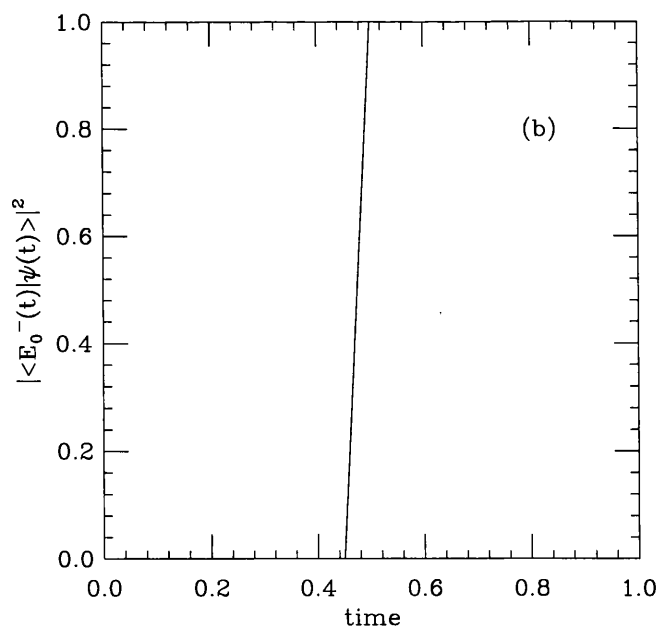
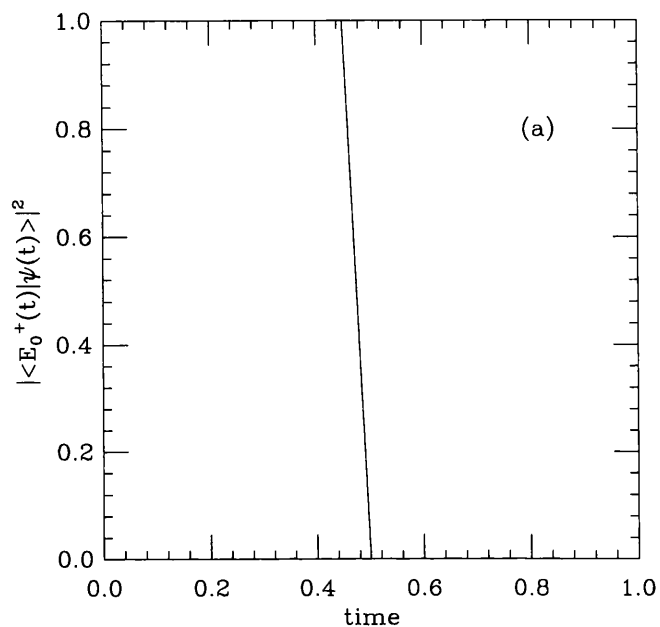


Figure 3.11: (a):  $|\langle E_0^+ | \psi \rangle|^2$  as a function of time for the configurations (3.3.33) for the massless Hamiltonian. (b):  $|\langle E_0^- | \psi \rangle|^2$  as a function of time for the configurations (3.3.33) for the massless Hamiltonian.

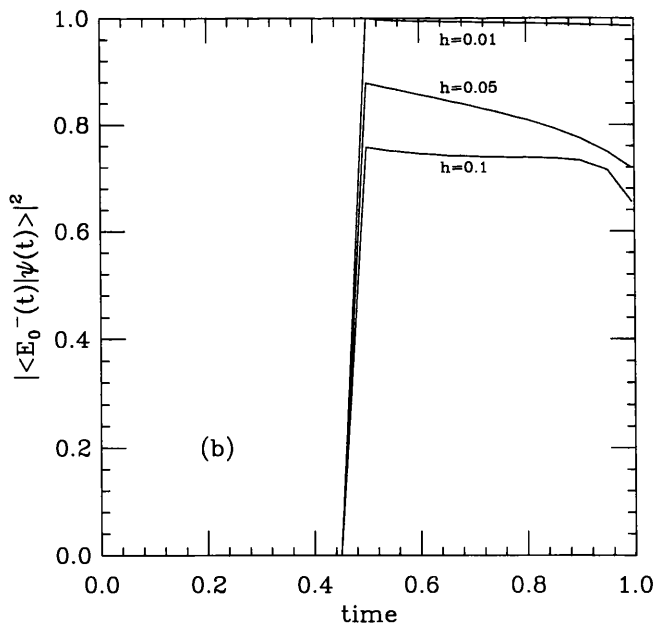
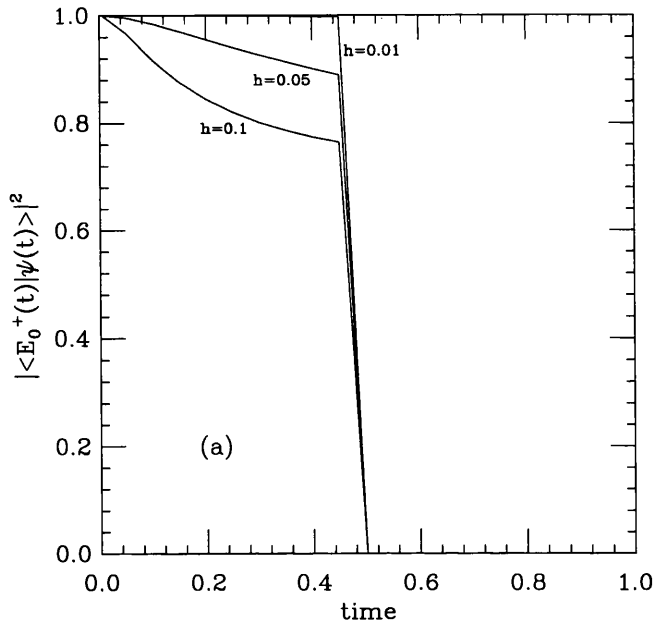


Figure 3.12: (a):  $|\langle E_0^+|\psi\rangle|^2$  as a function of time for the configurations (3.3.34) for Yukawa couplings  $h = 0.01, 0.05$  and  $0.1$ . (b):  $|\langle E_0^-|\psi\rangle|^2$  as a function of time for the configurations (3.3.34) for Yukawa couplings  $h = 0.01, 0.05$  and  $0.1$ .

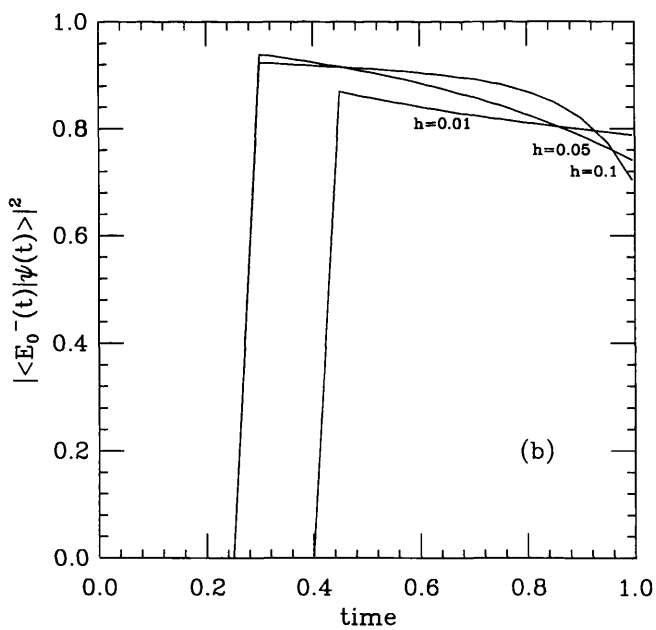
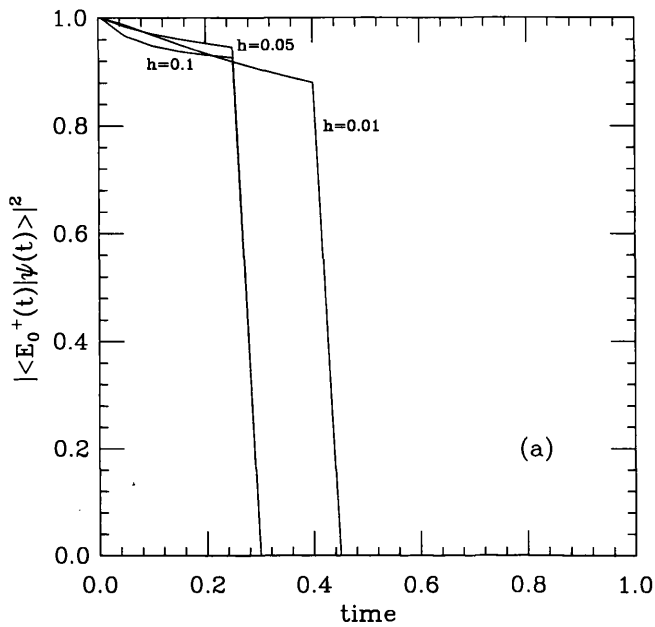


Figure 3.13: (a):  $|\langle E_0^+|\psi\rangle|^2$  as a function of time for the configurations (3.3.35) for Yukawa couplings  $h = 0.01, 0.05$  and  $0.1$ . (b):  $|\langle E_0^-|\psi\rangle|^2$  as a function of time for the configurations (3.3.35) for Yukawa couplings  $h = 0.01, 0.05$  and  $0.1$ .

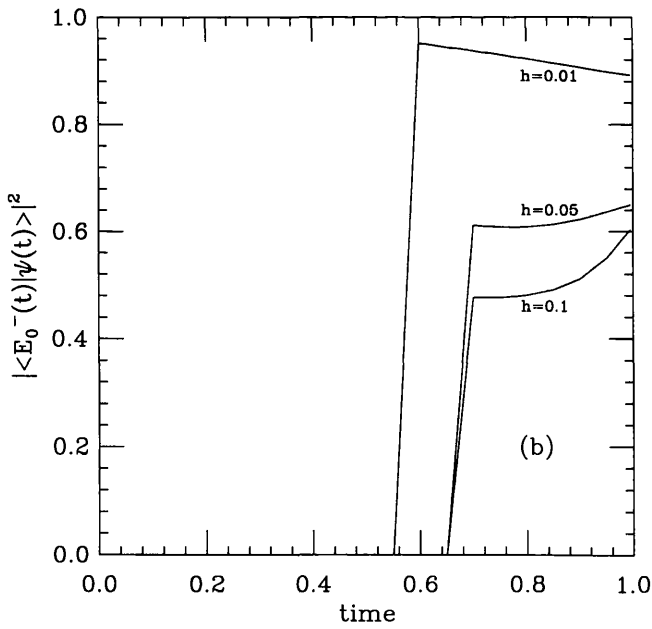
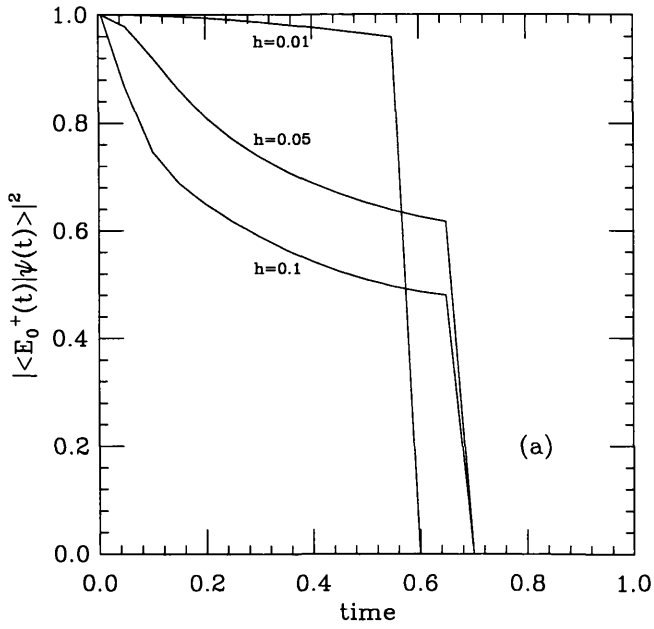


Figure 3.14: (a):  $|\langle E_0^+|\psi\rangle|^2$  as a function of time for the configurations (3.3.36) for Yukawa couplings  $h = 0.01, 0.05$  and  $0.1$ . (b):  $|\langle E_0^-|\psi\rangle|^2$  as a function of time for the configurations (3.3.36) for Yukawa couplings  $h = 0.01, 0.05$  and  $0.1$ .

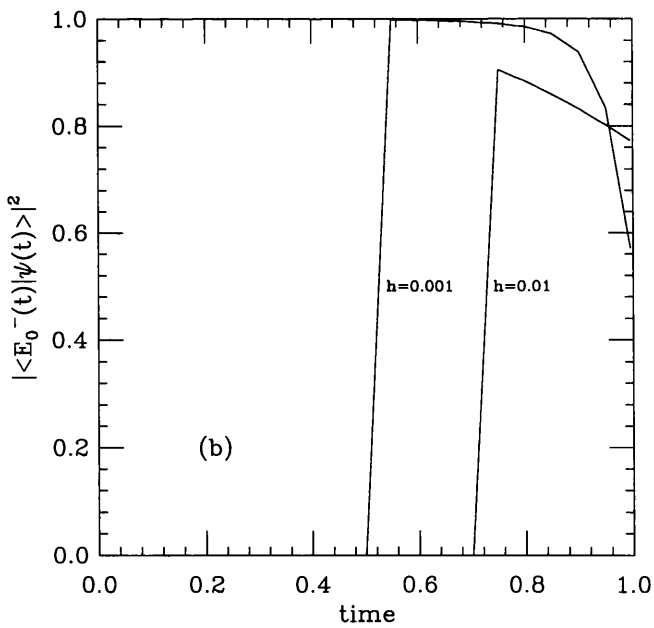
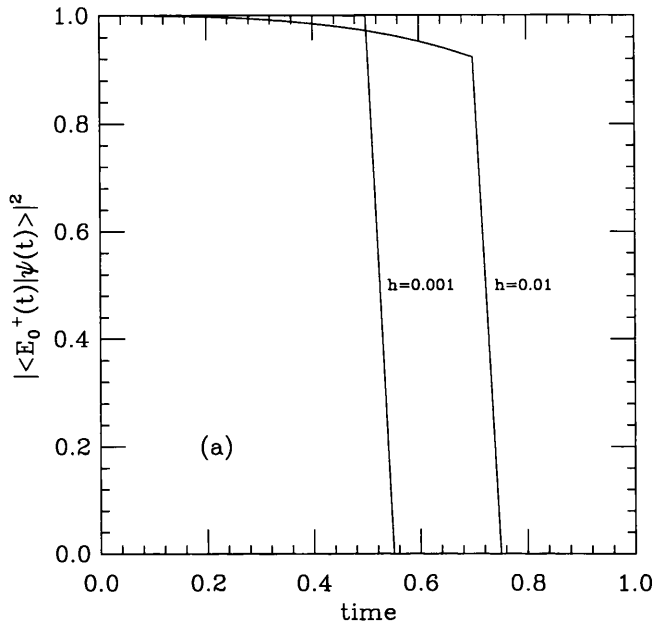


Figure 3.15: (a):  $|\langle E_0^+ | \psi \rangle|^2$  as a function of time for the configurations (3.3.37) for Yukawa couplings  $h = 0.001$  and  $0.01$ . (b):  $|\langle E_0^- | \psi \rangle|^2$  as a function of time for the configurations (3.3.37) for Yukawa couplings  $h = 0.001$  and  $0.01$ .

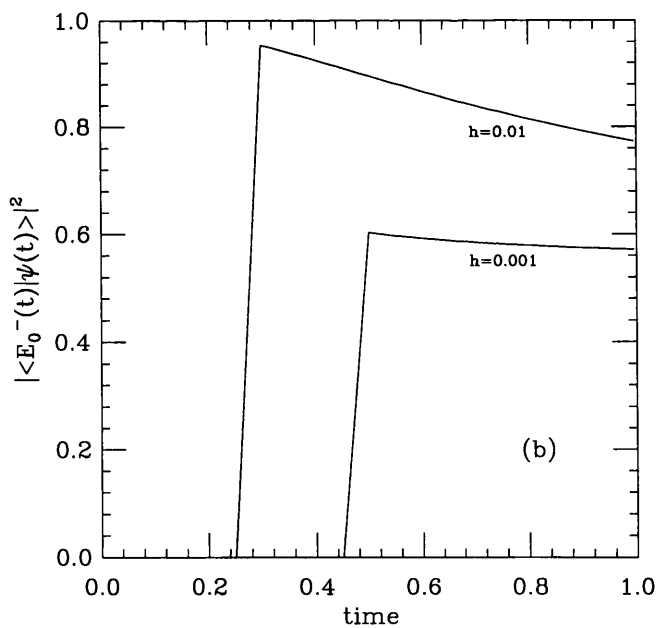
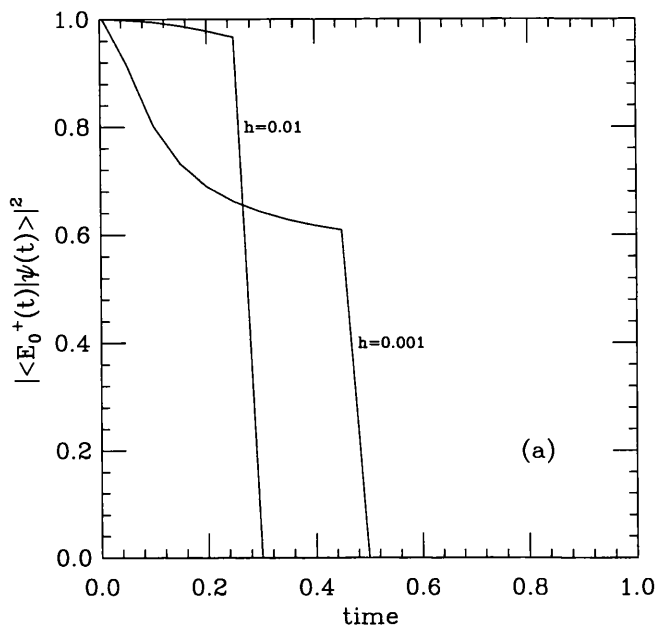


Figure 3.16: (a):  $|\langle E_0^+ | \psi \rangle|^2$  as a function of time for the configurations (3.3.38) for Yukawa couplings  $h = 0.001$  and  $0.01$ . (b):  $|\langle E_0^- | \psi \rangle|^2$  as a function of time for the configurations (3.3.38) for Yukawa couplings  $h = 0.001$  and  $0.01$ .

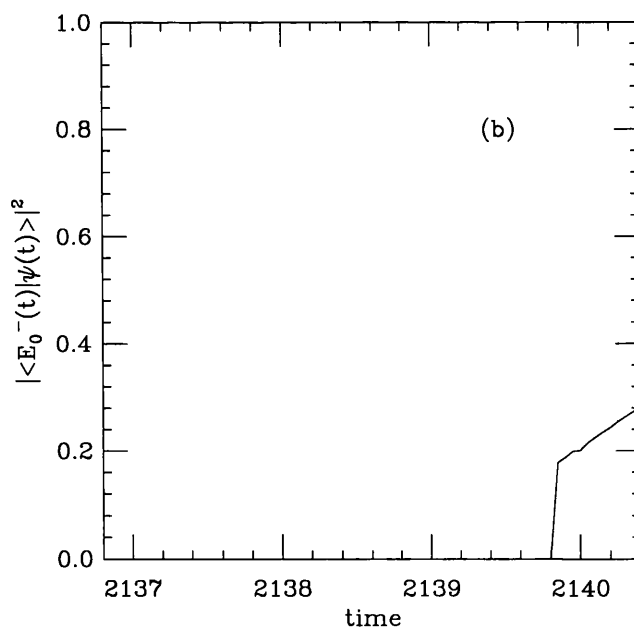
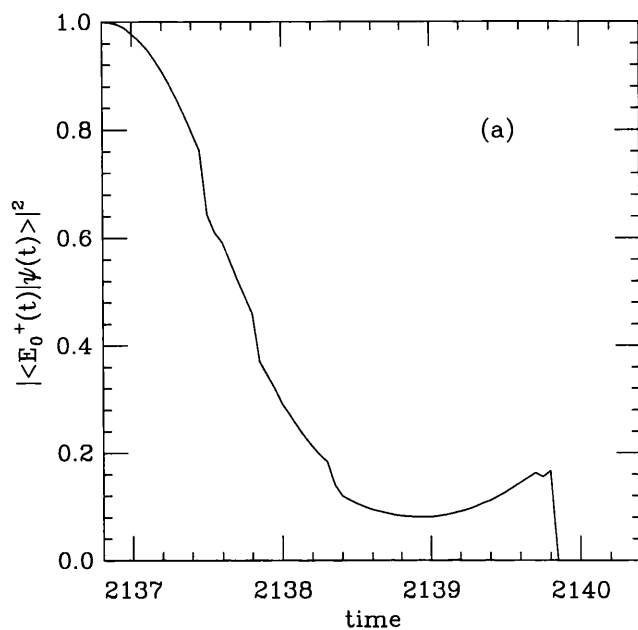


Figure 3.17: (a):  $|\langle E_0^+ | \psi \rangle|^2$  as a function of time for a typical sphaleron transition for the massless Hamiltonian. (b):  $|\langle E_0^- | \psi \rangle|^2$  as a function of time for a typical sphaleron transition for the massless Hamiltonian.

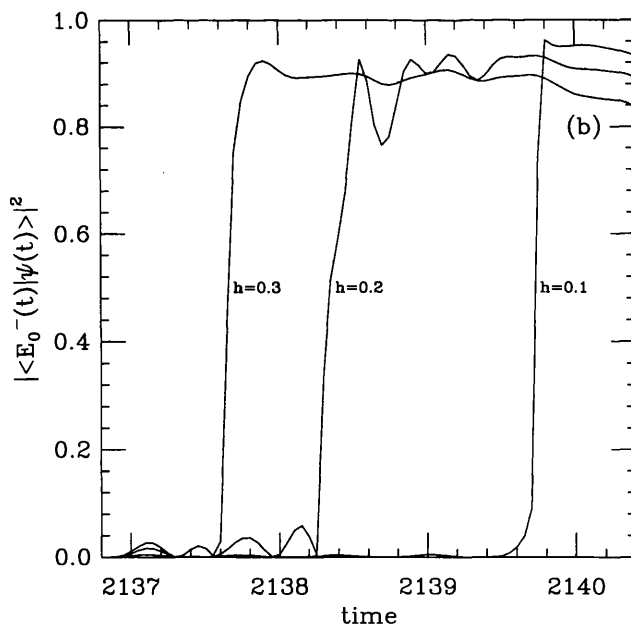
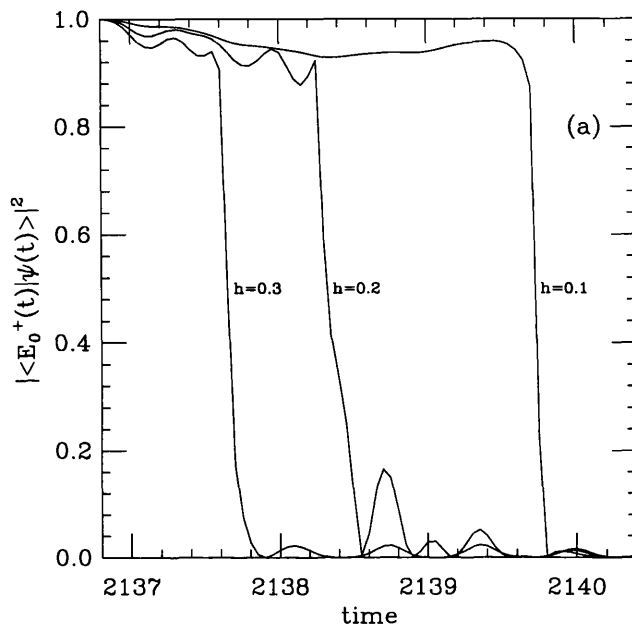


Figure 3.18: (a):  $|\langle E_0^+ | \psi \rangle|^2$  as a function of time for a typical sphaleron transition for Yukawa couplings  $h = 0.1, 0.2$  and  $0.3$ . (b):  $|\langle E_0^- | \psi \rangle|^2$  as a function of time for a typical sphaleron transition for Yukawa couplings  $h = 0.1, 0.2$  and  $0.3$ .

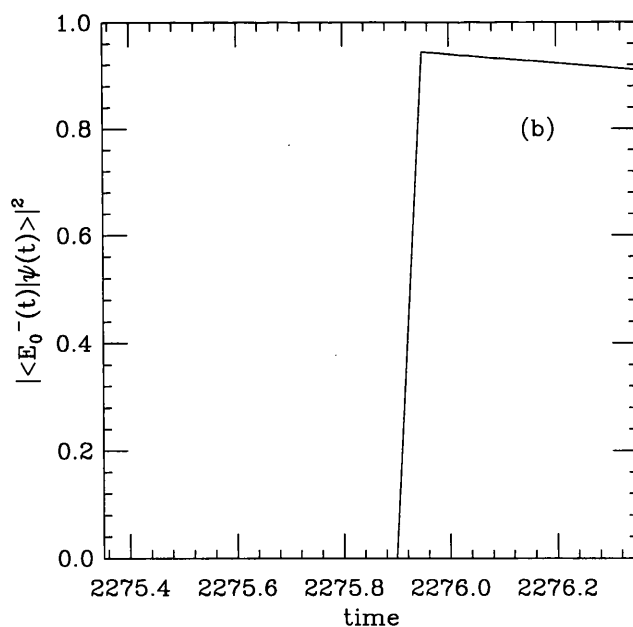
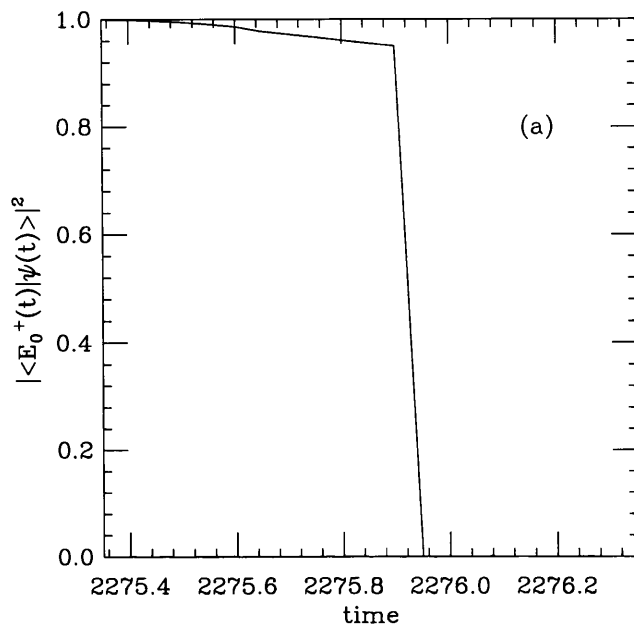


Figure 3.19: (a):  $|\langle E_0^+ | \psi \rangle|^2$  as a function of time for a typical sphaleron transition for the massless Hamiltonian. (b):  $|\langle E_0^- | \psi \rangle|^2$  as a function of time for a typical sphaleron transition for the massless Hamiltonian.

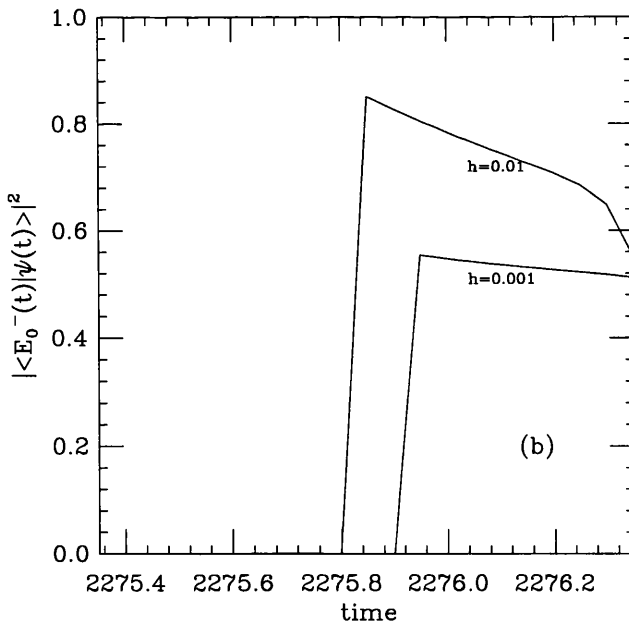
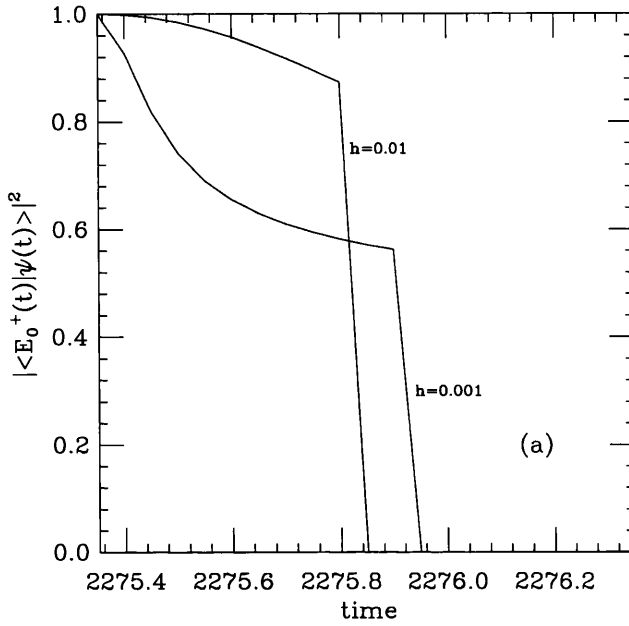


Figure 3.20: (a):  $|\langle E_0^+|\psi\rangle|^2$  as a function of time for a typical sphaleron transition for Yukawa couplings  $h = 0.001$  and  $0.01$ . (b):  $|\langle E_0^-|\psi\rangle|^2$  as a function of time for a typical sphaleron transition for Yukawa couplings  $h = 0.001$  and  $0.01$ .

# Chapter 4

## SU(2) Model in 3+1 Dimensions

### 4.1 Introduction

In Chapter 2 the real time microcanonical method for studying fermion number violation on the lattice was discussed and applied to the  $U(1)$  model in  $1 + 1$  dimensions. In this chapter we apply the same method to the  $SU(2)$  model in  $3 + 1$  dimensions. The methods and notation of [5, 24, 25] are used throughout this chapter.

### 4.2 Lattice Gauge-Higgs System

The continuum action of the  $SU(2)$  Higgs model in  $3 + 1$  dimensions is

$$S = \int dt d^3x \left[ -\frac{1}{4} \text{Tr} (F^{\mu\nu} F_{\mu\nu}) + (D^\mu \Phi)^\dagger (D_\mu \Phi) - M^2 \Phi^\dagger \Phi - \lambda (\Phi^\dagger \Phi)^2 \right] \quad (4.2.1)$$

We put this system on a space-time lattice with lattice spacing  $a$  in the spatial directions and  $a\Delta t$  in the temporal direction.

$$S = \beta_G \left\{ \frac{1}{\Delta t} \sum_{\square_t} \left( 1 - \frac{1}{2} \text{Re Tr } U_{\square_t} \right) - \Delta t \sum_{\square_s} \left( 1 - \frac{1}{2} \text{Re Tr } U_{\square_s} \right) \right\} \\ + \frac{\beta_H}{2} \left\{ \frac{1}{\Delta t} \sum_x \left( 2\Phi_x^\dagger \Phi_x - \Phi_x^\dagger U_{x,\hat{0}} \Phi_{x+\hat{0}} - \Phi_{x+\hat{0}}^\dagger U_{x,\hat{0}}^\dagger \Phi_x \right) \right\}$$

$$\begin{aligned}
& -\Delta t \sum_x \left( 6\Phi_x^\dagger \Phi_x - \sum_i \left( \Phi_x^\dagger U_{x,\hat{i}} \Phi_{x+\hat{i}} + \Phi_{x+\hat{i}}^\dagger U_{x,\hat{i}}^\dagger \Phi_x \right) \right) \Big\} \\
& -\beta_R \Delta t \sum_x \left( \Phi_x^\dagger \Phi_x - v^2 \right)^2
\end{aligned} \tag{4.2.2}$$

where  $\hat{i}$  and  $\hat{0}$  are spatial and time-like directions respectively. In Eq. (4.2.2)  $\Phi$  has been rescaled to be  $a\sqrt{\frac{2}{\beta_H}}$  of the continuum Higgs field.

The Higgs field  $\Phi_x$  is an  $SU(2)$  doublet sitting on lattice sites. The lattice gauge field  $U_{x,\hat{0}}$  is an  $SU(2)$  matrix sitting on the link connecting  $x$  and  $x + \hat{0}$  while  $U_{x,\hat{i}}$  sits on the link connecting  $x$  and  $x + \hat{i}$ .  $U_\square$  is the product of links around an elementary plaquette where  $\square_t$  is a plaquette in the  $0 - \hat{i}$  plane and  $\square_s$  is a plaquette in a  $\hat{i} - \hat{j}$  plane.

The lattice parameters in Eq. (4.2.2) and the continuum coupling constants in Eq. (4.2.1) have the following connection at tree-level

$$\begin{aligned}
M^2 &= -\frac{2\beta_R v^2}{\beta_H a^2} \\
\lambda &= \frac{4\beta_R}{\beta_H^2} \\
g^2 &= \frac{4}{\beta_G}
\end{aligned} \tag{4.2.3}$$

where  $a$  denotes the lattice spacing. In accordance with [5] we choose for the vacuum expectation value of the lattice Higgs field

$$v^2 = \frac{2\beta_R + 3\beta_H - 1}{2\beta_R} \tag{4.2.4}$$

The  $W$  and Higgs masses are given by

$$M_W^2 a^2 = \frac{\beta_H}{\beta_G} v^2, \quad M_H^2 a^2 = \frac{8\beta_R}{\beta_H} v^2 \tag{4.2.5}$$

In the following we choose the temporal gauge  $U_{x,\hat{0}} = 1$ . The lattice momenta fields are defined as follows

$$\begin{aligned}
E_{x,\hat{i}} &= \frac{1}{\Delta t} U_{x+\hat{0},\hat{i}} U_{x,\hat{i}}^\dagger \\
P_x &= \frac{1}{\Delta t} \left( \Phi_{x+\hat{0}} - \Phi_x \right)
\end{aligned} \tag{4.2.6}$$

From Eq. (4.2.6)  $\Delta t E_{x,\hat{i}} \in SU(2)$  and so we can write

$$E_{x,\hat{i}} = E_{x,\hat{i}}^4 + i\tau^a E_{x,\hat{i}}^a \quad (4.2.7)$$

where  $\tau^a$  are the Pauli matrices. Then  $\sum_{a=1}^4 E_{x,\hat{i}}^a E_{x,\hat{i}}^a = \frac{1}{\Delta t^2}$ .

Using the principle of least action we derive the equations of motion

$$\begin{aligned} E_{x,\hat{i}}^a &= E_{x-\hat{0},\hat{i}}^a - \frac{1}{2}\Delta t \sum_{j \neq i} \text{Im Tr} \left( \tau^a \left( U_{x,\hat{i}} U_{x+\hat{i},\hat{j}} U_{x+\hat{j},\hat{i}}^\dagger U_{x,\hat{j}}^\dagger + U_{x,\hat{i}} U_{x-\hat{j}+\hat{i},\hat{j}}^\dagger U_{x-\hat{j},\hat{i}}^\dagger U_{x-\hat{j},\hat{j}} \right) \right) \\ &\quad - \frac{\beta_G}{\beta_H} \text{Im} \left( \Phi_x^\dagger \tau^a U_{x,\hat{i}} \Phi_{x+\hat{i}} \right) \\ P_x &= P_{x-\hat{0}} + \Delta t \left\{ \sum_i \left( U_{x,\hat{i}} \Phi_{x+\hat{i}} + U_{x-\hat{i},\hat{i}}^\dagger \Phi_{x-\hat{i}} \right) \right. \\ &\quad \left. - \left( 6 + 4 \frac{\beta_R}{\beta_H} \left( \Phi_x^\dagger \Phi_x - v^2 \right) \right) \Phi_x \right\} \end{aligned} \quad (4.2.8)$$

and the Gauss constraints

$$\Delta_x^a = \frac{\beta_G}{4} \sum_i \text{Im Tr} \left( \tau^a \left( U_{x-\hat{i},\hat{i}}^\dagger E_{x-\hat{i},\hat{i}}^\dagger U_{x-\hat{i},\hat{i}}^\dagger - E_{x,\hat{i}}^\dagger \right) \right) + \frac{\beta_H}{2} \text{Im} \left( \Phi_x^\dagger \tau^a P_x \right) = 0 \quad (4.2.9)$$

which are constants of the motion.

To define a Hamiltonian we take the  $\Delta t \rightarrow 0$  limit of Eq. (4.2.2) and write it in the form

$$S = \int dt (E_K - E_P) \quad (4.2.10)$$

where  $E_K$  is the kinetic energy and  $E_P$  is the potential energy. We can then define a Hamiltonian  $H = E_K + E_P$ .

$$\begin{aligned} aH &= \frac{\beta_G}{2} \sum_{x,\hat{i}} E_{x,\hat{i}}^a E_{x,\hat{i}}^a + \frac{\beta_H}{2} \sum_x P_x^\dagger P_x \\ &\quad + \beta_G \sum_{\square_s} \left( 1 - \frac{1}{2} \text{Re Tr } U_{\square_s} \right) + 3\beta_H \sum_x \Phi_x^\dagger \Phi_x - \beta_H \sum_{x,\hat{i}} \text{Re} \left( \Phi_x^\dagger U_{x,\hat{i}} \Phi_{x+\hat{i}} \right) \\ &\quad + \beta_R \sum_x \left( \Phi_x^\dagger \Phi_x - v^2 \right)^2 \end{aligned} \quad (4.2.11)$$

In accordance with [5] we chose the temperature  $T = \frac{1}{a}$  (the motivation for this identification was discussed in Section 2.2). In addition we chose  $\Delta t = 0.05$  which ensures that the energy is well conserved as is the Gauss constraint.

### 4.3 Numerical Procedure

We follow the same numerical procedure as for the  $U(1)$  model in 3+1 dimensions. The modified Metropolis technique is used to take account of the 3 Gauss constraints per site. In this case the Hamiltonian is modified to

$$H' = H + G \sum_{x,a} \Delta_x^a \Delta_x^a \quad (4.3.12)$$

After thermalisation the Gauss constraint was further reduced by applying the following "Langevin" cooling equations.

$$\begin{aligned} E_{x,i}^a(t + \Delta t) &= E_{x,i}^a(t) + \Delta t \frac{\partial \Delta^2}{\partial E_{x,i}^a} \\ \Phi_x(t + \Delta t) &= \Phi_x(t) + \Delta t \frac{\partial \Delta^2}{\partial \Phi_x^\dagger} \\ U_{x,i}(t + \Delta t) &= e^{-\frac{1}{2} \Delta t r^a \nabla^a \Delta^2} U_{x,i}(t) \end{aligned} \quad (4.3.13)$$

where  $\Delta^2 = \sum \Delta_x^a \Delta_x^a$ .  $\nabla^a \Delta^2$  is the derivative of  $\Delta^2$  with respect to the link  $U_{x,i}$ .

$$\nabla^a \Delta^2(U_{x,i}) = \frac{\partial}{\partial \alpha} \Delta^2 \left[ e^{\frac{1}{2} i \alpha r^a} U_{x,i} \right]_{\alpha=0} \quad (4.3.14)$$

As before we minimised  $\Delta^2$  with 1000 cooling sweeps and cooling timestep  $\Delta t = 0.05$ . An alternative thermalisation method has been suggested in [32] which ensures that the constraint is exactly satisfied. The method has been applied to the full  $SU(2)$ -Higgs theory [7] and the pure  $SU(2)$  theory (which should be a good approximation to the full theory for temperatures  $T \gg T_C$ ) [6].

As before the system was thermalised with 5000 Metropolis sweeps and 5 hits per site/link in every sweep. As expected we found the total energy after thermalisation to agree well with that predicted by the classical equipartition theorem

$$\left\langle \frac{H}{T} \right\rangle = 10N^3 \quad (4.3.15)$$

on an  $N^3$  lattice, since in this case we have 20 degrees of freedom per site.

## 4.4 Choice of Parameters

In calculating the transition rate for the  $SU(2)$  model in  $3+1$  dimensions, Arnold and McLerran [20] worked in the approximation  $\lambda \sim g^2$ . We approximate this condition by setting  $M_W = M_H$  which from Eq. (4.2.5) gives

$$\beta_R = \frac{\beta_H^2}{8\beta_G} \quad (4.4.16)$$

so that  $\beta_R$  is fixed once we have chosen  $\beta_G, \beta_H$ .

If we denote the sphaleron radius in units  $a$  by  $k = \frac{1}{M_W a}$  then the lattice calculation is only valid in the range

$$2 \leq k \leq \frac{N}{4} \quad (4.4.17)$$

for an  $N^3$  lattice.

Finally we require  $x = \frac{E_{SPH}}{T} \gg 1$  for the rate equation Eq. (1.4.37) to be valid. Since  $E_{SPH} \sim \frac{2M_W}{\alpha_W}$  we have  $x = \frac{2M_W}{T\alpha_W}$ . Using  $\alpha_W = \frac{1}{\beta_G \pi}$ ,  $T = \frac{1}{a}$  and  $M_W = \frac{1}{ka}$  we thus require

$$x = \frac{2\pi\beta_G}{k} \gg 1 \quad (4.4.18)$$

On the other hand if  $x$  is too large then the sphaleron barrier far exceeds the temperature and the transition rate will be suppressed. As in the  $1+1$  dimensional case the choice  $x \sim 10$  seems reasonable. Choosing  $k$  in accordance with Eq. (4.4.17) we thus can find  $\beta_G = \frac{xk}{2\pi}$ . We thus have  $\beta_G \sim 3 - 6$  for reasonable lattice sizes ( $8^3$  to  $16^3$ ). Now using Eqs. (4.2.5) and (4.4.16) we have the following quadratic to solve for  $\beta_H$ .

$$\frac{1}{\beta_G}\beta_H^2 + \left(12 - \frac{1}{k^2}\right)\beta_H - 4 = 0 \quad (4.4.19)$$

Solving for  $\beta_H$  we find  $\beta_H \approx \frac{4}{12 - \frac{1}{k^2}}$ . This gives  $\beta_H \sim 0.34$  for typical values of  $k$  consistent with Eq. (4.4.17). Unfortunately as shown in [5] (by measuring  $\langle |\Phi|^2 \rangle$  for example) for such values of  $\beta_G, \beta_H$  the system is in the phase where  $SU(2)$  symmetry is restored.

We are thus forced to work in the symmetric phase where the analytic expression for the rate Eq. (1.4.37) fails. In this phase the rate is given by  $\Gamma = \kappa(\alpha_W T)^4$  where  $\kappa$  is a non-perturbative constant. In lattice units the number of transitions in lattice time  $t$  is thus

$$N = \frac{\kappa}{\pi^4} \frac{N^3}{\beta_G^4} t \quad (4.4.20)$$

So we would like  $\frac{N^3}{\beta_G^4}$  to be large. On the other hand it can be shown [5] that the thermal fluctuations of Chern-Simons number about a given  $N_{CS}$  sector  $\langle N_{CS}^2 \rangle \approx 0.001 \frac{N^3}{\beta_G^2}$  which we would like to be small. So we have a situation of competing interests. From [5] we know  $\beta_G = 12$  is a good choice for a  $16^3$  lattice. We choose  $\beta_H = 0.34$  which ensures the system is in the symmetric phase as discussed above and  $\beta_R$  is fixed by Eq. (4.4.16).

## 4.5 Topological Measurements

For the  $SU(2)$  theory in  $3 + 1$  dimensions there is no simple lattice expression for the Chern-Simons number. However the change in Chern-Simons number can be written as an integral over the gauge-invariant object  $\text{Tr} (F_{\mu\nu} \tilde{F}^{\mu\nu})$ , the "topological charge density".

$$N_{CS}(t) - N_{CS}(0) = \frac{1}{16\pi^2} \int_0^t dt \int d^3x \text{Tr} (F_{\mu\nu} \tilde{F}^{\mu\nu}) \quad (4.5.21)$$

On the lattice  $\int dt \int d^3x \text{Tr} (F_{\mu\nu} \tilde{F}^{\mu\nu})$  can be written [37]

$$\int dt \int d^3x \text{Tr} (F_{\mu\nu} \tilde{F}^{\mu\nu}) = \sum_x \frac{1}{16} \sum_{\mu, \nu, \rho, \sigma = \pm 0}^{\pm 3} \tilde{\epsilon}_{\mu\nu\rho\sigma} \left[ \frac{1}{2} \text{Tr} (U_{x,\mu\nu} U_{x,\rho\sigma}) - \frac{1}{4} \text{Tr} U_{x,\mu\nu} \text{Tr} U_{x,\rho\sigma} \right] \quad (4.5.22)$$

where  $\tilde{\epsilon}_{0123} = -\tilde{\epsilon}_{1023} = -\tilde{\epsilon}_{-0123} = 1$  etc.  $U_{x,\mu\nu}$  are plaquettes in the  $\mu\nu$  plane originating at the site  $x$ .

$$U_{x,\mu\nu} = U_{x,\hat{\mu}} U_{x+\hat{\mu},\hat{\nu}} U_{x+\hat{\nu},\hat{\mu}}^\dagger U_{x,\hat{\nu}}^\dagger \quad (4.5.23)$$

A typical measurement of the change in Chern-Simons number during the time evolution is shown in figure 4.1. As in the 1 + 1 dimensional case,  $N_{CS}$  spends most of the time fluctuating around integer values with occasional rapid jumps between integer values. Actually since we have used a simple version of  $\Delta N_{CS}$  we find typically  $\Delta N_{CS} \sim 0.75$  rather than 1 due to large fluctuations in the gauge field. In comparison using "smooth" backgrounds we find  $\Delta N_{CS}$  very close to 1. The picture can thus be improved [24] by smoothing the gauge field configurations, by applying the following "Langevin" cooling equations

$$\begin{aligned}\Phi_x(t + \Delta t) &= \Phi_x(t) + \Delta t \frac{\partial H}{\partial \Phi_x^\dagger} \\ U_{x,i}(t + \Delta t) &= e^{-\frac{1}{2}\Delta t \tau^a \nabla^a H} U_{x,i}(t)\end{aligned}\tag{4.5.24}$$

where  $H$  is the Hamiltonian.  $\nabla^a H$  is the derivative of  $H$  with respect to the link  $U_{x,i}$  (see Eq. (4.3.14) for the definition). The effect of applying these equations is shown in figure 4.2. Figure 4.2a shows a typical sphaleron transition where the Chern-Simons number changes by one unit. In figure 4.2b each of the configurations has been subjected to 60 cooling sweeps with  $\Delta t = 0.05$ . The effect of cooling is to smooth the configurations by stripping off the high momentum modes while at the same time the low momentum modes (which according to Section 2.2 are precisely those modes which are responsible for  $\Delta N_{CS} = 1$ ) survive.

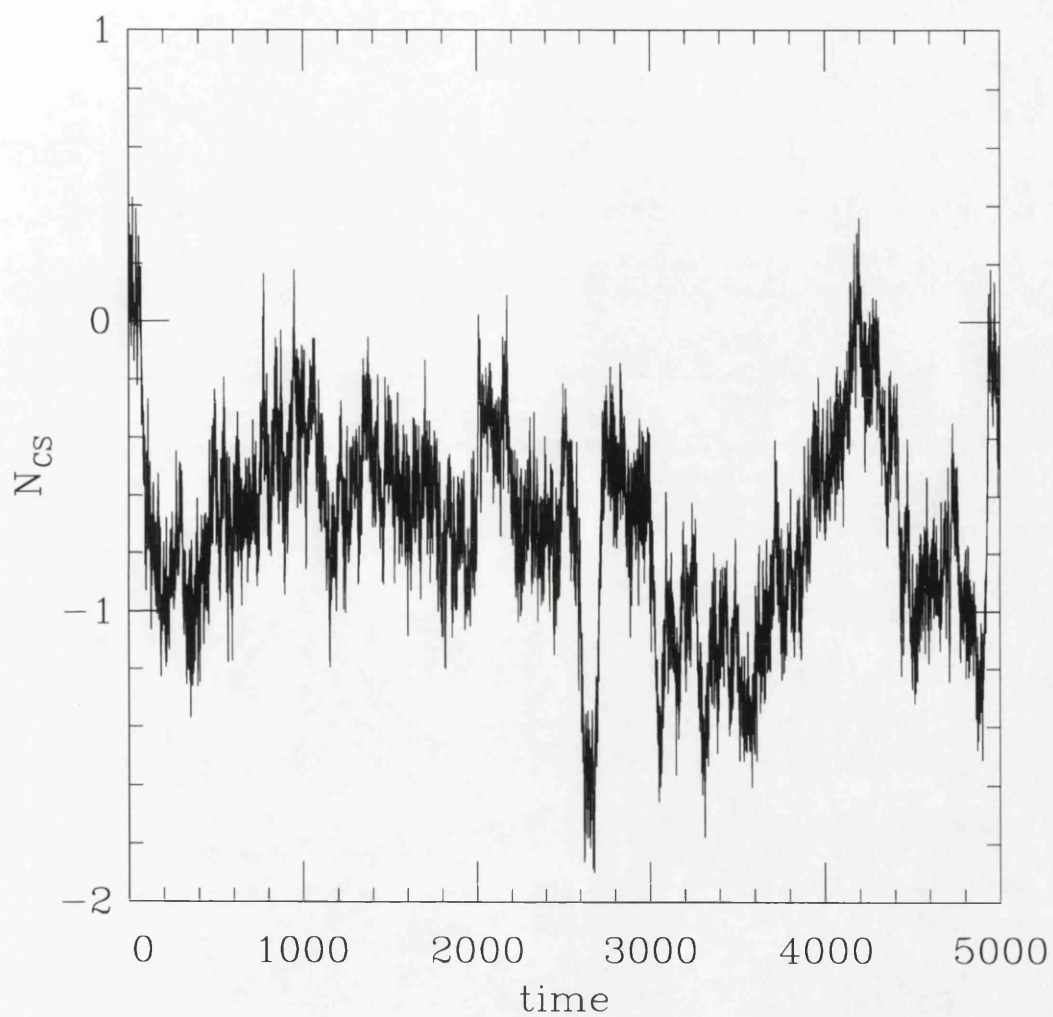


Figure 4.1: The Chern-Simons number as a function of time for  $\beta_G = 12$ ,  $\beta_H = 0.34$ ,  $\beta_R = 0.0012$ . The lattice size is  $16^3$ .

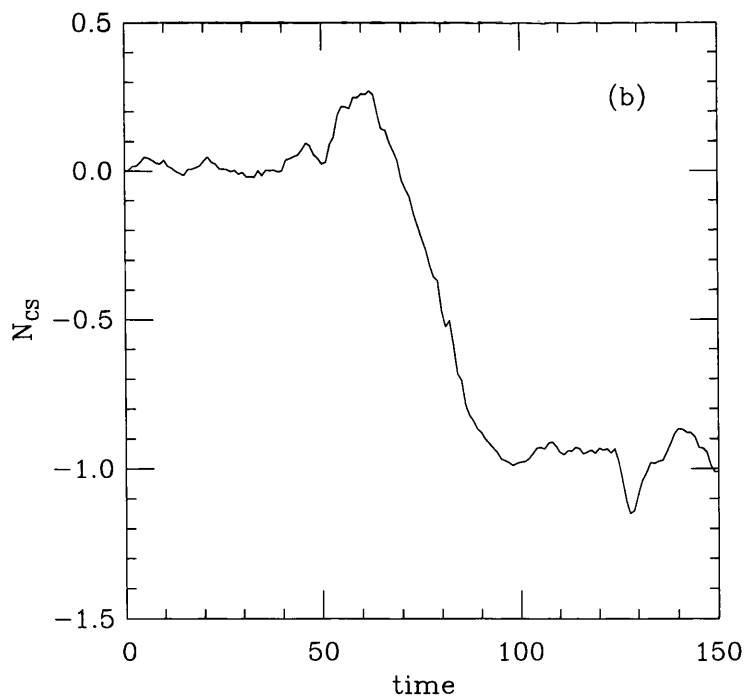
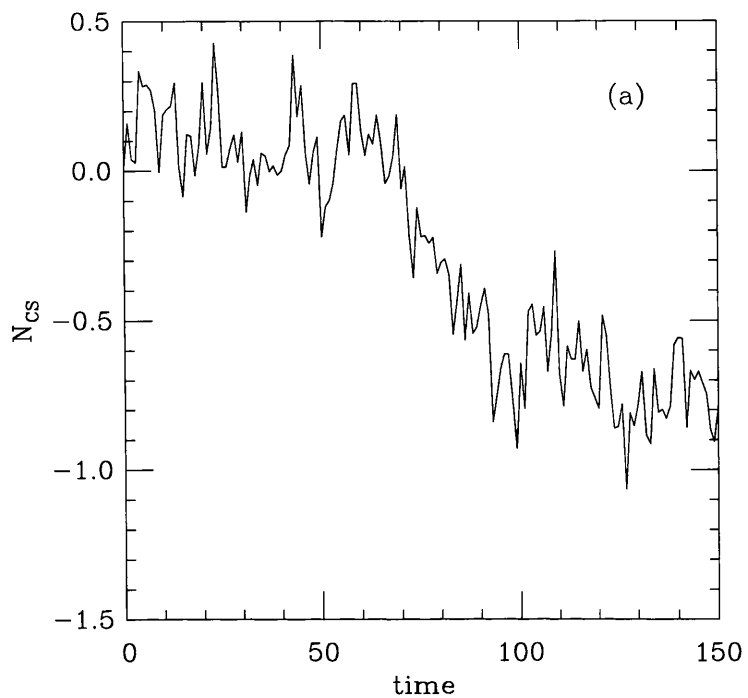


Figure 4.2: The Chern-Simons number as a function of time for a typical sphaleron transition. (a): no cooling. (b): 60 cooling sweeps.

# Chapter 5

## Level Crossing in $SU(2)$ Model in $3+1$ Dimensions

### 5.1 Introduction

In Chapter 3 the level crossing picture was verified for the  $U(1)$  model in  $1+1$  dimensions by measuring the eigenvalues and eigenvectors of the fermion Hamiltonian. In this chapter the same methods are applied to the  $SU(2)$  model in  $3+1$  dimensions. Firstly we measure the lowest energy eigenvalue and chirality, essentially reproducing the results of [25]. We then check the level crossing interpretation using the "overlap" method discussed in Section 3.4.

### 5.2 Lattice Eigenvalue Equations

The continuum time-independent Dirac equation for a free particle in  $3+1$  dimensions is

$$(-i\alpha_i \nabla_i + \beta m) \psi = E\psi \quad (5.2.1)$$

where the hermitian Dirac matrices  $\alpha_i, \beta$  satisfy

$$\{\alpha_i, \alpha_j\} = 2\delta_{ij}, \quad \{\alpha_i, \beta\} = 0, \quad \alpha_i^2 = \beta^2 = 1 \quad (5.2.2)$$

In 3+1 dimensions these relations can be satisfied by 4 by 4 matrices. One specific representation is

$$\alpha_i = \begin{pmatrix} \sigma_i & 0 \\ 0 & -\sigma_i \end{pmatrix}, \quad \beta = \begin{pmatrix} 0 & I \\ I & 0 \end{pmatrix} \quad (5.2.3)$$

where  $\sigma_i$  are the Pauli matrices. In this representation the upper 2-component spinor has chirality +1 and is denoted  $\psi^R$  while the lower 2-component spinor has chirality -1 and is denoted  $\psi^L$ .

$$\begin{aligned} -i\sigma_i \nabla_i \psi^R + m\psi^L &= E\psi^R \\ i\sigma_i \nabla_i \psi^L + m\psi^R &= E\psi^L \end{aligned} \quad (5.2.4)$$

As in the 1+1 dimensional case the "naive" discretisation of Eq. (5.2.4),

$$\begin{aligned} \frac{-i}{2a} \sum_{i=1}^3 \sigma_i (\chi_{x+i}^0 - \chi_{x-i}^0) + m\chi_x^1 &= E\chi_x^0 \\ \frac{i}{2a} \sum_{i=1}^3 \sigma_i (\chi_{x+i}^1 - \chi_{x-i}^1) + m\chi_x^0 &= E\chi_x^1 \end{aligned} \quad (5.2.5)$$

suffers from the doubling problem, i.e. gives additional copies of Eq. (5.2.4) in the continuum limit. In this case the lattice eigenvalues are given by

$$E^2 = \frac{1}{a^2} \sum_{i=1}^3 \sin^2(ak_i) + m^2 \quad (5.2.6)$$

where

$$-\frac{\pi}{a} < k_i \leq \frac{\pi}{a} \quad (5.2.7)$$

Now since  $\sin(k_i a + \pi) = -\sin(k_i a)$  for all  $i$  there is a doubling of states for each space dimension, i.e. 8 times too many states.

The number of extra states can be reduced by the process of "spin diagonalisation". If we make the following unitary transformation of the fermion fields,

$$\chi_x \rightarrow \sigma_1^{x_1} \sigma_2^{x_2} \sigma_3^{x_3} \chi_x \quad (5.2.8)$$

then Eq. (5.2.5) becomes

$$\begin{aligned} \frac{-i}{2a} \sum_{i=1}^3 \eta_i(x) (\chi_{x+i}^0 - \chi_{x-i}^0) + m\chi_x^1 &= E\chi_x^0 \\ \frac{i}{2a} \sum_{i=1}^3 \eta_i(x) (\chi_{x+i}^1 - \chi_{x-i}^1) + m\chi_x^0 &= E\chi_x^1 \end{aligned} \quad (5.2.9)$$

where  $\eta_i(x)$  are the Kawamoto-Smit phases defined as

$$\eta_1(x) = 1, \quad \eta_2(x) = (-1)^{x_1}, \quad \eta_3(x) = (-1)^{x_1+x_2} \quad (5.2.10)$$

Since the two spin components of  $\chi$  in Eq. (3.2.10) are now decoupled we can keep only one component, reducing the number of fermion degrees of freedom per site from 4 to 2. We are however still left with 4 times too many states. We interpret these remaining states as in the 1 + 1 dimensional case, i.e. as additional fermion flavours.

To identify the continuum fields we split the lattice into elementary cubes with origins at  $2x$  and define new fields  $\chi_{x,\rho}$  as follows

$$\chi_{x,\rho} = \chi_{2x+\hat{\rho}} \quad (5.2.11)$$

where  $\hat{\rho} = (\rho_1, \rho_2, \rho_3)$  is a vector whose components can be 0 or 1. Rewriting Eq. (5.2.9) in terms of these fields gives

$$\begin{aligned} -i \sum_{i=1}^3 \left( \Gamma_{\rho\rho'}^i \nabla_i \chi_{x,\rho'}^0 + a \Gamma_{\rho\rho'}^{5i} \nabla_i^2 \chi_{x,\rho'}^0 \right) + m\chi_{x,\rho}^1 &= E\chi_{x,\rho}^0 \\ i \sum_{i=1}^3 \left( \Gamma_{\rho\rho'}^i \nabla_i \chi_{x,\rho'}^1 + a \Gamma_{\rho\rho'}^{5i} \nabla_i^2 \chi_{x,\rho'}^1 \right) + m\chi_{x,\rho}^0 &= E\chi_{x,\rho}^1 \end{aligned} \quad (5.2.12)$$

where  $\nabla_i$  and  $\nabla_i^2$  are first and second central differences on the lattice with lattice spacing  $2a$

$$\begin{aligned} \nabla_i \chi_{x,\rho} &= \frac{1}{4a} (\chi_{x+i,\rho} - \chi_{x-i,\rho}) \\ \nabla_i^2 \chi_{x,\rho} &= \frac{1}{4a^2} (\chi_{x+i,\rho} + \chi_{x-i,\rho} - 2\chi_{x,\rho}) \end{aligned} \quad (5.2.13)$$

and  $\Gamma^i, \Gamma^{5i}$  are defined as

$$\begin{aligned}\Gamma_{\rho\rho'}^i &= (\delta_{\rho+i,\rho'} + \delta_{\rho-i,\rho'}) \eta_i(\rho) \\ \Gamma_{\rho\rho'}^{5i} &= (\delta_{\rho-i,\rho'} - \delta_{\rho+i,\rho'}) \eta_i(\rho)\end{aligned}\quad (5.2.14)$$

The continuum fields  $\psi_x^{\alpha a}$  are given as linear combinations of the  $\chi_{x,\rho}$  fields.

$$\psi_x^{\alpha a} = \frac{1}{2} \sum_{\rho,\rho_4} T_{\rho,\rho_4}^{\alpha a} \chi_{x,\rho}^{\rho_4} \quad (5.2.15)$$

where the matrices  $T_{\rho,\rho_4}$  are defined in terms of the Dirac matrices  $\alpha_i, \beta$  as

$$T_{\rho,\rho_4} = \beta^{\rho_4} \alpha_1^{\rho_1} \alpha_2^{\rho_2} \alpha_3^{\rho_3} \quad (5.2.16)$$

Eq. (5.2.12) can now be written

$$-i \sum_{i=1}^3 \left( \alpha_i^{\alpha\beta} \nabla_i \psi_x^{\beta a} + a (\beta\gamma_5)^{\alpha\beta} (\alpha_i \beta \gamma_5)^{ab} \psi_x^{\beta b} \right) + \beta^{\alpha\beta} m \psi_x^{\beta a} = E \psi_x^{\alpha a} \quad (5.2.17)$$

In the limit as  $a \rightarrow 0$  Eq. (5.2.17) gives 4 copies of Eq. (5.2.4), if we identify  $\alpha$  as the Dirac index and  $a$  as the flavour.

For the purposes of our numerical calculations we rescale the  $\chi$  fields, energy  $E$  and mass  $m$  according to

$$\chi^{0,1} \rightarrow \frac{1}{a^{3/2}} \chi^{0,1}, \quad E \rightarrow \frac{1}{a} E, \quad m \rightarrow \frac{1}{a} m \quad (5.2.18)$$

so that Eq. (5.2.9) becomes

$$\begin{aligned}\frac{-i}{2} \sum_{i=1}^3 \eta_i(x) (\chi_{x+i}^0 - \chi_{x-i}^0) + m \chi_x^1 &= E \chi_x^0 \\ \frac{i}{2} \sum_{i=1}^3 \eta_i(x) (\chi_{x+i}^1 - \chi_{x-i}^1) + m \chi_x^0 &= E \chi_x^1\end{aligned}\quad (5.2.19)$$

With this normalisation the total chirality on the lattice is

$$\langle \Gamma_5 \rangle = \sum_x \psi_x^{\dagger a\alpha} \gamma_5^{\alpha\beta} \psi_x^{\beta a} \quad (5.2.20)$$

Using Eq. (5.2.15) this can be expressed in terms of  $\chi^0, \chi^1$

$$\langle \Gamma_5 \rangle = \frac{i}{2^3} \sum_x \sum_{ijk=\pm 1} (-1)^{x_2} \left( \chi_x^{\dagger 0} \chi_{x+i+j\hat{2}+k\hat{3}}^0 - \chi_x^{\dagger 1} \chi_{x+i+j\hat{2}+k\hat{3}}^1 \right) \quad (5.2.21)$$

We can consider  $\chi^1, \chi^2$  to be  $SU(2)$  doublets in Eq. (5.2.9) and couple them to the lattice gauge field  $U_{x,i}$  in the usual gauge invariant way

$$\begin{aligned} \frac{-i}{2} \sum_{i=1}^3 \eta_i(x) \left( U_{x,i} \chi_{x+i}^0 - U_{x-i,i}^\dagger \chi_{x-i}^0 \right) + m \chi_x^1 &= E \chi_x^0 \\ \frac{i}{2} \sum_{i=1}^3 \eta_i(x) \left( U_{x,i} \chi_{x+i}^1 - U_{x-i,i}^\dagger \chi_{x-i}^1 \right) + m \chi_x^0 &= E \chi_x^1 \end{aligned} \quad (5.2.22)$$

The chirality is modified to

$$\langle \Gamma_5 \rangle = \frac{i}{2} \sum_x \sum_{ijk=\pm 1} (-1)^{x_2} \left( \chi_x^0 U_{111} \chi_{x+i\hat{1}+j\hat{2}+k\hat{3}}^0 - \chi_x^1 U_{111} \chi_{x+i\hat{1}+j\hat{2}+k\hat{3}}^1 \right) \quad (5.2.23)$$

where  $U_{111}$  is the average of the link products over the 6 paths connecting the sites  $x$  and  $x + i\hat{1} + j\hat{2} + k\hat{3}$ . This ensures that the definition is gauge invariant.

In the massless case  $\chi^0, \chi^1$  decouple and we can keep a single doublet  $\chi^0$  so that Eq. (5.2.22) becomes

$$\frac{-i}{2} \sum_{i=1}^3 \eta_i(x) \left( U_{x,i} \chi_{x+i}^0 - U_{x-i,i}^\dagger \chi_{x-i}^0 \right) = E \chi_x^0 \quad (5.2.24)$$

Since the number of degrees of freedom has been halved we now have 4 Weyl fermions in the continuum limit. The chirality is modified to

$$\langle \Gamma_5 \rangle = \frac{i}{2} \sum_x \sum_{ijk=\pm 1} (-1)^{x_2} \chi_x^0 U_{111} \chi_{x+i\hat{1}+j\hat{2}+k\hat{3}}^0 \quad (5.2.25)$$

which is a conserved quantum number in the continuum limit (though the order  $a$  term in the lattice Hamiltonian breaks the chiral symmetry). In the continuum there is a chiral anomaly which in this case is

$$\Delta \Gamma_5 = 4 \Delta N_{CS} \quad (5.2.26)$$

since we have 4 Weyl fermions.

Alternatively we can consider the case where  $\chi^0$  is an  $SU(2)$  doublet but  $\chi^1$  is a singlet. In this case the requirement of gauge invariance forbids an explicit mass term and the fermion mass is introduced by a Yukawa coupling to the lattice

Higgs field.

$$\begin{aligned} \frac{-i}{2} \sum_{i=1}^3 \eta_i(x) \left( U_{x,i} \chi_{x+i}^0 - U_{x-i,i}^\dagger \chi_{x-i}^0 \right) + M_x \chi_x^1 &= E \chi_x^0 \\ \frac{i}{2} \sum_{i=1}^3 \eta_i(x) \left( \chi_{x+i}^1 - \chi_{x-i}^1 \right) + M_x^\dagger \chi_x^0 &= E \chi_x^1 \end{aligned} \quad (5.2.27)$$

where  $M_x$  is constructed from the Higgs doublet  $\Phi_x$  as follows

$$M_x = \begin{pmatrix} \phi_0^* & \phi_+ \\ -\phi_+^* & \phi_0 \end{pmatrix} \begin{pmatrix} h_u & 0 \\ 0 & h_d \end{pmatrix}, \quad \Phi_x = \begin{pmatrix} \phi_+ \\ \phi_0 \end{pmatrix} \quad (5.2.28)$$

$h_u$  and  $h_d$  are independent Yukawa couplings. Since  $\chi^1$  is now a singlet the gauge invariant definition of chirality is

$$\langle \Gamma_5 \rangle = \frac{i}{2} \sum_x \sum_{ijk=\pm 1} (-1)^{x_2} \left( \chi_x^0 U_{111} \chi_{x+i\hat{1}+j\hat{2}+k\hat{3}}^0 - \chi_x^1 \chi_{x+i\hat{1}+j\hat{2}+k\hat{3}}^1 \right) \quad (5.2.29)$$

As in the free field case there are lattice doublers so that Eq. (5.2.27) describes four flavours with common Yukawa couplings  $h_u, h_d$  in the continuum limit (in practice we choose for simplicity  $h_u = h_d$  so that all 4 flavours are degenerate in mass). In the continuum limit Eq. (5.2.27) gives

$$\begin{pmatrix} -i\alpha_i D_i & \beta M \\ \beta M^\dagger & -i\alpha_i \partial_i \end{pmatrix} \begin{pmatrix} \psi \\ \chi \end{pmatrix} = E \begin{pmatrix} \psi \\ \chi \end{pmatrix} \quad (5.2.30)$$

where  $\psi = \begin{pmatrix} \psi^{1,R} \\ \psi^{3,L} \end{pmatrix}$ ,  $\begin{pmatrix} \psi^{2,R} \\ \psi^{4,L} \end{pmatrix}$ ,  $\chi = \begin{pmatrix} \psi^{3,R} \\ \psi^{1,L} \end{pmatrix}$ ,  $\begin{pmatrix} \psi^{4,R} \\ \psi^{2,L} \end{pmatrix}$ . ( $\psi^{a,R}, \psi^{a,L}$  are the

upper and lower 2 components of  $\psi^{\alpha a}$  in the chiral representation). Note that for two of these flavours ( $a = 1, 2$ ) only the right handed component couples to the gauge field, while for flavours  $a = 3, 4$  only the left handed component couples to

the gauge field. Hence the total fermion number  $N_F^1 + N_F^2 + N_F^3 + N_F^4$  is conserved for the lattice system since

$$\Delta N_F^1 = \Delta N_F^2 = -\Delta N_F^3 = -\Delta N_F^4 = \Delta N_{CS} \quad (5.2.31)$$

However as discussed in Section 3.2 we can still study fermion number violation by considering the generalised chirality  $\tilde{\Gamma}_5$  defined here as  $\langle \tilde{\Gamma}_5 \rangle = N_F^1 + N_F^2 - N_F^3 - N_F^4$ .  $\tilde{\Gamma}_5$  labels the particular fermion species with  $\psi^1$  and  $\psi^2$  having  $\tilde{\Gamma}_5 = +1$  and  $\psi^3$  and  $\psi^4$  having  $\tilde{\Gamma}_5 = -1$ . From Eq. (5.2.31)  $\tilde{\Gamma}_5$  has an anomaly

$$\Delta \tilde{\Gamma}_5 = 4\Delta N_{CS} \quad (5.2.32)$$

$\tilde{\Gamma}_5$  can be written in terms of the lattice fields  $\psi^{\alpha a}$

$$\langle \tilde{\Gamma}_5 \rangle = \int d^3x \psi_x^{\dagger a \alpha} \gamma_5^{ab} \psi_x^{\alpha b} \quad (5.2.33)$$

Note that Eq. (5.2.33)  $\gamma_5$  acts on flavour indices. In terms of the lattice fields  $\chi^1, \chi^2$  we have

$$\langle \Gamma_5 \rangle = \frac{i}{2} \sum_x \sum_{ijk=\pm 1} (-1)^{x_2} \left( \chi_x^{\dagger 0} U_{111} \chi_{x+i\hat{1}+j\hat{2}+k\hat{3}}^0 + \chi_x^{\dagger 1} \chi_{x+i\hat{1}+j\hat{2}+k\hat{3}}^1 \right) \quad (5.2.34)$$

As in the 1+1 dimensional model this differs from the "normal" chirality, Eq. (5.2.29) in the sign of the second term.

### 5.3 Eigenvalue and Chirality Measurements

As in the  $U(1)$  model firstly we investigated the level crossing picture for a set of smooth configurations which interpolate between two topologically distinct vacua. For our  $SU(2)$  model the trivial vacuum with winding number zero is given by

$$U_{x,i}^{(0)} = I, \quad \phi_x^{(0)} = \begin{pmatrix} 0 \\ 1 \end{pmatrix} \quad (5.3.35)$$

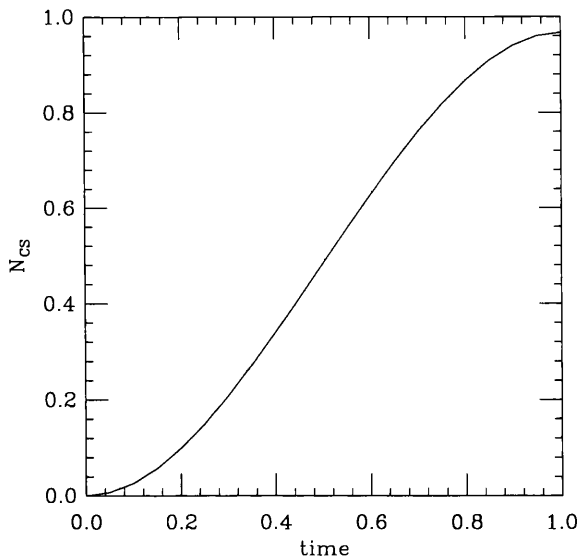


Figure 5.1: The Chern-Simons Number as a function of time for the configurations (5.3.38).

while a vacuum with winding number one is given by

$$\begin{aligned} U_{x,\hat{i}}^{(1)} &= V(x)V^{-1}(x + \hat{i}) = \exp(i\sigma_i u_i(x)) \\ \phi_x^{(1)} &= V(x)\phi_x^{(0)} \end{aligned} \quad (5.3.36)$$

where  $V(x)$  is the following gauge transformation

$$V(x) = (-1) \exp\left(\frac{2\pi i \sigma_i v_i}{L |v(x)|} \max\{|v_j(x)|, j = 1, 2, 3\}\right) \quad (5.3.37)$$

where  $L$  is the linear size of the lattice and  $v_i(x) = x_i - \frac{1}{2}L$ . Different trial cases were investigated as in Section 3.3. In each case we chose the gauge field to smoothly interpolate between  $U^{(0)}$  and  $U^{(1)}$  as follows.

$$U_{x,\hat{i}} = \exp(it \sigma_i u_i(x)) \quad (5.3.38)$$

where the "time" parameter  $t$  varies from 0 to 1.  $u_i(x)$  is defined in Eq. (5.3.36). In figure 5.1 we show the Chern-Simons number as a function of time for the gauge field given by Eq. (5.3.38).

Firstly we considered the Hamiltonian with an explicit mass term, Eq. (5.2.22) (in the case  $m = 0$ , Eq. (5.2.24)). Figure 5.2 shows the lowest positive eigenvalue and chirality  $\Gamma_5$  of the corresponding eigenvector for a variety of masses. In each case we observe the diving of the lowest eigenvalue and chirality flip from positive to negative. The lowest eigenvalue reaches its minimum at  $t = 0.5$  (which corresponds to the time  $t_{CS}$  where  $N_{CS} = \frac{1}{2}$ ). The results are thus very similar to the analogous  $U(1)$  results (see figure 3.1).

In the  $1 + 1$  dimensional case these results were interpreted using the fact that the eigenvalues come in pairs. In the current case there is an analogous symmetry in the spectrum. From Eq. (5.2.27), if  $(\chi_x^0, \chi_x^1)$  is an eigenvector with eigenvalue  $E$  and chirality  $\Gamma_5$  then  $((-1)^{x_1+x_2+x_3} \chi_x^0, -(-1)^{x_1+x_2+x_3} \chi_x^1)$  is an eigenvector with eigenvalue  $-E$  and chirality  $-\Gamma_5$ . As discussed in Section 3.3 for  $m = 0$  this allows us to interpret the results as showing a positive chirality mode crossing zero from above and a negative chirality mode crossing zero from below. For the  $SU(2)$  model we have an additional symmetry. If  $(\chi_x^0, \chi_x^1)$  is an eigenvector with eigenvalue  $E$  and chirality  $\Gamma_5$  then  $(\sigma_2 \chi^{0*}, -\sigma_2 \chi^{1*})$  is an eigenvector with eigenvalue  $-E$  and chirality  $-\Gamma_5$ . Using both these symmetries we can see that each eigenvalue is two-fold degenerate. Hence we can interpret the results as showing two  $\Gamma_5 = +1$  modes crossing zero from above and two  $\Gamma_5 = -1$  modes crossing zero from below. The total change in chiral charge is thus  $|\Delta\Gamma_5| = 4$  in agreement with Eq. (5.2.26).

For the case of the Hamiltonian with a Yukawa term, Eq. (5.2.27), we have investigated a variety of Higgs field configurations with different topological characteristics. We have considered the  $SU(2)$  versions of all 5 trial cases discussed in Section 3.3 for the  $U(1)$  model. The results in each case are in fact very similar to the results of that Section and we present results for just two cases.

#### CASE 1.

$$U_{x,\hat{i}} = \exp(it \sigma_i u_i(x))$$

$$\phi_x = (1-t)\phi_x^{(0)} + t\phi_x^{(1)} \quad (5.3.39)$$

In this case the Higgs field has a zero at time  $t_h = t_{CS} = \frac{1}{2}$ . Measurements of the lowest eigenvalue and generalised chirality  $\tilde{\Gamma}_5$  are shown in figure 5.3 (see figure 3.2 for the analogous  $U(1)$  results). For all values of  $h$  we see the lowest eigenvalue fall to zero and flip in sign of  $\tilde{\Gamma}_5$  from positive to negative. Furthermore for all  $h$  the zero eigenvalue occurs at time  $t_0 = t_{CS} = t_h$ . From Eq. (5.2.27) we have the following symmetries in the spectrum. If  $(\chi_x^0, \chi_x^1)$  is an eigenvector with eigenvalue  $E$  and generalised chirality  $\tilde{\Gamma}_5$  then  $((-1)^{x_1+x_2+x_3}\chi_x^0, -(-1)^{x_1+x_2+x_3}\chi_x^1)$  is an eigenvector with eigenvalue  $-E$  and generalised chirality  $-\tilde{\Gamma}_5$ . In addition for  $h_u = h_d$  (which we always assume for simplicity)  $(\sigma_2\chi^{0*}, -\sigma_2\chi^{1*})$  is an eigenvector with eigenvalue  $-E$  and generalised chirality  $-\tilde{\Gamma}_5$ . Using both these symmetries each eigenvalue is two-fold degenerate and so our results are interpreted as showing two  $\tilde{\Gamma}_5 = +1$  crossing zero from above and two  $\tilde{\Gamma}_5 = -1$  modes crossing zero from below. In the notation of Section 5.2 modes with  $\tilde{\Gamma}_5 = +1$  correspond to flavours  $a = 1, 2$  and modes with  $\tilde{\Gamma}_5 = -1$  to flavours  $a = 3, 4$ . Hence if the level crossing interpretation is correct our results give  $|\Delta(N_F^1 + N_F^2)| = |\Delta(N_F^3 + N_F^4)| = 2$  and  $|\Delta\tilde{\Gamma}_5| = 4$ , in agreement with Eqs. (5.2.31) and (5.2.32).

## CASE 2.

$$\begin{aligned} U_{x,i} &= \exp(it\sigma_i u_i(x)) \\ \phi_x &= (1-\sqrt{t})\phi_x^{(0)} + \sqrt{t}\phi_x^{(1)} \end{aligned} \quad (5.3.40)$$

In this case  $t_h = 0.25$ ,  $t_h < t_{CS}$ . The lowest eigenvalue and generalised chirality  $\tilde{\Gamma}_5$  are shown in figure 5.4 (see figure 3.3 for the analogous  $U(1)$  results). For this case the point  $t_0$  at which level crossing occurs depends upon  $h$ ,  $t_0$  varying continuously from  $t_{CS}$  to  $t_h$  as  $h$  is increased. The other 3 trial cases give very similar results to their  $U(1)$  counterparts (see also [25] for further examples).

We have also investigated the behaviour of the lowest eigenvalue and chirality in the presence of the high temperature gauge and Higgs fields discussed

in Chapter 4. In Section 4.5 fermion number violating "sphaleron" transitions were identified by measuring the change in Chern-Simons number of the gauge fields. As discussed in that section the measurement of  $\Delta N_{CS}$  is sensitive to high momentum fluctuations in the gauge field and is greatly improved by applying Langevin cooling equations, Eq. 4.5.24. This is shown in figure 4.2 with figure 4.2a corresponding to the "raw" configurations and figure 4.2b corresponding to the configurations subjected to 60 cooling sweeps.

Figure 5.5 shows the lowest eigenvalue and chirality for the massless Hamiltonian in the gauge field background without cooling. The effect of the high momentum fluctuations in the gauge field is clear. The lowest eigenvalue doesn't reach zero but just gets below 0.01, while the chirality  $\Gamma_5$  changes gradually from  $\sim -0.75$  to  $\sim +0.75$  rather than the sudden jump from  $-1$  to  $+1$  expected in the ideal massless case. Since  $|\Gamma_5|$  is quite far from 1 chirality is far from being a good quantum number. Indeed our results are closer to what we might expect if the fermion was massive (the mass term of course explicitly breaks chiral symmetry). This reduction in  $\Gamma_5$  due to fluctuations is well known (see for example [25, 38, 39]). As with the measurement of  $\Delta N_{CS}$  the picture is greatly improved after applying cooling equations. Figure 5.6 shows the lowest eigenvalue and chirality for the massless Hamiltonian in the gauge field background after 60 cooling sweeps. The lowest eigenvalue now gets very close to zero while  $\Gamma_5$  suddenly flips from (approximately)  $-1$  to  $+1$ . Since we are using only a simple version of  $\Delta N_{CS}$  we are unable to identify the exact value of the Chern-Simons number where the zero eigenvalue occurs but from our measurements we estimate  $N_{CS} \sim -0.7$ . This contrasts with the  $U(1)$  case where we know that  $N_{CS}$  must be half-integer.

Results for the Hamiltonian with a Yukawa term for 3 values of the Yukawa coupling  $h$  are shown in figures 5.7 and 5.8 for the uncooled and cooled backgrounds respectively. Firstly consider the uncooled case shown in figure 5.7. The results show similar behaviour to the massless case discussed above with fluctu-

ations in the background fields resulting in  $|\tilde{\Gamma}_5|$  less than one. As a function of Yukawa coupling,  $|\tilde{\Gamma}_5|$  decreases with increasing  $h$  showing the effect of fluctuations in the Higgs field. For the largest Yukawa coupling shown  $h = 0.5$  we find  $|\tilde{\Gamma}_5| \sim 0.1$ . As  $h$  is increased further we find  $\tilde{\Gamma}_5$  very close to zero so that it becomes impossible to identify any definite chirality flip. Note also that the time scale over which  $\tilde{\Gamma}_5$  changes from negative to positive gets shorter as  $h$  increases. After 60 cooling sweeps (see figure 5.8) the results are much better with  $\tilde{\Gamma}_5$  close to  $\pm 1$  for all 3 values of  $h$  investigated. Even for  $h = 0.5$  we find  $|\tilde{\Gamma}_5| \sim 0.92$ . However for such large values of  $h$  many cooling sweeps are needed to get  $|\tilde{\Gamma}_5| \sim 1$  whereas for smaller  $h$  we get good results after only a few cooling sweeps. This is shown in figure 5.9 which shows the effect on  $\tilde{\Gamma}_5$  of varying the number of cooling sweeps for  $h = 0.1$  and  $h = 0.5$ . For  $h = 0.1$  20 cooling sweeps are more than sufficient, while for  $h = 0.5$  we need many more sweeps. As discussed in [24] the Langevin cooling equations cause the magnitude of the Higgs field to relax much slower than the gauge field. Hence for large values of  $h$  fluctuations in the Higgs field can still affect the chirality measurements even though the gauge field is already quite smooth.

Note that the exact point at which level crossing occurs  $t_0$  depends upon  $h$ . As shown using the trial configurations this is to be expected for a general Higgs background. Our trial results indicate that  $t_0$  depends on the topology of the Higgs field with the point at which the Higgs winding number changes (the point at which the Higgs field has a zero) becoming increasingly significant as  $h$  is increased. It would be interesting to have some direct measurement of the Higgs topology to verify this as in the case of the  $U(1)$  model (see Section 5.3). Unfortunately we have been unable to locate the zeros of the Higgs field in the  $SU(2)$  model. As discussed in Section 4.4 restrictions on our choice of coupling constants forces us to work in the phase where  $SU(2)$  symmetry is restored and so the expectation value of the Higgs field is small compared to its expectation value

at zero temperature. In addition the thermal fluctuations are large in this phase. The Higgs field thus frequently gets close to zero and it is difficult to distinguish those points where it actually passes through zero. Unfortunately our cooling equations don't help much since they work rather slowly on the magnitude of the Higgs field as mentioned above.

## 5.4 Transition Probability Measurements

In Section 3.4 we discussed a method for investigating the level crossing interpretation directly by following the time evolution of the fermion states. In this section we apply the method to the  $SU(2)$  model. The fermion state  $|\psi\rangle$  was initially chosen to be the lowest positive energy eigenstate. As it evolved the overlap with the lowest positive energy eigenstates  $|\langle E_0^+|\psi\rangle|^2$  and the overlap with the highest negative energy eigenstates  $|\langle E_0^-|\psi\rangle|^2$  were measured. Note that in the  $SU(2)$  model each eigenvalue is two-fold degenerate as discussed in Section 5.3 so that for example  $|\langle E_0^+|\psi\rangle|^2$  is the total probability of finding the fermion in either of the 2 lowest positive energy eigenstates.

Firstly we applied the method to the trial backgrounds discussed in Section 5.3. Figure 5.10 shows  $|\langle E_0^+|\psi\rangle|^2$  and  $|\langle E_0^-|\psi\rangle|^2$  for the massless Hamiltonian in the gauge field background given by Eq. (5.3.38). The sharp drop in  $|\langle E_0^+|\psi\rangle|^2$  and simultaneous rise in  $|\langle E_0^-|\psi\rangle|^2$  at  $t_0 = \frac{1}{2}$  verifies that level crossing occurs at this point. There is however a slight fall in both  $|\langle E_0^+|\psi\rangle|^2$  and  $|\langle E_0^-|\psi\rangle|^2$  away from one indicating a slight dispersion into states other than  $|E_0^+\rangle$  and  $|E_0^-\rangle$ . This is in contrast to the analogous  $U(1)$  results (see figure 3.11) which show almost perfect adiabatic behaviour. For the Hamiltonian with a Yukawa term we have investigated all 5 trial cases and the results are similar to those for the  $U(1)$  model. For example results for CASE 1 and CASE 2 are shown in figures 5.11 and 5.12 respectively. As with the eigenvalue and chirality measurements discussed in the previous section these results are very similar to their  $U(1)$  counterparts (fig-

ures 3.12 and 3.13). As discussed in Section 3.5 the behaviour of  $|\langle E_0^+|\psi\rangle|^2$  and  $|\langle E_0^-|\psi\rangle|^2$  depends upon the Yukawa coupling  $h$ . Unfortunately the relationship is complicated and strongly dependent on the particular gauge-Higgs background.

In the previous section the lowest eigenvalue and chirality were also measured for a high temperature "sphaleron" background. Recall that in this case the level crossing picture was less obvious due to large fluctuations in the background fields. The picture was significantly improved after smoothing the fields using the Langevin cooling equations. Figure 5.13 shows  $|\langle E_0^+|\psi\rangle|^2$  and  $|\langle E_0^-|\psi\rangle|^2$  for the massless Hamiltonian for both uncooled and cooled gauge field backgrounds. In the uncooled case we see a gradual fall in  $|\langle E_0^+|\psi\rangle|^2$  as  $|\psi\rangle$  disperses among the various eigenstates, indicating that the uncooled gauge field is far from adiabatic. In addition we see  $|\langle E_0^-|\psi\rangle|^2$  gradually increasing as  $|\psi\rangle$  becomes the most probable state. Thus  $|\psi\rangle$  gradually evolves from  $|E_0^+\rangle$  into  $|E_0^-\rangle$  in contrast to the sudden transition associated with level crossing. However from the results of the previous section we know that the chirality flip also occurs gradually and in addition the lowest eigenvalue doesn't quite reach zero so that there is a gap separating positive and negative energy states. As noted in that section these results are similar to what we would expect if the fermion was massive. In that case we know (see Section 1.3) that the state doesn't "cross" zero but gradually "hops" across the gap with the amount of "hopping" depending upon the particular gauge field background (for example in the adiabatic limit no hopping occurs). This is exactly what is observed here. The results of the previous section suggests that level crossing only occurs after cooling the backgrounds and this is confirmed here. After 60 cooling sweeps we find the sudden drop drop in  $|\langle E_0^+|\psi\rangle|^2$  and rise in  $|\langle E_0^-|\psi\rangle|^2$  which shows  $|\psi\rangle$  evolving suddenly into  $|E_0^-\rangle$  and is interpreted as showing level crossing. Note that  $|\psi\rangle$  stays in  $|E_0^-\rangle$  with almost unit probability indicating that the cooled gauge field is almost adiabatic.

Similar behaviour is observed for the Hamiltonian with a Yukawa term as

shown in figures 5.14 and 5.15 which give the overlaps for the uncooled and cooled cases respectively. For the uncooled backgrounds the transition from  $|E_0^+\rangle$  to  $|E_0^-\rangle$  is gradual as opposed to the sudden transition expected for level crossing. As discussed above this is to be expected given the corresponding results for the lowest eigenvalue and generalised chirality (see figures 5.7 and 5.8). The transition becomes sharper as  $h$  is increased which is also reflected in the generalised chirality measurements. As expected from the eigenvalue and chirality measurements the level crossing picture is only obtained after cooling the background fields. This is shown in figure 5.15 which indicates  $|\psi\rangle$  evolving suddenly from  $|E_0^+\rangle$  to  $|E_0^-\rangle$ . There is of course a gradual fall in both  $|\langle E_0^+|\psi\rangle|^2$  and  $|\langle E_0^-|\psi\rangle|^2$  away from one showing that the background fields are not adiabatic. For these particular fields this effect increases with increasing  $h$  though as noted in the trial cases above there is no reason to expect this behaviour in general.

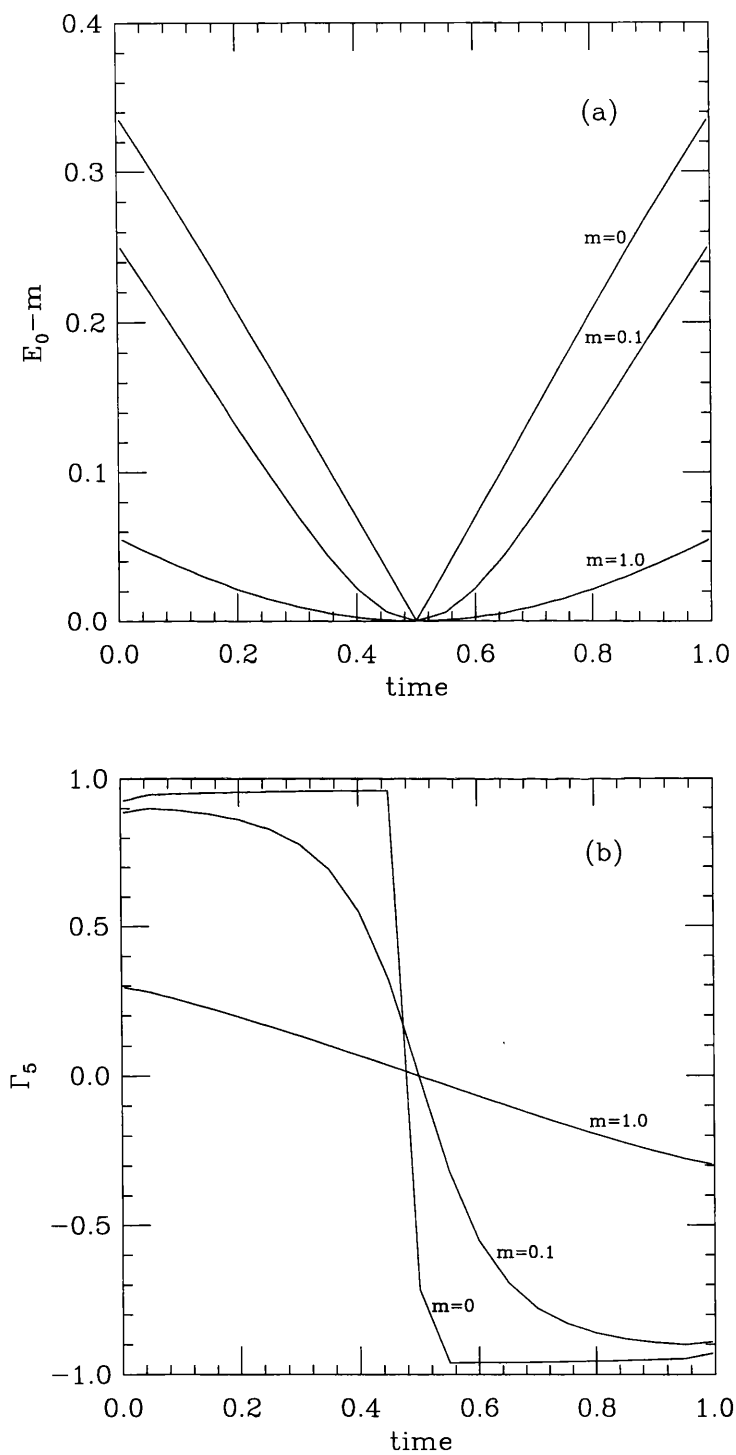


Figure 5.2: (a): The lowest eigenvalue  $E_0$  as a function of time for the configurations (5.3.38) for masses  $m = 0, 0.1$  and  $1.0$ . (b): The chirality  $\Gamma_5$  of the corresponding eigenvector.

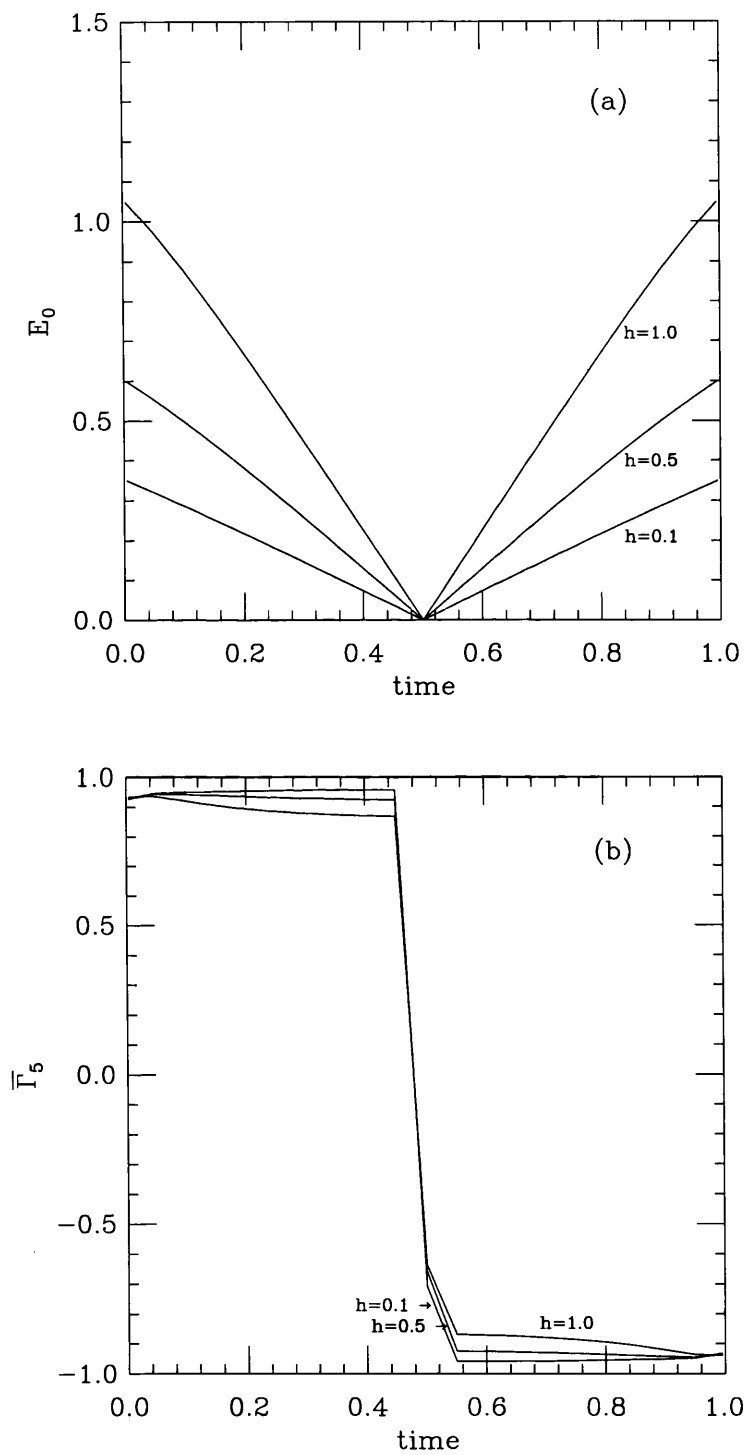


Figure 5.3: (a): The lowest eigenvalue  $E_0$  as a function of time for the configurations (5.3.39) for Yukawa couplings  $h = 0.1, 0.5$  and  $1.0$ . (b): The generalised chirality  $\hat{\Gamma}_5$  of the corresponding eigenvector.

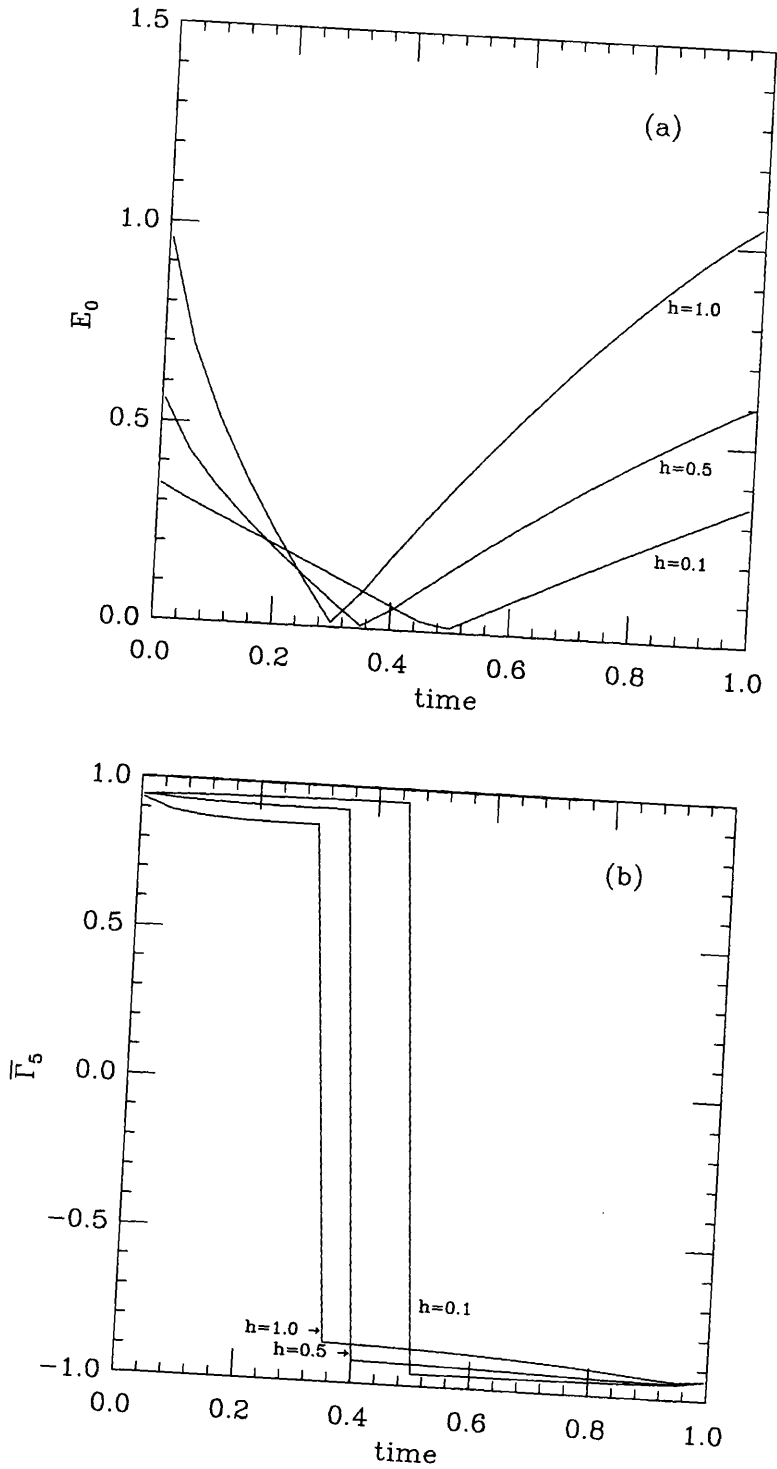


Figure 5.4: (a): The lowest eigenvalue  $E_0$  as a function of time for the configurations (5.3.40) for Yukawa couplings  $h = 0.1, 0.5$  and  $1.0$ . (b): The generalised chirality  $\tilde{\Gamma}_5$  of the corresponding eigenvector.

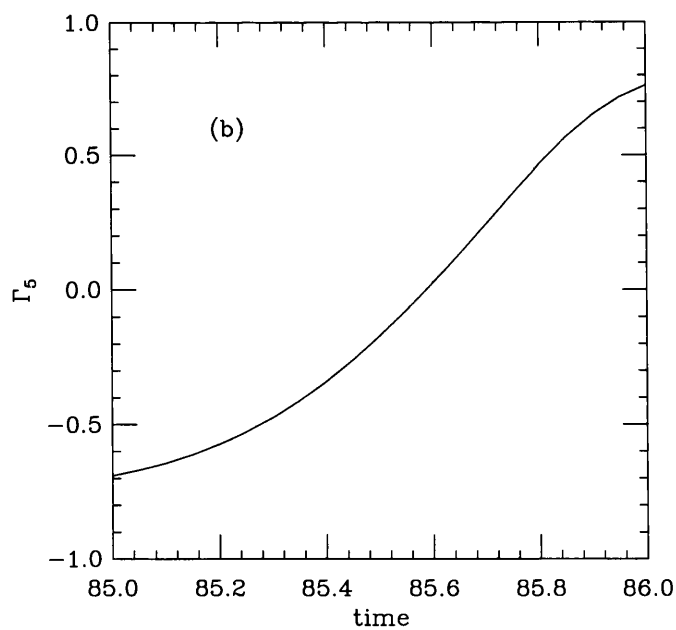
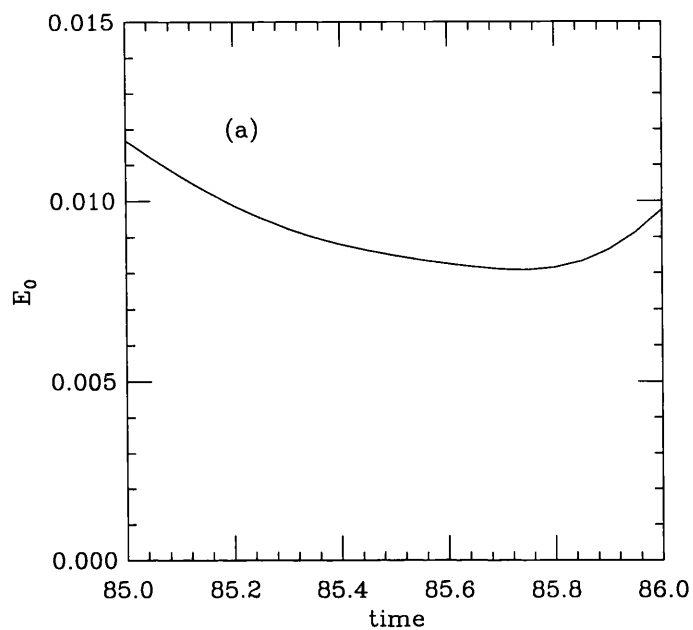


Figure 5.5: (a): The lowest eigenvalue  $E_0$  as a function of time for a typical sphaleron transition (no cooling) for the massless Hamiltonian. (b): The chirality  $\Gamma_5$  of the corresponding eigenvector.

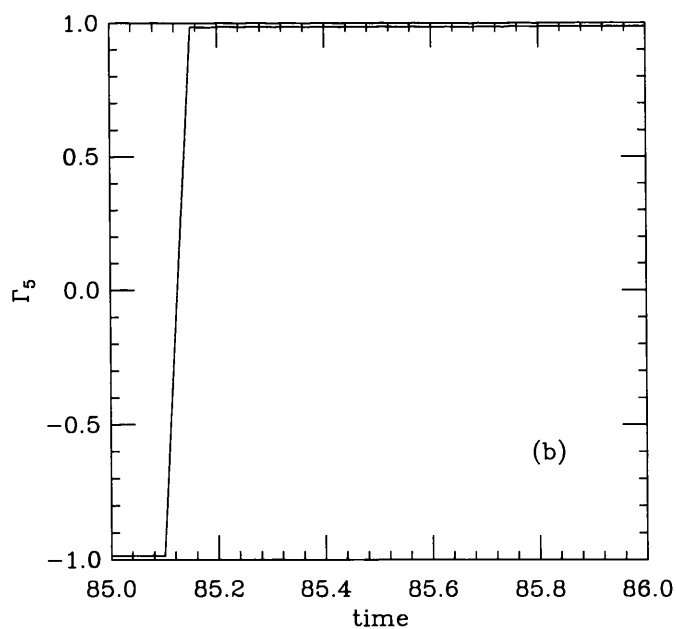
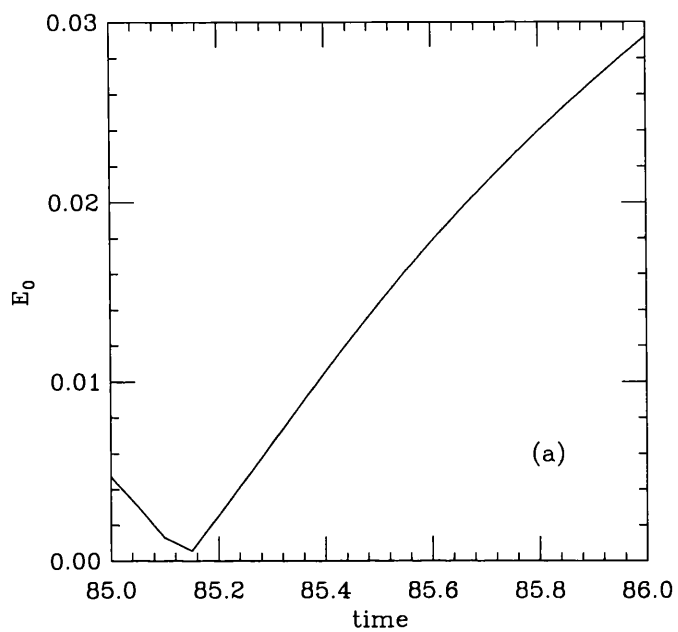


Figure 5.6: (a): The lowest eigenvalue  $E_0$  as a function of time for a typical sphaleron transition (60 cooling sweeps) for the massless Hamiltonian. (b): The chirality  $\Gamma_5$  of the corresponding eigenvector.

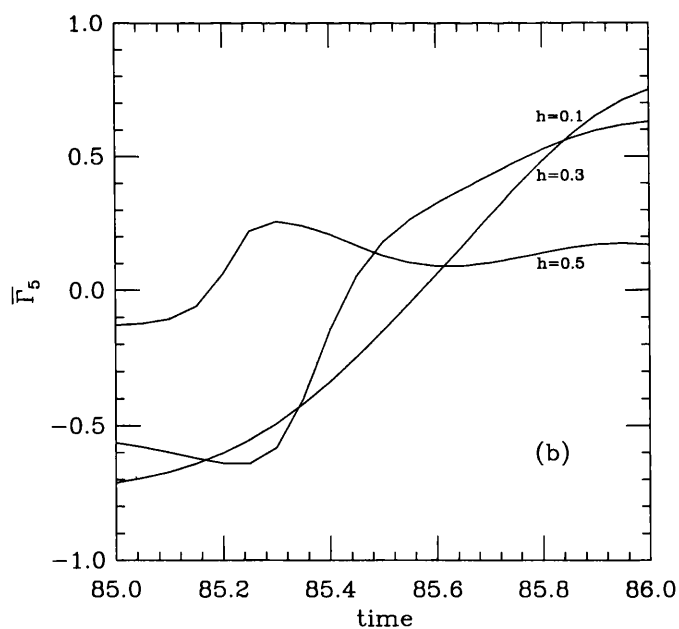
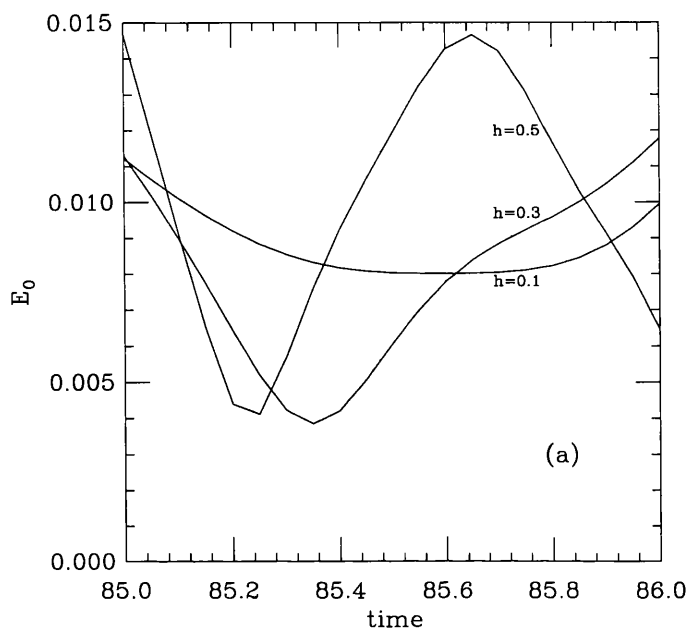


Figure 5.7: (a): The lowest eigenvalue  $E_0$  as a function of time for a typical sphaleron transition (no cooling) for Yukawa couplings  $h = 0.1, 0.3$  and  $0.5$ . (b): The generalised chirality  $\tilde{\Gamma}_5$  of the corresponding eigenvector.

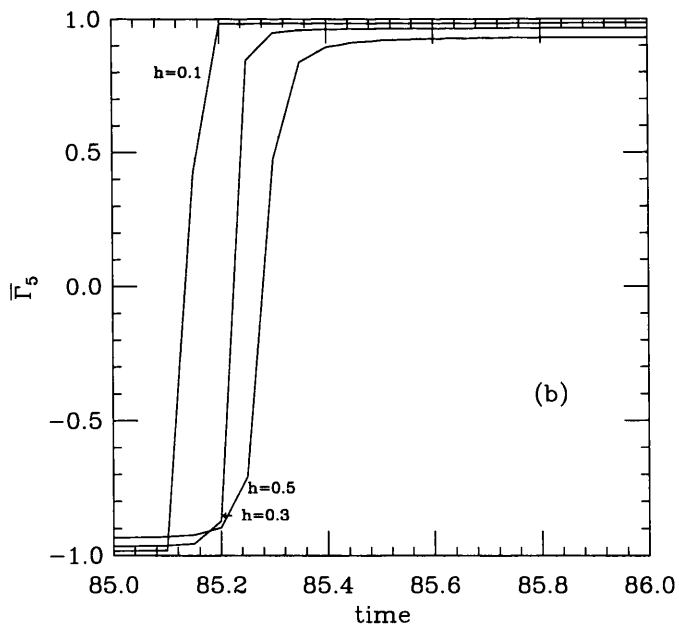
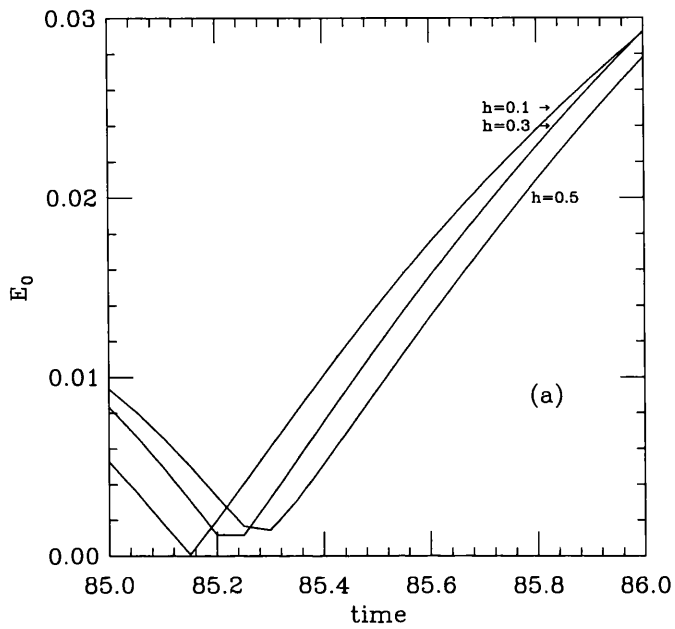


Figure 5.8: (a): The lowest eigenvalue  $E_0$  as a function of time for a typical sphaleron transition (60 cooling sweeps) for Yukawa couplings  $h = 0.1, 0.3$  and  $0.5$ . (b): The generalised chirality  $\tilde{\Gamma}_5$  of the corresponding eigenvector.

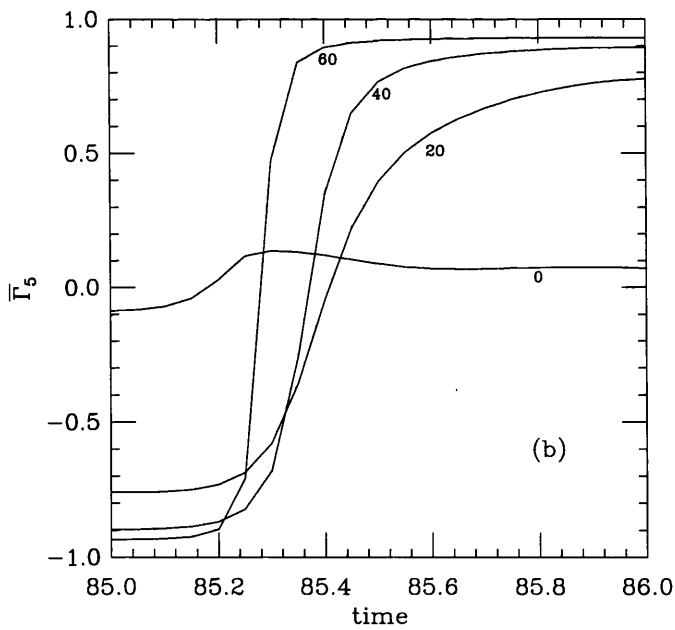
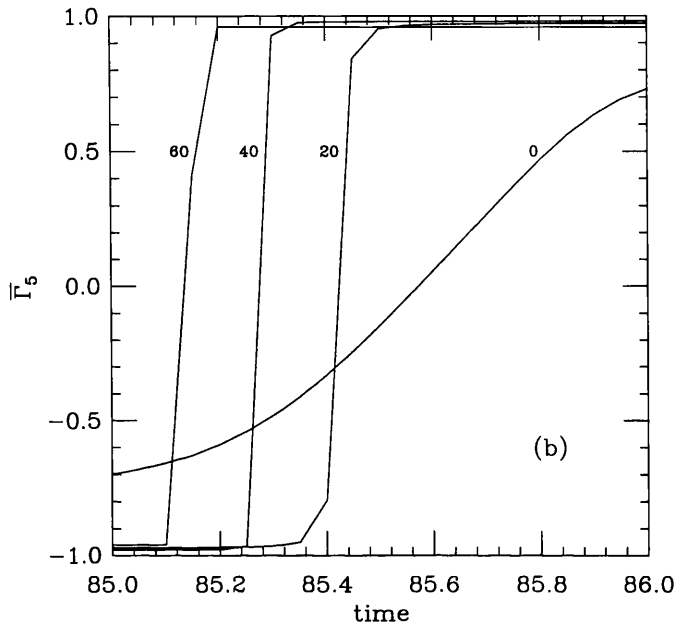


Figure 5.9: The generalised chirality  $\tilde{\Gamma}_5$  as a function of time for a typical sphaleron transition for 0, 20, 40 and 60 cooling sweeps. (a):  $h = 0.1$ . (b):  $h = 0.5$ .

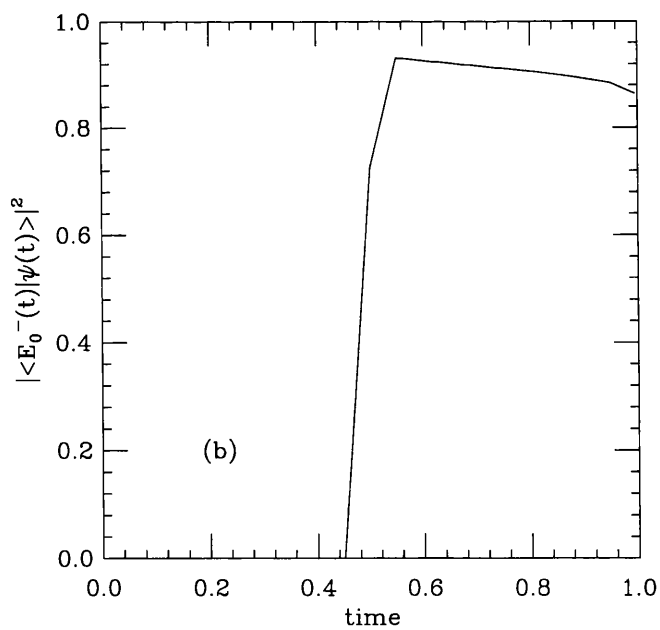
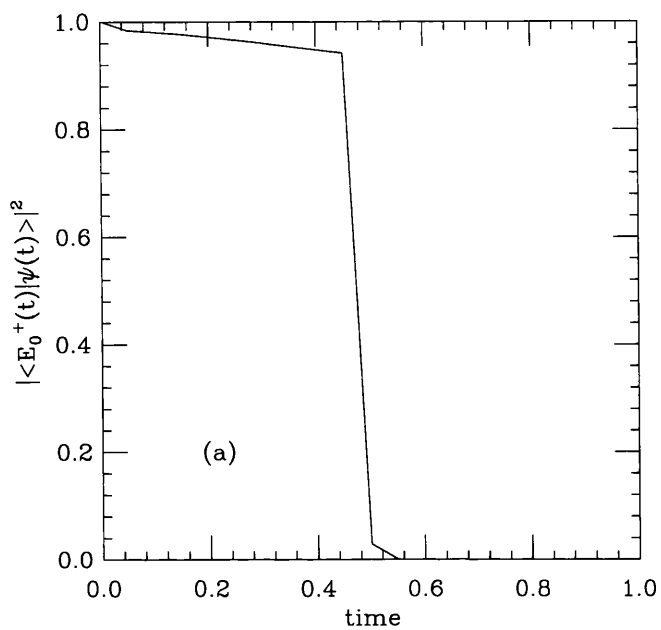


Figure 5.10: (a):  $|\langle E_0^+ | \psi \rangle|^2$  as a function of time for the configurations (5.3.38) for the massless Hamiltonian. (b):  $|\langle E_0^- | \psi \rangle|^2$  as a function of time for the configurations (5.3.38) for the massless Hamiltonian.

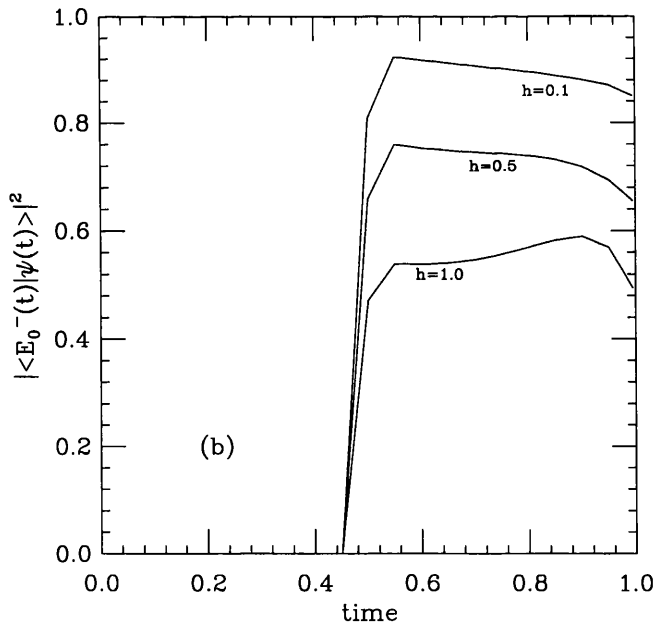
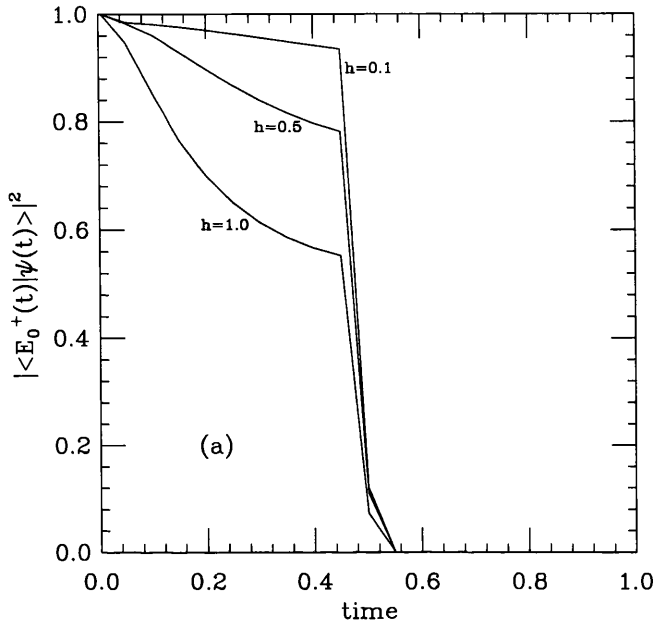


Figure 5.11: (a):  $|\langle E_0^+ | \psi \rangle|^2$  as a function of time for the configurations (5.3.39) for Yukawa couplings  $h = 0.1, 0.5$  and  $1.0$ . (b):  $|\langle E_0^- | \psi \rangle|^2$  as a function of time for the configurations (5.3.39) for Yukawa couplings  $h = 0.1, 0.5$  and  $1.0$ .

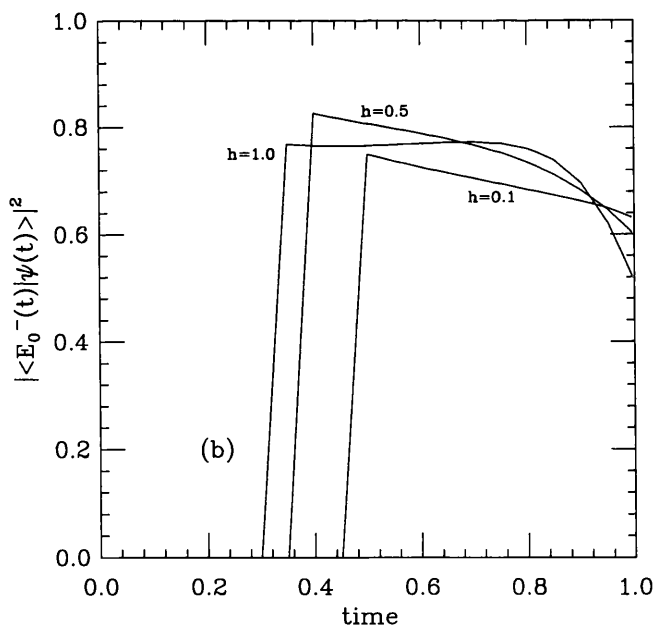
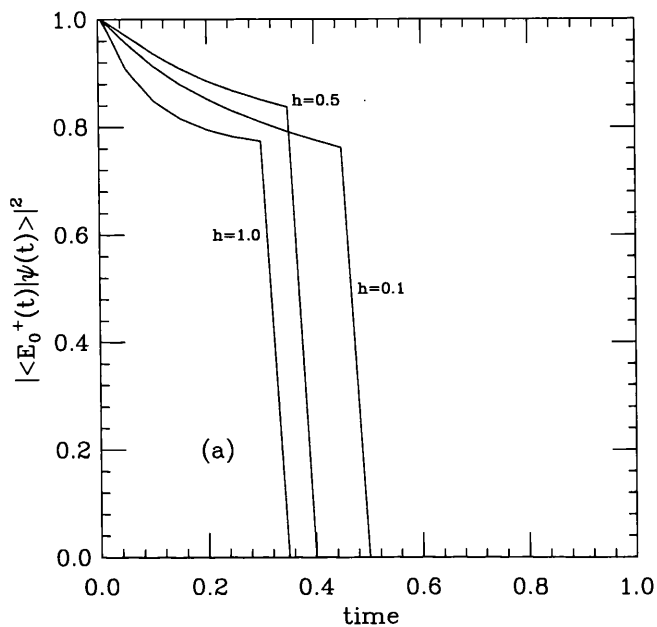


Figure 5.12: (a):  $|\langle E_0^+|\psi\rangle|^2$  as a function of time for the configurations (5.3.40) for Yukawa couplings  $h = 0.1, 0.5$  and  $1.0$ . (b):  $|\langle E_0^-|\psi\rangle|^2$  as a function of time for the configurations (5.3.40) for Yukawa couplings  $h = 0.1, 0.5$  and  $1.0$ .

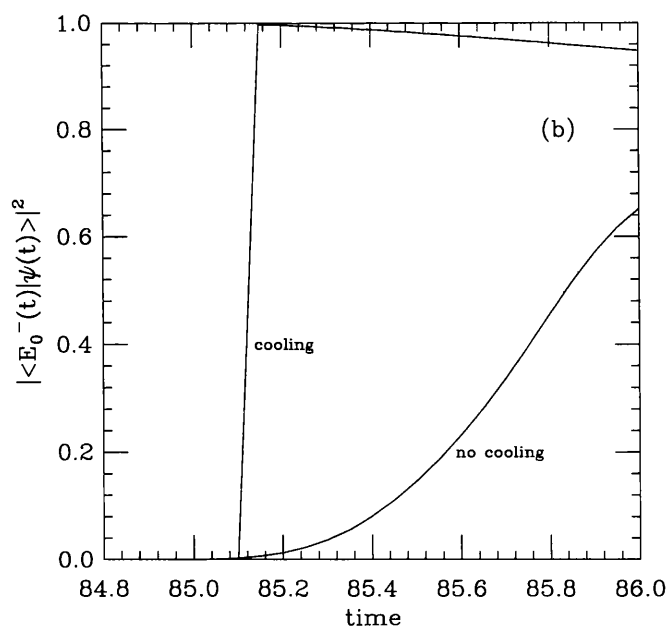
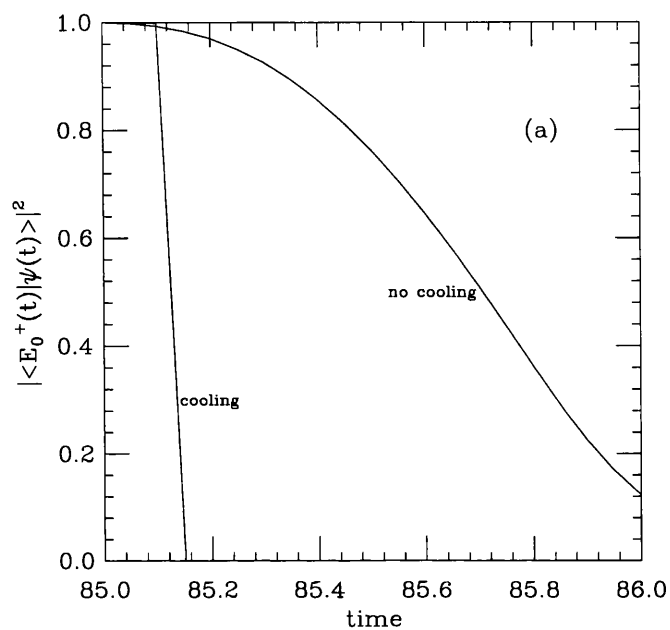


Figure 5.13: (a):  $|\langle E_0^+ | \psi \rangle|^2$  as a function of time for a typical sphaleron transition for the massless Hamiltonian. (b):  $|\langle E_0^- | \psi \rangle|^2$  as a function of time for a typical sphaleron transition for the massless Hamiltonian.

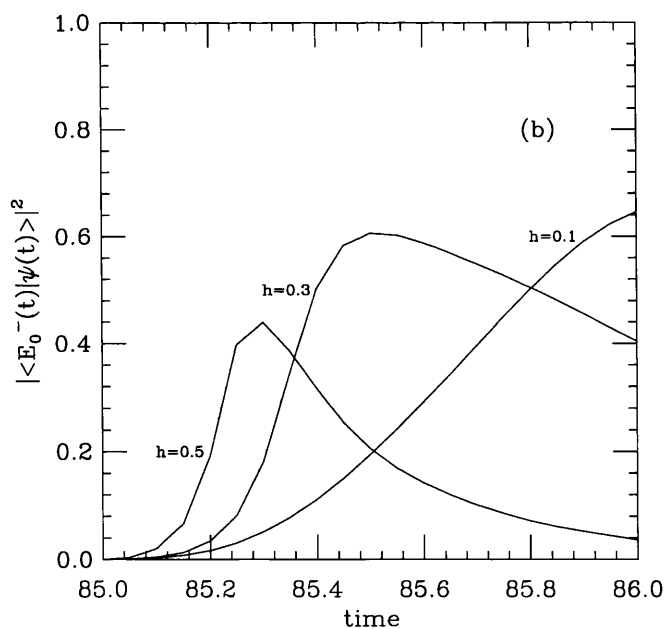
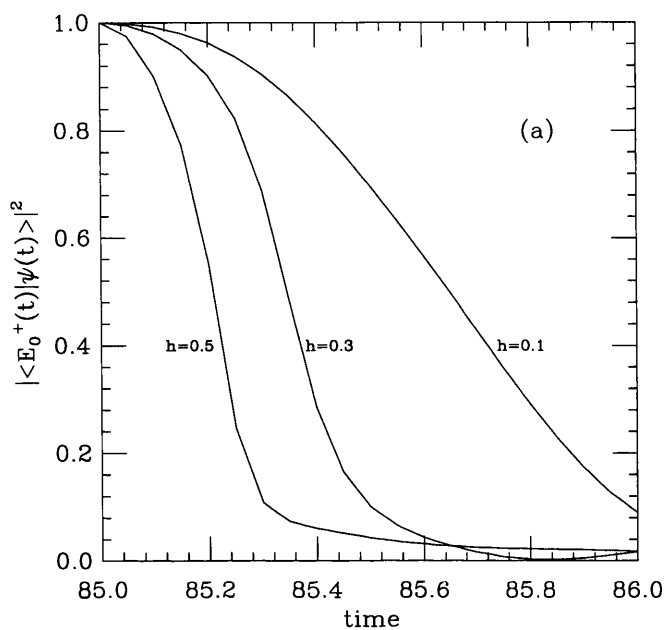


Figure 5.14: (a):  $|\langle E_0^+|\psi\rangle|^2$  as a function of time for a typical sphaleron transition (no cooling) for Yukawa couplings  $h = 0.1, 0.3$  and  $0.5$ . (b):  $|\langle E_0^-|\psi\rangle|^2$  as a function of time for a Yukawa couplings  $h = 0.1, 0.3$  and  $0.5$ .

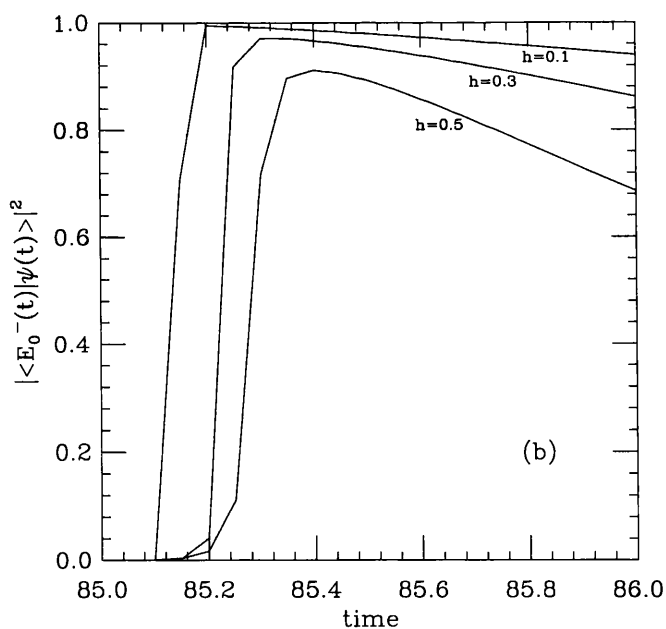
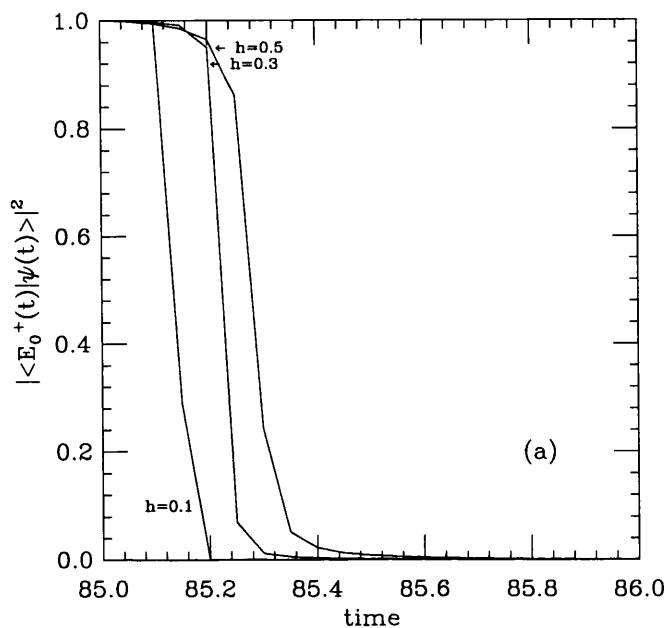


Figure 5.15: (a):  $|\langle E_0^+ | \psi \rangle|^2$  as a function of time for a typical sphaleron transition (60 cooling sweeps) for Yukawa couplings  $h = 0.1, 0.3$  and  $0.5$ . (b):  $|\langle E_0^- | \psi \rangle|^2$  as a function of time for a typical sphaleron transition (60 cooling sweeps) for Yukawa couplings  $h = 0.1, 0.3$  and  $0.5$ .

# Chapter 6

## Conclusions

In the first part of this thesis we presented evidence for level crossing in the lattice  $U(1)$  model in  $1 + 1$  dimensions. Using both "artificial" smooth and "realistic" high temperature background fields, where the Chern-Simons number changes by unity, we observe the diving of the lowest positive eigenvalue and flip in sign of the generalised chirality which we interpret as showing energy levels crossing zero.

The interpretation that the eigenvalue crosses zero is supported by solving the Dirac equation to follow the time development of the lowest energy eigenstates. In all cases the lowest positive energy eigenstate evolves suddenly into the highest negative energy eigenstate at the point where the eigenvalue crosses zero, confirming the level crossing picture. For general gauge-Higgs backgrounds there is also non-adiabatic behaviour resulting in a drift into higher energy states, the extent of this drift depending upon the particular background and Yukawa coupling. However in all the cases investigated level crossing can still be identified, despite this non-adiabatic behaviour.

In agreement with [15] for massless fermions the level crossing always occurs at half-integer  $N_{CS}$ , while the presence of a Yukawa term displaces the zero eigenvalue away from half-integer  $N_{CS}$ . Our results using smooth configurations indicate that the zero eigenvalue is displaced towards the point where the Higgs field has a

zero. For the high temperature fields this behaviour is verified by measuring the topology of the Higgs field.

Similar results were obtained for the  $SU(2)$  model in  $3 + 1$  dimensions, at least for the trial background fields. However, for the high temperature fields the generalised chirality  $|\tilde{\Gamma}_5|$  is significantly different from 1 and decreases as the Yukawa coupling  $h$  is increased. In addition the lowest eigenvalue doesn't reach zero so that there is a gap separating positive and negative energy states. Eventually we find  $\tilde{\Gamma}_5 \approx 0$  and it becomes increasingly difficult to identify the chirality flip. This effect is due to fluctuations in the background fields. Indeed using the relatively "smooth" trial backgrounds we find  $|\tilde{\Gamma}_5|$  close to one for large values of  $h$ . For the high temperature backgrounds it is convenient to artificially smooth the backgrounds by applying cooling equations. After cooling we find the lowest eigenvalue gets much closer to zero and  $\tilde{\Gamma}_5$  is close to  $\pm 1$  which we interpret as showing level crossing. Since our cooling equations work relatively slowly on the magnitude of the Higgs field, the number of cooling sweeps required increases with increasing  $h$ .

These results are in agreement with results of [25] where the above method was originally introduced and applied to the  $SU(2)$  model. To check the level crossing interpretation we have used the time-dependent Dirac equation. For smooth background fields the results show the lowest positive energy eigenstate evolving suddenly into the highest negative energy eigenstate, confirming the level crossing of energy eigenvalues. Using the high temperature fields the state doesn't cross zero but rather gradually "hops" across the eigenvalue gap described above. Level crossing is only observed after cooling the backgrounds in agreement with the eigenvalue and chirality measurements.

As in the  $U(1)$  model the exact point at which the zero eigenvalue occurs depends upon the Yukawa coupling. In fact using trial configurations very similar results are obtained for both models. However unlike the  $U(1)$  model it is not necessary for  $N_{CS}$  to be half-integer to have a zero eigenvalue of the massless

Hamiltonian in the  $SU(2)$  case. An example is the particular high temperature configuration described in this thesis, where we find a zero eigenvalue for  $N_{CS} \sim -0.7$ . For non-zero Yukawa coupling our trial results indicate that the zero eigenvalue is displaced towards the point where the Higgs field has a zero. Unfortunately we have been unable to check this for our high temperature fields, due to difficulty in locating the zeros of the Higgs field in the symmetric phase. This may be possible in the broken phase though such simulations are expected to require significantly larger lattices.

The results of this thesis thus provide further evidence that the high temperature configurations with  $\Delta N_{CS} = 1$  observed in lattice simulations are accompanied by level crossing and hence fermion number non-conservation.

# Appendix A

## Lattice Gauge Theory

As discussed in Section 2.2 the real time microcanonical method relies on the assumption that the dynamics of sphaleron transitions at high temperatures is described well by classical statistical mechanics. However due to the Rayleigh Jeans divergence the classical statistical mechanics of a continuum field theory are ill defined. This ultraviolet divergence is conveniently regularised by putting the system on a spatial lattice.

The simplest spatial lattice is a cubic lattice (a chain in 1 space dimension) with equal lattice spacing  $a$  in all directions. Scalar fields are put on lattice sites  $x_i = an_i$  (where  $n_i$  are integers),  $\phi(x) \rightarrow \phi_n$ . The lattice provides the necessary momentum cut-off as can be seen by Fourier transforming to momentum space. In  $d$  space dimensions we have

$$\phi(k) = \sum_n a^d e^{ik \cdot na} \quad (\text{A. 1})$$

which is periodic in momentum  $k_i$  with period  $\frac{2\pi}{a}$ . Hence we can restrict  $k_i$  to lie in the first Brillouin zone  $-\frac{\pi}{a} < k_i \leq \frac{\pi}{a}$ .

On the lattice  $\partial_i \phi(x)$  becomes

$$\partial_i \phi(x) \rightarrow \frac{\phi_{n+i} - \phi_n}{a} \quad (\text{A. 2})$$

so that a derivative term in the Hamiltonian  $\int d^d x \partial_i \phi^\dagger \partial_i \phi$  becomes

$$\int d^d x \partial_i \phi^\dagger \partial_i \phi \rightarrow \sum_n a^{d-2} \sum_{i=1}^d \left( 2\phi_n^\dagger \phi_n - 2\text{Re} \left( \phi_n^\dagger \phi_{n+\hat{i}} \right) \right) \quad (\text{A. 3})$$

Eq. (A. 3) is invariant under a global phase transformation

$$\phi_n \rightarrow G \phi_n \quad (\text{A. 4})$$

where  $G \in U(1)$ . Suppose we want to gauge this symmetry i.e. let  $G = G_n$ . Then  $\phi_n^\dagger \phi_{n+\hat{i}} \rightarrow \phi_n^\dagger G_n^\dagger G_{n+\hat{i}} \phi_{n+\hat{i}}$ . To make this term gauge invariant we introduce the lattice gauge field or link variable  $U_{n,\hat{i}} \in U(1)$  lying on the link connecting sites  $n$  and  $n + \hat{i}$  which transforms as

$$U_{n,\hat{i}} \rightarrow G_n U_{n,\hat{i}} G_{n+\hat{i}}^\dagger \quad (\text{A. 5})$$

Then the covariant version of Eq, (A. 3) is

$$\int d^d x \partial_i \phi^\dagger \partial_i \phi \rightarrow \sum_n a^{d-2} \sum_{i=1}^d \left( 2\phi_n^\dagger \phi_n - 2\text{Re} \left( \phi_n^\dagger U_{n,\hat{i}} \phi_{n+\hat{i}} \right) \right) \quad (\text{A. 6})$$

We can also construct gauge invariant terms entirely from link variables. From Eq. (A. 5) we can see that the trace of the path ordered product of link variables around any closed loop is gauge invariant. The simplest of these is the plaquette consisting of 4 links. The product of links around a plaquette  $\square$  is

$$U_\square = U_{n,\hat{i}} U_{n+\hat{i},\hat{j}} U_{n+\hat{j},\hat{i}}^\dagger U_{n,\hat{j}}^\dagger \quad (\text{A. 7})$$

from which we can construct the Wilson action [34]

$$\beta \sum_\square (1 - \text{Re} U_\square) \quad (\text{A. 8})$$

$\beta$  is a normalisation constant.

The connection between the link variable  $U_{n,\hat{i}}$  and the vector potential  $A_i(n)$  is

$$U_{n,\hat{i}} = \exp(iga A_i(n)) \quad (\text{A. 9})$$

where  $g$  is the continuum (bare) coupling constant. With this identification we find in the continuum limit Eq. (A. 3) becomes

$$\sum_n a^{d-2} \sum_{i=1}^d \left( 2\phi_n^\dagger \phi_n - 2\text{Re} \left( \phi_n^\dagger U_{n,i} \phi_{n+i} \right) \right) \rightarrow \int d^d x D_i \phi^\dagger D_i \phi \quad (\text{A. 10})$$

where  $D_i$  is the covariant derivative,  $D_i = \partial_i + igA_i$ . The continuum limit of the Wilson action is just the continuum gauge field action

$$\beta \sum_{\square} (1 - \text{Re} U_{\square}) \rightarrow \frac{1}{4} \int d^d x F_{ij} F_{ij} \quad (\text{A. 11})$$

if we identify  $\beta = \frac{1}{g^2}$ .

It is easy to generalise to the case where  $G_n \in SU(N)$ . Instead of Eq. (A. 9) we now have

$$U_{n,i} = \exp(igaT^a A_i^a(n)) \in SU(N) \quad (\text{A. 12})$$

where  $T^a$  are the generators of  $SU(N)$ . The Wilson action is now

$$\beta \sum_{\square} \left( 1 - \frac{1}{2} \text{Re Tr} U_{\square} \right) \quad (\text{A. 13})$$

where  $\beta = \frac{2N}{g^2}$ .

# Appendix B

## Monte Carlo Methods

The probability of any particular field configuration  $C$  in thermal equilibrium at temperature  $T$  is given by

$$P_{eq}(C) = \frac{1}{Z} e^{-\frac{H(C)}{T}} \quad (\text{B. 1})$$

where  $Z$  is the partition function

$$Z = \sum_C e^{-\frac{H(C)}{T}} \quad (\text{B. 2})$$

We want to pick an initial configuration with this statistical weight. Monte Carlo methods produce a sequence of configurations  $C_i$  such that for large  $i$  the the probability of finding any particular configuration is given by Eq. (B. 1) independently of the starting configuration  $C_0$  used. At any given stage in the Monte Carlo process given the current configuration  $C$  we choose a new configuration  $C'$  with probability  $P(C \rightarrow C')$ . Then  $P(C \rightarrow C')$  must satisfy

$$P_{eq}(C) = \sum_{C'} P_{eq}(C') P(C \rightarrow C') \quad (\text{B. 3})$$

In practice most Monte Carlo algorithms are based on the detailed balance condition

$$P(C \rightarrow C') e^{-\frac{H(C)}{T}} = P(C' \rightarrow C) e^{-\frac{H(C')}{T}} \quad (\text{B. 4})$$

which is a sufficient condition for  $P(C \rightarrow C')$  to satisfy Eq. (B. 3).

The Monte Carlo method used in our simulations is the Metropolis algorithm [41]. Here a test configuration  $C'$  is suggested with probability  $P_0(C \rightarrow C')$  such that  $P_0(C \rightarrow C') = P_0(C' \rightarrow C)$ . If  $H(C') < H(C)$  then  $C'$  is accepted as the new configuration. If  $H(C') > H(C)$  a random number  $r$  in the range  $[0, 1]$  is picked and  $C'$  is accepted if  $r < e^{-\frac{H(C') - H(C)}{T}}$ . Otherwise  $C'$  is rejected and we keep the configuration  $C$ . We have considerable freedom in our choice of a test configuration  $C'$ . In practice it is convenient to change a single site/link at a time. We sweep through the lattice sequentially with 5 hits per site/link before moving on to the next.

# Appendix C

## The Lanczos Algorithm

The Lanczos algorithm [43] is used to perform a unitary transformation on a Hermitian matrix  $H$

$$X^\dagger H X = T, \quad X^\dagger X = I \quad (\text{C. 1})$$

such that  $T$  is tridiagonal

$$T = \begin{pmatrix} \alpha_1 & \beta_1 & & & \\ \beta_1 & \alpha_2 & \beta_2 & & \\ & \beta_2 & \alpha_3 & & \\ & & & \ddots & \\ & & & & \ddots \end{pmatrix} \quad (\text{C. 2})$$

The columns of the matrix  $X$  are the mutually orthonormal Lanczos vectors  $x_i$ . Choosing  $x_1$  to be any unit vector the  $x_i$ ,  $\alpha_i$  and  $\beta_i$  can be calculated recursively using

$$\begin{aligned} \alpha_i &= x_i^\dagger H x_i \\ u_1 &= H x_1 - \alpha_1 x_1 \\ u_i &= H x_i - \beta_{i-1} x_{i-1} - \alpha_i x_i, \quad i \geq 2 \\ \beta_i^2 &= u_i^\dagger u_i \end{aligned}$$

$$x_{i+1} = \frac{1}{\beta_i} u_i \quad (\text{C. 3})$$

The eigenvalues of  $H$  can now be found easily using the method of Sturm sequences. This method uses the fact that if  $V$  is an  $N \times N$  Hermitian matrix and  $d_i$  is the minor determinant of  $V - \lambda I$  formed by the first  $i$  rows and columns then the number of eigenvalues less than  $\lambda$  equals the number of sign changes in the sequence  $d_0, d_1, \dots, d_N$ . For the tridiagonal form  $T$  the  $d_i$  are easily calculated recursively.

$$\begin{aligned} d_0 &= 1 \\ d_1 &= \alpha_i - \lambda \\ d_i &= (\alpha_i - \lambda) d_{i-1} - \beta_{i-1}^2 d_{i-2}, \quad i \geq 2 \end{aligned} \quad (\text{C. 4})$$

The eigenvalues can be found by picking an interval  $[\lambda_{min}, \lambda_{max}]$  containing the eigenvalue  $\lambda_i$  and using the above theorem to find whether  $\lambda_i$  is in the lower or upper half. By repeatedly halving the interval the eigenvalue can be found to any required precision.

To reduce the amount of computation required we make use of the even-odd block structure of the Fermion Hamiltonian. For example in  $1 + 1$  dimensions Eq. (3.2.10) is written explicitly in terms of odd and even sites. In matrix notation we have

$$H\psi = \begin{pmatrix} 0 & M \\ M^\dagger & 0 \end{pmatrix} \begin{pmatrix} \psi^{even} \\ \psi^{odd} \end{pmatrix} = E \begin{pmatrix} \psi^{even} \\ \psi^{odd} \end{pmatrix} \quad (\text{C. 5})$$

where  $\psi^{even} = \begin{pmatrix} \chi^{1,even} \\ \chi^{2,odd} \end{pmatrix}$ ,  $\psi^{odd} = \begin{pmatrix} \chi^{1,odd} \\ \chi^{2,even} \end{pmatrix}$ . Now if we multiply Eq. (C. 5) by

$H$  the two components  $\psi^{even}, \psi^{odd}$  decouple. Hence we only need to solve

$$MM^\dagger \psi^{even} = E^2 \psi^{even} \quad (\text{C. 6})$$

for  $E^2$ .

# Appendix D

## Inverse Iteration

Let  $H$  be the Hamiltonian matrix with eigenvalues  $E_i$  and eigenvectors  $\psi_i$ .

$$H\psi_i = E\psi_i \quad (\text{D. 1})$$

The method of inverse iteration [42] is used to find the eigenvectors given that we already know (approximately) the eigenvalues. We start with some random vector  $r$  and solve

$$(H - E)\psi = r \quad (\text{D. 2})$$

for  $\psi$ , where  $E$  is close to some eigenvalue, say  $E \approx E_n$ . Then  $\psi$  will be close to the eigenvector  $\psi_n$ . To see this note that if we expand  $r = \sum_j \alpha_j \psi_j$  then substituting into Eq. (D. 2) gives

$$\psi = \sum_j \frac{\alpha_j}{E_j - E} \psi_j \quad (\text{D. 3})$$

Since  $E \approx E_n$  then  $\psi \approx \psi_n$  (provided  $\alpha_n \neq 0$ ). This procedure can be iterated with  $\psi$  replacing the random vector  $r$  in Eq. (D. 2). In practice we find a single iteration sufficient since we accurately know the energy eigenvalues.

Again the even-odd structure of the Hamiltonian can be used to simplify the computation. Given  $E^2$  we solve Eq. (C. 6) for  $\psi_{\text{even}}$ . Rather than Eq. (D. 2) we want to solve

$$(MM^\dagger - E^2)\psi_{\text{even}} = r \quad (\text{D. 4})$$

Then  $\psi_{odd}$  is easily deduced from Eq. (C. 5)  $\psi_{odd} = \frac{1}{E} M^\dagger \psi_{even}$ .

To solve Eq. (D. 2) we use Lanczos matrix inversion [44] to find  $\psi_{even} = (MM^\dagger - E^2)^{-1} r$ . Lanczos matrix inversion uses the  $\alpha_i$  and  $\beta_i$  of the tridiagonal matrix and the Lanczos vectors  $x_i$  to build up an iterative solution to

$$H\psi = \eta \quad (\text{D. 5})$$

where  $H$  is any Hermitean matrix. The solution is given by the following recurrence relations

$$\begin{aligned} A_{k+1} &= -\frac{\alpha_{k+1}}{\beta_k} A_k + B_k \\ B_{k+1} &= -\frac{\beta_{k+1}}{\beta_k} A_k \\ y_{k+1} &= y_k + \frac{t_k}{A_{k+1}} \\ t_{k+1} &= -\frac{B_{k+1}}{A_{k+1}} t_k \\ U_{k+1} &= U_k + \frac{A_k}{\beta_k} x_{k+1} \\ V_{k+1} &= V_k - \frac{t_k}{A_{k+1}} U_{k+1} \end{aligned} \quad (\text{D. 6})$$

with initial conditions  $A_1 = t_1 = 1$ ,  $U_1 = B_1 = y_1 = 0$ ,  $x_1 = \eta$ ,  $V_1 = -\frac{x_1}{\beta_1}$  and  $U_1 = 0$ . Then the solution to Eq. (D. 5) is found as

$$\psi_k = -\frac{1}{y_k + \frac{\alpha_1}{\beta_1}} V_k \rightarrow \psi \quad \text{as} \quad t_k \rightarrow 0 \quad (\text{D. 7})$$

# Bibliography

- [1] S. Adler, Phys. Rev. 177 (1969) 2426; J. Bell and R. Jackiw, Nuovo Cimento 60 (1969) 47; W. Bardeen, Phys. Rev. 184 (1969) 1848
- [2] R. Rajaraman, "Solitons and Instantons" (North-Holland Publishing Company, 1982)
- [3] F. R. Klinkhamer and N. S. Manton, Phys. Rev. D30 (1984) 2212
- [4] A. I. Bochkaev and M. E. Shaposnikov, Mod. Phys. Lett. A2 (1987) 991
- [5] J. Ambjørn, T. Askgaard, H. Porter and M. E. Shaposnikov; Phys. Lett. B244 (1990) 479; Nucl. Phys. B353 (1990) 346
- [6] J. Ambjørn and A. Krasnitz, Phys. Lett. B362 (1985) 97
- [7] J. Smit and W. Tang, hep-lat/9605016
- [8] H. B. Nielsen and M. Ninomiya, Phys. Lett. B130 (1983) 389
- [9] J. Ambjørn, J. Greensite and C. Peterson, Nucl. Phys. B221 (1983) 381
- [10] C.G. Callen, R. Dashen and D. J. Gross, Phys. Rev. D17 (1978) 2717
- [11] N. Christ, Phys. Rev. D (19980) 1591
- [12] Z. Guralnik, Phys. Rev. D49 (1994) 49
- [13] A. Ringwald, Phys. Lett. B213 (1988) 61

- [14] M. Axenides, A. Johansen and H. Nielsen, Nucl. Phys. B414 (1994) 53
- [15] M. Axenides, A. Johansen and H. Nielsen, Mod. Phys. Lett. A9 (1994) 1529
- [16] G. 't Hooft, Phys. Rev. Lett. 37 (1976) 8; Phys. Rev. D14 (1976) 3432
- [17] A. D. Sakharov, Sov. Phys. JETP Lett. 5 (1967) 24
- [18] V. Kuzmin, V. Rubakov and M. Shaposnikov, Phys. Lett. B155 (1985) 36
- [19] J. Langer, Ann. Phys. 41 (1967) 108; Ann. Phys. 54 (1969) 258; I. Affleck, Phys. Rev. Lett. 46 (1981) 388
- [20] P. Arnold and L. McLerran, Phys. Rev. D36 (1987) 581; Phys. Rev. D37 (1988) 1020
- [21] J. I. Kapusta, "Finite Temperature Field Theory" (Cambridge University Press, 1989)
- [22] A. Bochkarev and M. Shaposnikov, Mod. Phys. Lett. A2 (1987) 417
- [23] A. Cohen, D. Kaplan and A. Nelson, Ann. Rev. Nucl. Part. Sci. 43 (1993) 27
- [24] J. Ambjørn and K. Farakos, Phys. Lett. B294 (1992) 248
- [25] J. Ambjørn, K. Farakos, S. Hands, G. Koutsoumbas and G. Thorleifsson, Nucl. Phys. B425 (1994) 39
- [26] D. Grigoriev, V. Rubakov and M. Shaposnikov, Phys. Lett. B216 (1989) 172; Nucl. Phys. B326 (1989) 737
- [27] D. Grigoriev and V. Rubakov, Nucl. Phys. B299 (1988) 67
- [28] S. Klebnikov and M. Shaposnikov, Nucl. Phys. B308 (1988) 885
- [29] A. Bochkarev and P. de Forcrand, Phys. Rev. D47 (1993) 3476
- [30] A. Krasnitz and R. Potting, Nucl. Phys. B (Proc. Suppl.) 34 (1994) 613

- [31] J. Smit and W. Tang, Nucl. Phys. B (Proc. Suppl.) 34 (1994) 616
- [32] A. Krasnitz, Nucl.Phys. B455 (1995) 320
- [33] J. Kuti, in "Computational Physics", ed. R. D. Kenway and G. S. Pawley (SUSSP Publications, 1987)
- [34] K. Wilson, in "New Phenomena in Subnuclear Physics", ed. A. Zichichi (Plenum, 1977)
- [35] L. Susskind, Phys. Rev. D16 (1977) 3031
- [36] H. B. Nielsen and M. Ninomiya, Nucl. Phys. B185 (1980) 20; Phys. Lett. B105 (1981) 209
- [37] P. Di Vecchia, K. Fabricus, G. C. Rossi and G. Veneziano, Nucl. Phys. B192 (1981) 392
- [38] S. J. Hands, Nucl. Phys. B329 (1990) 205
- [39] S. J. Hands and M. Teper, Nucl. Phys. B347 (1990) 819
- [40] K. Wilson, Phys. Rev. D10 (1974) 2445
- [41] N. Metropolis, M. Rosenbluth, A. Rosenbluth, E. Teller and J. Teller, J. Chem. Phys. 21 (1953) 1057
- [42] W. Press, B. Flannery, S. Teukolsky and W. Vetterling, "Numerical Recipes" (Cambridge University Press, 1989)
- [43] C. Lanczos, J. Res. Nat. Bur. Stand. 49 (1952) 409
- [44] P. Gibbs, "Applications of the Lanczos Algorithm to Lattice QCD", Glasgow University thesis 1985

